ReproMIA: A Comprehensive Analysis of Model Reprogramming for Proactive Membership Inference Attacks

Chihan Huang
HKUST
Hong Kong, China
huangchihan1@gmail.com

Huaijin Wang
HKUST
Hong Kong, China
hwangdz@cse.ust.hk

Shuai Wang
HKUST
Hong Kong, China
shuaiw@cse.ust.hk

Abstract

The pervasive deployment of deep learning models across critical domains has concurrently intensified privacy concerns due to their inherent propensity for data memorization. While Membership Inference Attacks (MIAs) serve as the gold standard for auditing these privacy vulnerabilities, conventional MIA paradigms are increasingly constrained by the prohibitive computational costs of shadow model training and a precipitous performance degradation under low False Positive Rate constraints. To overcome these challenges, we introduce a novel perspective by leveraging the principles of model reprogramming as an active signal amplifier for privacy leakage. Building upon this insight, we present ReproMIA, a unified and efficient proactive framework for membership inference. We rigorously substantiate, both theoretically and empirically, how our methodology proactively induces and magnifies latent privacy footprints embedded within the model's representations. We provide specialized instantiations of ReproMIA across diverse architectural paradigms, including LLMs, Diffusion Models, and Classification Models. Comprehensive experimental evaluations across more than ten benchmarks and a variety of model architectures demonstrate that ReproMIA consistently and substantially outperforms existing state-of-the-art baselines, achieving a transformative leap in performance specifically within low-FPR regimes, such as an average of 5.25% AUC and 10.68% TPR@1%FPR increase over the runner-up for LLMs, as well as 3.70% and 12.40% respectively for Diffusion Models.

CCS Concepts

• **Security and privacy** → **Privacy-preserving protocols**; • **Computing methodologies** → **Machine learning algorithms**; **Natural language generation**; **Computer vision**; **Transfer learning**.

Keywords

Membership Inference Attack, Model Reprogramming, Large Language Model, Diffusion Model, Computer Vision

1 Introduction

Machine learning technologies, especially deep neural networks [46] have become essential to modern infrastructure, powering critical fields from high-precision medical diagnostics [22] and automated financial risk mitigation [24] to large-scale Generative AI [28]. However, their performance relies on internalizing massive datasets [64] that often contain sensitive personal, medical, or proprietary information [7]. As data demands grow, preventing model leakage of this sensitive information has become a paramount concern.

In this context, Membership Inference Attack [74] has been proposed as a rigorous benchmark for quantifying the degree of privacy leakage inherent in a model. MIA aims to determine whether a specific data record was incorporated into a model's training set by analyzing its output responses. This modality of attack has garnered significant scholarly attention and has been extensively investigated [8, 53, 54, 60]. Beyond serving as a direct threat vector for assessing privacy vulnerabilities, MIA functions as a critical evaluation for various privacy-centric tasks, including privacy auditing [41, 62], the verification of machine unlearning [45], and the performance benchmarking of privacy-enhancing technologies [20, 65]. Consequently, it represents an indispensable core technology in the architecture of Trustworthy AI.

Despite the considerable strides made in MIA over the past decade, existing attack paradigms are confronting unprecedented technical bottlenecks and performance ceilings when faced with increasingly sophisticated deep learning architectures and highly optimized training stratagems. First, traditional attack frameworks using shadow models [6] necessitate the optimization of multiple surrogate models mirroring the target architecture, which requires significant computational resources, making such methods increasingly impractical in the era of LLMs with billions of parameters [73]. Second, the evolution of modern training techniques like regularization and label smoothing has significantly converged the output distributions of member and non-member samples [23, 40, 77]. This signal attenuation phenomenon increasingly neutralizes detection methods predicated on simple posterior probabilities or entropy values, making it difficult to provide reliable privacy inference under the stringent security constraints of low False Positive Rates.

Most critically, contemporary MIA research remains largely confined to the passive observation of raw model outputs, lacking a universal mechanism capable of actively probing, inducing, and amplifying the subtle privacy vestiges embedded within deep neural representations. Particularly within the domains of LLMs and generative models, the security community urgently requires a novel evaluative framework that can transcend task boundaries to actively bolster privacy identification signals.

To address the limitations of conventional passive paradigms, we innovatively propose the integration of model reprogramming into the MIA framework. This serves as an active privacy probe designed to accentuate the latent behavioral discrepancies between member and non-member samples. The core of model reprogramming lies in its ability to keep the model parameters frozen while introducing learnable transformation operators within the input space to induce the model to perform novel downstream tasks or enhance existing ones. Our fundamental insight is that this reprogramming process essentially constitutes a deep stress test of the model's latent feature

space. By applying strategic transformations in the input domain, we can artificially evoke and magnify the subtle memory footprints of member samples embedded within deep neural layers, thereby proactively amplifying the feature divergence between members and non-members.

Based on these insights, we introduce ReproMIA, a unified evaluative framework that leverages the principles of model reprogramming to actively bolster membership inference signals. The pivotal mechanism of ReproMIA involves the construction of a lightweight reprogramming layer. While keeping the target model parameters frozen, the framework learns specific input-space transformations and employs an optimization objective decoupled from the original model task to elicit and intensify the target model's latent memorization properties. The advantages of this framework are twofold:

(1) ReproMIA is not localized to a single data modality or target architecture, it is a generalized framework applicable across diverse model structures, objectives, and data domains. We have successfully instantiated the framework for LLMs, Diffusion Models, Image Classification Models, and Graph Neural Networks.
(2) By inducing the overfitting-driven memorization effects associated with member samples, ReproMIA captures nuanced neural activation variances that elude traditional methodologies. Consequently, it achieves high-fidelity membership adjudication even under a low FPR.

To rigorously validate the efficacy and robustness of ReproMIA, we conducted a systematic evaluation across more than ten benchmark datasets spanning the core domains of machine learning, including NLP, Computer Vision, AIGC, and GNNs. In comparative analyses against a spectrum of state-of-the-art baselines, ReproMIA consistently demonstrated substantial performance gains across all evaluations. Of particular significance is the framework's performance in low FPR scenarios, which is the most critical metric in security auditing, where ReproMIA achieved a profound escalation in TPR across numerous challenging datasets. For instance, on the WikiMIA benchmark [73], ReproMIA outperformed the runner-up baseline by an average of 5.25% in AUC and 10.68% in TPR@1%FPR. When targeting Stable Diffusion [66], ReproMIA secured an average improvement of 3.70% in AUC and 12.40% in TPR@1%FPR over the runner-up baseline, all while maintaining minimal query overhead. Furthermore, we provide an in-depth exploration of ReproMIA's resilience against potential defensive countermeasures, with empirical results confirming that its high-fidelity MIA performance remains largely uncompromised. This comprehensive and multifaceted empirical study underscores the immense potential of ReproMIA as a unified and indispensable tool for privacy auditing in the modern AI era.

In summary, our contributions are summarized as follows:

(1) We provide a rigorous investigation into the underlying mechanisms of model reprogramming from both theoretical and empirical dimensions. We demonstrate how our approach proactively accentuates the latent behavioral discrepancies between member and non-member samples through multiple analytical perspectives.
(2) We propose a unified and computationally efficient framework, ReproMIA, providing specialized instantiations for both generative and discriminative paradigms. By successfully deploying the framework across LLMs, Diffusion Models, and Classification Models, we substantiate its architectural universality and robust generalizability.
(3) We conducted an extensive empirical study across more than ten benchmark datasets spanning multiple modalities and numerous target architectures. The experimental results consistently indicate that ReproMIA substantially exceeds current state-of-the-art baselines across all scenarios, achieving a significant breakthrough in the critical security metric of TPR at low FPR. Furthermore, we provide a detailed analysis of its resilience against prevailing defensive mechanisms.

The structure of our paper is organized as follows: Section 2 introduces the background knowledge of model reprogramming and MIA, Section 3 defines the threat model, Section 4 introduces the overall framework of ReproMIA and provides our insights from both theoretical and empirical perspectives, Sections 5, 6 and C instantiate ReproMIA on LLMs, Diffusion Models, and Classification Models with experimental results, Section 7 discuss ReproMIA in another perspective, Section 8 provides related works and Section 9 concludes our paper, Appendix A provides all theoretical proofs, B provides more details, D provides more experimental results, and E discusses the unification of ReproMIA.

2 Preliminaries

2.1 Model Reprogramming

2.1.1 Model Reprogramming Definition. Model reprogramming [21] aims to repurpose a pre-trained model from a source task to a distinct target objective through data-level manipulation. Unlike conventional transfer learning, which often requires structural modifications or parameter fine-tuning, model reprogramming keeps the base model's parameters frozen throughout the entire training procedure [2]. This approach involves designing an input-agnostic perturbation or transformation function, alongside a label mapping function that bridges the source and target output spaces [81].

Formally, let $\mathcal{M}_\theta : \mathcal{X} \to \mathcal{Y}$ denote a model pre-trained on a source task, where $\mathcal{X}$ and $\mathcal{Y}$ represent the original input and output domains, respectively. Given a target task defined over a different manifold $(x', y') \sim \mathcal{D}'$, with $x' \in \mathcal{X}'$ and $y' \in \mathcal{Y}'$ where $\mathcal{X}'$ and $\mathcal{Y}'$ represent the target input and output domains, the objective of model reprogramming is to optimize a reprogramming function $f : \mathcal{X}' \to \mathcal{X}$. When integrated with a predefined output mapping $h : \mathcal{Y} \to \mathcal{Y}'$, this yields a reprogrammed model $\mathcal{F}(x') \triangleq h\left(\mathcal{M}_\theta(f(x'))\right)$ capable of operating on the target domain $\mathcal{D}'$. The optimization objective is formulated as:

$$\min \mathbb{E}_{(x',y')\sim\mathcal{D}'}\left[\mathcal{L}'(\mathcal{F}(x'), y')\right]. \tag{1}$$

By optimizing only a minimal set of parameters, model reprogramming significantly reduces the need for labeled data and computational overhead while effectively leveraging the inherent feature-extraction capabilities of large-scale pre-trained models.

2.1.2 Model Reprogramming Example. As illustrated in Figure 1, the methodology for reprogramming an ImageNet classifier for

MNIST classification involves specific data-level mapping. Specifically, 28×28 grayscale MNIST images are replicated across three channels and centered within a 224×224 ImageNet-compatible canvas. The peripheral regions are filled by a learnable global perturbation tensor W, constrained by a binary mask M to ensure the perturbation applies only to non-MNIST pixels. This composite input is then processed via a sigmoid activation for numerical stability.

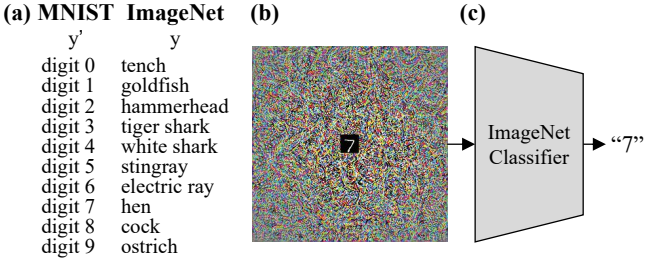

Figure 1: An example of the process of reprogramming an Inception V3 ImageNet model as an MNIST classifier, referred from [21].

The synthesized input undergoes standard ImageNet normalization before being fed into the frozen classifier. The resulting 1,000-dimensional softmax vector is truncated to its first 10 dimensions, serving as the predictive distribution for MNIST classes. During training, optimization is strictly confined to the parameters W. The objective function minimizes the Binary Cross-Entropy loss on the MNIST task, augmented by an ℓ_2 regularization term on W to promote numerical smoothness and prevent overfitting.

2.2 Membership Inference Attacks

MIA Definition. Membership Inference Attack is a pivotal privacy-centric paradigm that has garnered significant scholarly attention due to its ease of deployment and profound privacy implications [6, 8–10, 61, 73, 85]. The fundamental objective of MIA is to determine whether a specific sample x was included in the training set $\mathcal{D}_{train}$ of a target model $\mathcal{M}_\theta$. Formally, given $\mathcal{M}_\theta$ and restricted auxiliary information $\mathcal{I}$, the attacker $\mathcal{A}$ seeks to infer:

$$\mathcal{A} : (x, \mathcal{M}_\theta, \mathcal{I}) \rightarrow \{0, 1\}, \tag{2}$$

where 1 signifies that the sample x is a member of the training set, i.e. $x \in \mathcal{D}_{train}$, and 0 indicates otherwise. In this capacity, $\mathcal{A}$ functions essentially as a binary classifier. Typically, the process involves computing a membership score, $\text{Score}(x)$, which is then compared against a predefined threshold to determine the sample's membership status.

2.3 Metrics for MIA

The following metrics are frequently utilized to evaluate the performance and efficacy of MIAs [6, 10]:

Balanced Accuracy: This metric assesses the overall discriminative capacity of a binary classifier. Under a balanced prior distribution, it measures the precision of membership predictions across the evaluation set, ensuring the performance reflects an unbiased capability to distinguish between members and non-members.

AUC (Area Under the ROC Curve): AUC provides a scalar representation of an attack's global discriminative power by calculating the area beneath the Receiver Operating Characteristic (ROC) curve, which elucidates the trade-off between TPR and FPR across thresholds. Ranging from 0.5 to 1.0, a higher AUC indicates superior performance regardless of the specific decision threshold, characterizing the overall evolution of MIA effectiveness.

TPR@Low FPR: This metric quantifies the True Positive Rate achievable under an exceedingly low False Positive Rate. Since attackers typically cannot tolerate misclassifying many non-members as members, a high TPR@Low FPR signifies the ability to identify a substantial portion of training data while maintaining high precision and minimal false positives.

3 Threat Model

Despite the divergent data modalities and architectural configurations inherent to image classification models, graph neural networks, diffusion models, and LLMs, the privacy vulnerabilities they manifest exhibit a profound logical congruence.

3.1 Attacker's Objective

The quintessential objective of an attack is to exploit the marginal disparities in model behavior when processing seen versus unseen samples to infer sensitive privacy attributes. Adopting the notation established in Section 2.2, the attacker seeks to formulate an optimal inference function $\mathcal{A}$ capable of accurately discerning whether a target sample was present during the training phase. Formally, this necessitates the maximization of Balanced Accuracy, AUC, and TPR@Low FPR, while ensuring that computational overhead remains within a strictly defined threshold.

3.2 Attacker's Capabilities

The capabilities of an attacker are fundamentally predicated on their level of access to the target model and the extent of their available auxiliary information. We categorize these adversarial capabilities into the following three dimensions:

White-box / Black-box Access: In a white-box setting, the attacker possesses comprehensive knowledge of the model's internal states, including its architecture and backpropagated gradients. However, such transparency is seldom granted in practical deployment, particularly regarding commercial models served via APIs. Consequently, we focus on the black-box environment, which reflects the most common practical deployment setting. In this setting, the attacker has no access to the model architecture, internal states, or backpropagated gradients, but can query the model and observe its outputs, such as logits, softmax scores, or loss values. This assumption is well aligned with real-world commercial systems exposed via APIs [51, 80], where internal details are intentionally hidden, and has been widely adopted in prior work [6, 43, 73, 87].

Resource Constraints: Adversarial efficacy is further constrained by a query budget. For instance, in high-parameter LLMs or diffusion models, high-frequency querying is not only prohibitively expensive but also susceptible to detection by robust defense mechanisms. Thus, the attacker must reliably infer membership within a minimal number of queries.

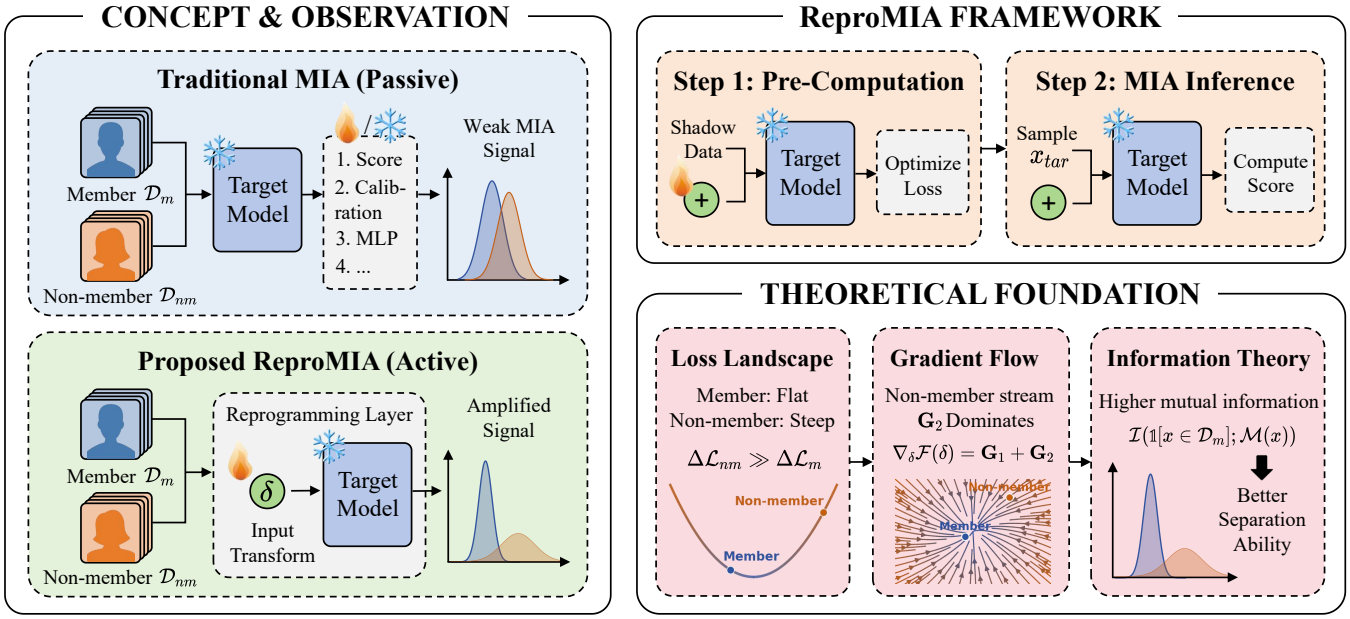

Figure 2: The overall framework of our ReproMIA, which includes the difference between it and the traditional MIA methods, and the process of our theoretical overview.

Auxiliary Knowledge: Auxiliary knowledge encompasses auxiliary datasets and the training of shadow and reference models. For classification models with lower computational costs, we grant them access to the full spectrum of auxiliary information. Regarding LLMs and large-scale diffusion models, the specific subsets of auxiliary knowledge available to them are explicitly delineated in the corresponding sections.

4 Theoretical Foundation

4.1 Overall Framework

Traditional MIA methodologies typically rely on the passive exploitation of behavioral discrepancies exhibited by the target model $\mathcal{M}_\theta$ when processing training versus non-training data. However, as contemporary deep learning architectures continue to scale in parameter volume, such marginal differences often become negligible, making it difficult to enhance adversarial performance.

To transcend these limitations, we introduce ReproMIA, a novel reprogramming-based MIA paradigm. Our fundamental insight posits that while the intrinsic signal variance of the original input sample x may be faint, we can leverage model reprogramming techniques to learn a specialized discriminative pattern δ in the pre-computation step. As illustrated in Figure 2, unlike traditional MIA that passively observes output statistics, our ReproMIA framework introduces an active probing mechanism. By freezing the target model $\mathcal{M}_\theta$ and optimizing an input-space transformation δ, we dynamically amplify the latent privacy footprints. During the MIA inference, injecting δ into the input space can guide the model to forcibly amplify the behavioral divergence between members and non-members.

Formally, we characterize ReproMIA as a bilevel optimization problem. Given a target model $\mathcal{M}_\theta$ and a shadow dataset $\mathcal{D}_{shadow} = \mathcal{D}^s_m \cup \mathcal{D}^s_{nm}$ denoting the member and non-member dataset, the objective is to identify the optimal reprogramming pattern δ^*:

$$\delta^* = \arg\max_{\delta \in \Omega} \mathbb{E}_{x \sim \mathcal{D}^s_m, z \sim \mathcal{D}^s_{nm}} \left[\Phi \left(\mathcal{M}_\theta(x \oplus \delta), \mathcal{M}_\theta(z \oplus \delta) \right) \right], \quad (3)$$

where $\oplus$ denotes the injection operator, encompassing additive perturbations, concatenations, or frame embeddings. Ω signifies the constrained perturbation manifold, and Φ represents the difference measurement function with $\Phi(a, b) = \phi(g(a) - g(b))$, where $g : \mathbb{R}^K \to \mathbb{R}$ is the scoring function, and $\phi : \mathbb{R} \to \mathbb{R}$ is monotonically increasing and differentiable.

The theoretical efficacy of ReproMIA is established through a three-stage progressive derivation: ❶ the Loss Landscape Curvature analysis, showing that members reside in locally flatter minima, making them more sensitive to reprogramming; ❷ the Gradient Flow Analysis, demonstrating that member samples induce larger and faster initial gradients during the optimization of δ; and ❸ an Information Theoretic Perspective, which quantifies the higher mutual information between member samples and the learned perturbation. They will be elaborated in Sections 4.3, 4.4 and 7.1, respectively.

By optimizing δ^* on a shadow model, we derive a generalized discriminative pattern. During the inference phase, for any arbitrary target sample x_{tar}, the attacker merely needs to query $\mathcal{M}_\theta(x_{tar} \oplus \delta^*)$ and evaluate the resulting score to achieve high-precision membership inference. In the Sections 5, 6, and C, we will detail the specific methodological designs tailored for LLMs, Diffusion Models, and Classification Models, respectively.

4.2 Core Hypothesis

Prior to delineating the specific instantiations of ReproMIA across various model architectures, we establish a unified theoretical foundation to explain why the learned reprogramming pattern δ^* fundamentally amplifies membership signals. The analysis proceeds from three complementary perspectives and culminates in a unified framework that subsumes all three instantiations, with empirical experiments that directly validate each theoretical claim.

Hypothesis 1. *Given a model $\mathcal{M}_\theta$ optimized on a dataset $\mathcal{D}_{train}$, the learned reprogramming pattern δ^* acts as an active diagnostic probe that selectively exploits the asymmetry in the model's loss landscape between member and non-member samples, formally characterized as:*

$$\mathbb{E}_{x_m \sim \mathcal{D}_m^s}\left[\phi(\mathcal{M}_\theta(x_m \oplus \delta^*))\right] \gg \mathbb{E}_{x_{nm} \sim \mathcal{D}_{nm}^s}\left[\phi(\mathcal{M}_\theta(x_{nm} \oplus \delta^*))\right], \tag{4}$$

with a substantially greater margin than when $\delta = 0$. We substantiate this hypothesis through the following theoretical discourse and a series of foundational experiments.

4.3 Loss Landscape Curvature

The intuition underlying model reprogramming can be elucidated through the geometric characteristics of the loss landscape. Within the framework of Empirical Risk Minimization, models optimized to convergence on $\mathcal{D}_m$ inevitably manifest varying degrees of overfitting, especially for high-capacity models. Geometrically, this phenomenon is characterized by a loss surface that is locally flatter around member samples x_m compared to the regions around non-member samples x_{nm}.

To formalize this observation, consider the second-order Taylor expansion of the loss function $\mathcal{L}$ with respect to the input x:

$$\mathcal{L}\left(\mathcal{M}_\theta(x+\delta)\right) \approx \mathcal{L}\left(\mathcal{M}_\theta(x)\right) + \nabla_x \mathcal{L}^\top \delta + \frac{1}{2}\delta^\top \mathbf{H}_x \delta, \tag{5}$$

where $\mathbf{H}_x = \nabla_x^2 \mathcal{L}(\mathcal{M}_\theta(x))$ denotes the input-space Hessian matrix of the loss function at point x. For a member x_m that has been memorized by the model, the model's output satisfies $p_y(x_m) \approx 1$, so the first-order gradient $\nabla_x \mathcal{L} = \mathbf{J}(x_m)^\top (p(x_m) - \mathbb{1}[k = y]_{k=1}^K) \approx 0$ is negligible, so the curvature term $\frac{1}{2}\delta^\top \mathbf{H}_{x_m} \delta$ becomes the dominant factor.

Consistent with classical overfitting theory [42, 63], the Hessian eigenvalues corresponding to overfitted samples x_m tend to be smaller, i.e., $\lambda_{\max}(\mathbf{H}_{x_m})$ is minimized. Intuitively, the model exhibits localized robustness toward small perturbations of training data. Conversely, for non-members x_{nm}, the absence of memorization effects results in a significantly more precipitous loss landscape, where the Hessian matrix exhibits ill-conditioned properties and substantially larger eigenvalues, such that $\lambda_{\max}(\mathbf{H}_{x_{nm}}) \gg \lambda_{\max}(\mathbf{H}_{x_m})$.

Proposition 1. *Let $\mathcal{M}_\theta$ be a model with an overfitting ratio $\rho = \mathcal{L}_{test}/\mathcal{L}_{train} > 1$. Under moderate regularity conditions of the loss function, the spectral gap between the Hessians of members and non-members satisfies:*

$$\mathbb{E}_{x_{nm}}\left[\lambda_{\max}(\mathbf{H}_{x_{nm}})\right] - \mathbb{E}_{x_m}\left[\lambda_{\max}(\mathbf{H}_{x_m})\right] \geq C(\rho - 1), \tag{6}$$

where $C > 0$ is a constant contingent upon the network architecture and the training distribution. This implies that upon the application of a reprogramming pattern δ, the resultant loss increment for non-members is markedly higher than that for members, thereby generating an observable signal that ReproMIA can exploit.

The pivotal advantage of learning δ instead of utilizing stochastic perturbations is that δ^* is directionally guided toward the subspace that maximally segregates these two populations, rather than relying on indiscriminate sampling within the input space.

The proof for Proposition 1 is in Appendix A.2.

Empirical Validation. We select different models to empirically substantiate the aforementioned proposition. Specifically, we select Mamba-1.4B [29], Pythia-6.9B [4], LLaMA-30B [79], OPT-66B [94] as target models, recording the loss discrepancies between members and non-members both with and without ReproMIA on the WikiMIA benchmark [73] with length of 128. A broadened loss gap under the influence of the reprogramming pattern serves as a direct observable consequence of a more pronounced spectral gap. As illustrated in Figure 3, the deployment of ReproMIA significantly amplifies the loss divergence between members and non-members. This enhancement remains consistent across different model architectures and varying parameter scales, thereby providing robust empirical validation for our theoretical conjecture.

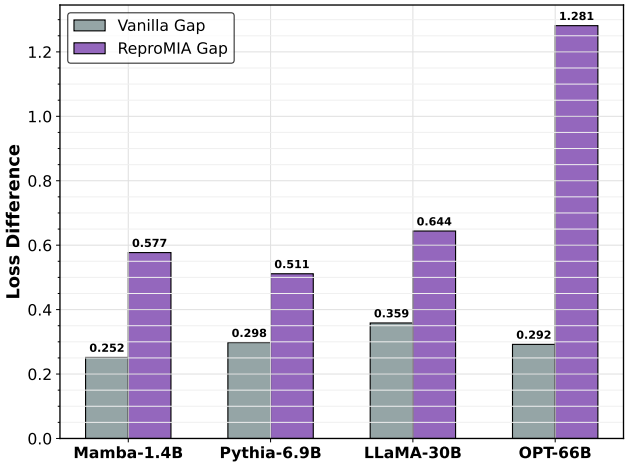

Figure 3: The loss difference with and without model reprogramming on different target models.

4.4 Gradient Flow Analysis

We now elucidate why the reprogramming objective function facilitates the generation of a well-behaved gradient signal, which subsequently yields a pattern δ^* that is optimally aligned with the membership-sensitive subspace. By decomposing the gradient into constituent member and non-member streams, we demonstrate that a significant magnitude discrepancy exists between these flows, thereby deriving a geometric interpretation for the directional efficacy of δ^*.

Let the reprogramming objective on the right-hand side of Equation (3) be denoted by $\mathcal{F}(\delta)$, and let $\Phi(a, b) = \phi_1(a) - \phi_2(b)$, where

ϕ_1 incentivizes high membership scores and ϕ_2 penalizes low non-member scores. By leveraging the linearity of expectation and the chain rule, the gradient can be decomposed as follows:

$$\nabla_\delta \mathcal{F}(\delta) = \underbrace{\mathbb{E}_{x_m}\left[\left(\frac{\partial \mathcal{M}_\theta(\tilde{x}_m)}{\partial \delta}\right)^\top \cdot \nabla_{o_m}\phi_1(o_m)\right]}_{\mathbf{G}_1 \text{ (member stream)}} - \underbrace{\mathbb{E}_{x_{nm}}\left[\left(\frac{\partial \mathcal{M}_\theta(\tilde{x}_{nm})}{\partial \delta}\right)^\top \cdot \nabla_{o_{nm}}\phi_2(o_{nm})\right]}_{\mathbf{G}_2 \text{ (non-member stream)}}, \tag{7}$$

where $\tilde{x} = x \oplus \delta$, while $o_m = \mathcal{M}_\theta(\tilde{x}_m)$ and $o_{nm} = \mathcal{M}_\theta(\tilde{x}_{nm})$.

Member Stream $\mathbf{G}_1$. In the case of an additive injection operator $\oplus$, the Jacobian matrix of the reprogramming pattern collapses into the model's input-space Jacobian:

$$\frac{\partial \mathcal{M}(\tilde{x}_m)}{\partial \delta} = \frac{\partial \mathcal{M}_\theta(x_m+\delta)}{\partial (x_m+\delta)}\frac{\partial (x_m+\delta)}{\partial \delta} = \mathbf{J}_x(\tilde{x}_m)\cdot \mathbf{I} = \mathbf{J}_x(\tilde{x}_m), \tag{8}$$

where $\mathbf{J}_x(\tilde{x}_m) \in \mathbb{R}^{K\times|\delta|}$ denotes the Jacobian of the model output evaluated at the reprogrammed input. As established in Proposition 1, a model that has memorized x_m exhibits a locally flat loss landscape at that coordinate. In expectation, this phenomenon manifests as a smaller Frobenius norm of the Jacobian, $\mathbb{E}_{x_m}[\|\mathbf{J}_x(\tilde{x}_m)\|_F]$. Consequently, during the gradient ascent process, $\mathbf{G}_1$ generates a mild yet consistent impetus, directionally nudging the pattern toward higher membership scores without precipitously reshaping the underlying loss surface.

Non-member Stream $\mathbf{G}_2$. In contrast, the Jacobian matrix for non-member samples satisfies:

$$\mathbb{E}_{x_{nm}}\left[\|\mathbf{J}_x(\tilde{x}_{nm})\|_F\right] > \mathbb{E}_{x_m}\left[\|\mathbf{J}_x(\tilde{x}_m)\|_F\right]. \tag{9}$$

In expectation, this relationship is strongly motivated by the spectral gap articulated in Proposition 1. The mathematical nexus between the input-space Hessian and the Jacobian is precisely established via the decomposition: $\mathbf{H}(x) = \mathbf{J}(x)^\top \mathbf{C}(p)\mathbf{J}(x) + \mathbf{R}(x)$ (see Appendix A.1), where $\mathbf{C}$ represents the curvature tensor of the output distribution and $\mathbf{R}(x)$ denotes the residual term. For non-member entities, the heightened eigenvalues of $\mathbf{H}(x_{nm})$ necessitate that $\mathbf{J}(\tilde{x}_{nm})$ possesses a substantially larger spectral norm in expectation. Consequently, the non-member stream $\mathbf{G}_2$ exerts a dominant influence over the total gradient $\nabla_\delta \mathcal{F}$, steering the direction of δ to induce maximal perturbation in non-member output distributions. The explanation can be found in Appendix A.3.

Geometric Interpretation of Gradient Direction. By factoring out the Jacobian matrices, we can reformulate the reprogramming objective gradient from Equation (7) as follows:

$$\nabla_\delta \mathcal{F}(\delta) = \mathbb{E}_{x_m}\left[\mathbf{J}(\tilde{x}_m)^\top w_m\right] - \mathbb{E}_{x_{nm}}\left[\mathbf{J}(\tilde{x}_{nm})^\top w_{nm}\right], \tag{10}$$

where $w_m = \nabla_{o_m}\phi_1 \in \mathbb{R}^K$ and $w_{nm} = \nabla_{o_{nm}}\phi_2 \in \mathbb{R}^K$ represent the vectors of localized score improvement within the output space.

The first term backpropagates w_m into the perturbation manifold via $\mathbf{J}^\top$, identifying input-space trajectories that marginally enhance member scores. Given that $\|\mathbf{J}(\tilde{x}_m)\|$ is inherently constrained by the model's localized flatness at training points, this term provides a stabilizing bias without exerting dominant influence. Conversely, the second term backpropagates w_{nm} through $\mathbf{J}(\tilde{x}_{nm})^\top$, identifying the specific directions in the perturbation space that most rapidly destabilize non-member outputs, subsequently subtracting them from the aggregate gradient. Since $\|\mathbf{J}(\tilde{x}_{nm})\|$ is significantly larger in magnitude, this term acts as the primary driving force, steering δ toward a configuration that exacerbates non-member uncertainty while maintaining the relative stability of member outputs.

Taken together, as the gradient of δ iterates, member samples maintain high-confidence and low-loss behavior under the influence of the reprogramming pattern, whereas non-member samples are systematically driven into high-entropy, high-loss regimes. This alignment with the fundamental objectives of MIA emerges autonomously from the bilevel optimization structure, necessitating no explicit architectural supervision.

Empirical Validation. Figure 4 provides compelling visual substantiation for the previous gradient flow analysis. Following the experimental setup of Section 4.3, on the LLaMA-30B architecture, the vanilla score distributions for members and non-members exhibit substantial overlap, complicating precise threshold selection. However, with the application of `ReproMIA`, the member distribution undergoes significant sharpening, while the non-member distribution markedly broadens, dramatically mitigating distributional overlap. Moreover, the variation of non-members is significantly larger than that of members, also providing an empirical validation of Proposition 2.

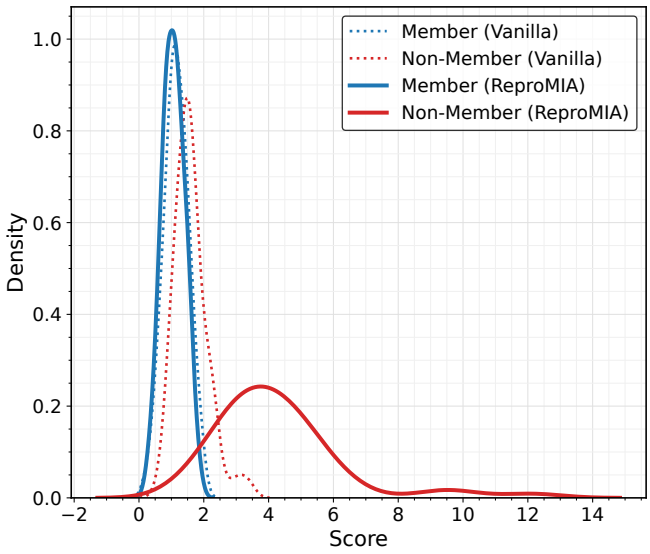

Figure 4: The separation scores with and without model reprogramming on LLaMA-30B.

5 `ReproMIA` for Large Language Models

5.1 Methodology

For LLMs, we instantiate the reprogramming paradigm as soft prompt tuning. Our core insight is that model memorization of training data is often latent within specific parameter subspaces. By optimizing a prefix prompt within a continuous embedding space,

Table 1: AUC and TPR@1%FPR results on WikiMIA benchmark. The best results are bolded, and the second best results are underlined.

Len.	Method	Mamba-1.4B		Pythia-6.9B		LLaMA-13B		NeoX-20B		LLaMA-30B		OPT-66B		Average	
		AUC	T@1%F	AUC	T1%F	AUC	T1%F	AUC	T1%F	AUC	T1%F	AUC	T1%F	AUC	T1%F
32	Loss	60.09	4.75	63.57	7.72	66.47	5.64	68.22	9.20	68.29	3.86	64.39	3.86	65.17	5.84
	Ref	61.86	0.59	61.98	1.48	66.23	0.30	68.39	7.42	62.08	0.59	62.08	0.59	63.77	1.83
	Zlib	61.21	3.86	63.89	4.75	66.77	5.93	68.32	8.61	68.71	4.75	68.71	4.75	66.27	5.44
	Neighbor	60.46	/	60.78	/	62.43	/	66.72	/	62.41	/	62.41	/	62.54	/
	Min-K%	62.87	7.12	66.37	9.20	66.79	6.53	70.93	10.39	68.87	7.12	68.87	3.86	67.45	7.37
	Min-K%++	66.21	4.45	71.12	7.12	84.52	12.17	75.32	6.53	84.13	9.20	82.50	8.61	77.30	8.01
	ReCaLL	88.05	11.57	86.64	19.29	88.08	14.54	86.03	17.80	88.55	10.98	78.28	6.82	85.94	13.50
	ReproMIA	**90.70**	**14.24**	**93.28**	**21.07**	**92.45**	**16.02**	**88.94**	**18.03**	**94.33**	**20.18**	**92.62**	**17.80**	**92.05**	**17.89**
64	Loss	56.98	2.40	61.62	1.92	64.17	3.85	66.56	4.81	66.12	5.29	66.12	5.29	63.60	3.93
	Ref	62.54	0.48	62.56	0.96	63.71	2.88	73.14	8.17	69.34	1.44	69.34	1.44	66.77	2.56
	Zlib	59.31	5.29	63.21	9.62	65.77	7.69	68.66	6.73	67.55	9.13	67.55	9.13	65.34	7.93
	Neighbor	58.62	/	60.60	/	62.32	/	66.67	/	62.09	/	62.09	/	62.07	/
	Min-K%	61.65	11.54	65.97	12.02	66.46	7.21	71.50	7.21	68.41	8.65	68.41	8.65	67.07	9.21
	Min-K%++	66.84	8.17	72.68	11.55	86.71	14.42	75.67	9.13	85.35	7.69	85.35	8.17	78.77	9.86
	ReCaLL	90.18	13.94	92.37	24.52	92.47	28.85	**90.87**	7.21	93.95	26.64	83.69	10.58	90.59	18.62
	ReproMIA	**90.38**	**16.83**	**95.56**	**36.06**	**94.17**	**37.70**	84.82	**10.58**	**95.20**	**35.10**	**93.14**	**16.83**	**92.21**	**25.52**
128	Loss	63.19	1.23	60.83	3.28	66.73	9.86	66.64	4.92	72.13	8.20	65.49	3.28	65.84	5.13
	Ref	66.45	3.70	56.29	0.00	63.26	0.98	75.77	0.00	72.21	0.00	68.93	4.92	67.15	1.60
	Zlib	66.70	9.88	61.65	6.56	69.29	15.49	67.37	4.92	73.85	16.39	67.00	6.56	67.64	9.97
	Neighbor	62.20	/	55.55	/	64.21	/	67.00	/	67.65	/	63.45	/	63.34	/
	Min-K%	66.16	6.17	63.69	8.20	70.98	14.08	71.30	3.28	76.24	9.84	70.71	3.28	69.85	7.48
	Min-K%++	68.71	2.47	64.15	8.20	84.33	12.68	75.40	1.64	72.61	8.20	71.85	8.20	72.84	6.90
	ReCaLL	87.58	19.67	86.94	26.23	90.67	19.67	87.85	**19.67**	90.08	18.03	73.26	6.56	86.06	18.31
	ReproMIA	**89.60**	**36.07**	**96.96**	**49.18**	**94.60**	**49.18**	**90.22**	**19.67**	**98.84**	**59.02**	**94.28**	**21.31**	**94.08**	**39.07**

we can effectively create a trigger that directionally awakens the model's overfitted memory of member data while simultaneously inducing significant interference for non-member samples.

Given an input token sequence $T = [t_1, t_2, \ldots, t_N]$ and its corresponding embedding sequence $\mathbf{E} \in \mathbb{R}^{N \times d}$, where N denotes the sequence length and d represents the hidden dimension, we introduce a learnable soft prompt $\mathbf{P} \in \mathbb{R}^{L \times d}$ with prompt length L. We concatenate $\mathbf{P}$ and $\mathbf{E}$ along the sequence dimension to serve as the model input:

$$\mathbf{H}_0 = [\mathbf{P}; \mathbf{E}] \in \mathbb{R}^{(L+N) \times d}. \tag{11}$$

This soft prompt allows us to navigate the continuous gradient manifold to identify the optimal solution, capturing feature directions that are acutely sensitive to the model's internal memorization. While model architecture and scale may cause the optimal length L to fluctuate, the difference is so slight that a fixed L can be used to achieve optimal results.

Traditional MIA typically focus on the overall sequence perplexity; however, this metric is frequently dominated by high-frequency tokens, thereby obscuring the memory signals of specific long-tail content [87, 93]. Inspired by anomaly detection in statistics, we designed a self-calibrated tail-probability amplification mechanism as the primary driver of our optimization. The crux of distinguishing members from non-members lies in the most difficult tokens within a sequence. For non-members, these tokens exhibit extremely low probabilities; conversely, due to overfitting, the model assigns anomalously high confidence to these inherently low-probability tokens [73].

To eliminate inherent bias stemming from the model's internal distribution, we design the self-calibration mechanism based on vocabulary statistics. For the i-th token t_i, we compute not only the raw log-likelihood $\log p(t_i|h_{<i})$ but also the mean μ_i and standard deviation σ_i across the entire vocabulary $\mathcal{V}$ for the current context:

$$\begin{aligned} \mu_i &= \mathbb{E}_{v \in \mathcal{V}} \left[\log p\left(v \mid h_{<i}\right) \right] \\ \sigma_i &= \sqrt{\mathrm{Var}_{v \in \mathcal{V}} \left[\log p\left(v \mid h_{<i}\right) \right]} \end{aligned}. \tag{12}$$

We define the calibrated score in the form of a z-score:

$$z(t_i) = \frac{\log p(t_i|h_{<i}) - \mu_i}{\sigma_i}. \tag{13}$$

This approach dynamically standardizes the prediction difficulty at each position, rendering scores strictly comparable across different samples. Furthermore, rather than averaging across all tokens, we employ a Top-K% selection [73] to isolate the $K\%$ of tokens with the lowest $z(t_i)$ values. Let Ω_k denote this set of indices; the calibrated score for the sequence is defined as:

$$\mathcal{S}(x) = \frac{1}{|\Omega_k|} \sum_{j \in \Omega_k} z(t_j). \tag{14}$$

To effectively steer the LLM's output for membership distinction, we optimize the soft prompt $\mathbf{P}$ by maximizing the discrepancy between member and non-member scores. However, a naive global mean divergence tends to ignore boundary samples. To address this,

Table 2: AUC results on MIMIR benchmark. The best results are bolded, and the second best results are underlined.

Method	Wikipedia					Github					Pile CC					PubMed Central				
	160M	1.4B	2.8B	6.9B	12B	160M	1.4B	2.8B	6.9B	12B	160M	1.4B	2.8B	6.9B	12B	160M	1.4B	2.8B	6.9B	12B
Loss	51.2	51.0	51.7	52.7	53.0	65.2	69.6	70.8	72.6	73.6	49.5	50.1	50.3	50.6	51.2	49.8	49.9	50.0	50.6	51.3
Ref	**51.9**	52.6	52.5	54.1	54.9	63.5	65.6	66.4	67.2	67.7	49.9	50.3	50.7	**51.9**	**52.3**	48.5	49.5	49.7	51.1	51.5
Zlib	51.0	51.8	52.3	53.4	54.0	**67.2**	**70.9**	**72.0**	72.7	**74.6**	49.7	50.3	50.4	50.8	51.2	49.9	50.1	50.2	50.6	51.2
Neighbor	50.2	51.1	51.7	53.5	54.1	67.1	70.3	71.1	72.7	73.5	47.8	48.7	49.6	50.1	50.6	49.2	50.2	50.4	50.9	51.5
Min-K%	48.9	50.7	51.4	53.0	53.8	65.0	69.8	71.0	**72.8**	73.9	**50.2**	50.0	50.7	51.3	51.7	50.3	50.6	50.7	51.3	52.4
Min-K%++	49.3	52.9	53.7	**56.1**	55.6	65.1	69.5	70.5	72.4	73.8	50.1	50.2	49.9	51.3	52.0	**50.3**	51.1	51.0	52.8	53.2
ReCaLL	51.4	52.4	52.6	53.9	54.5	65.3	69.0	71.3	72.2	74.8	48.3	49.5	50.3	50.4	50.9	48.7	50.0	49.1	50.4	51.3
ReproMIA	49.3	**53.5**	**53.9**	55.8	**57.9**	65.1	66.5	69.1	71.9	74.3	50.1	**51.0**	**51.4**	51.5	52.1	**50.3**	**52.3**	**53.3**	**54.1**	**54.0**
Method	Arxiv					DM Mathematics					HackerNews					Average				
	160M	1.4B	2.8B	6.9B	12B	160M	1.4B	2.8B	6.9B	12B	160M	1.4B	2.8B	6.9B	12B	160M	1.4B	2.8B	6.9B	12B
Loss	50.5	51.5	52.4	53.4	53.9	49.3	48.9	48.8	48.9	48.8	49.8	50.3	51.0	51.8	52.6	39.0	45.7	37.7	43.5	45.0
Ref	50.2	51.0	52.6	52.4	54.3	48.5	48.6	48.4	48.8	48.8	43.2	50.9	53.0	54.2	54.6	37.6	47.5	40.7	48.2	48.0
Zlib	50.4	50.9	51.6	52.6	53.0	48.0	48.3	47.8	47.9	47.8	49.6	49.9	50.4	50.6	51.2	53.7	53.6	54.4	53.8	53.9
Neighbor	50.5	50.9	51.8	51.9	53.2	49.1	49.0	49.1	49.2	48.4	48.3	50.4	51.1	51.8	52.5	38.1	47.8	40.7	46.8	47.8
Min-K%	50.8	51.3	52.7	53.8	54.6	**49.7**	49.6	49.5	49.6	49.6	50.8	50.8	52.0	53.3	54.3	39.6	48.4	40.3	49.8	48.6
Min-K%++	51.0	50.8	53.1	54.0	55.9	49.7	50.4	50.9	50.6	50.3	50.1	51.1	52.4	53.8	54.6	44.1	57.5	48.5	53.4	50.8
ReCaLL	**52.7**	52.5	52.9	54.7	**56.2**	49.5	50.0	49.4	49.3	49.0	**51.5**	51.8	**53.4**	54.2	55.0	**50.2**	60.8	57.1	62.4	60.7
ReproMIA	51.0	**53.5**	**53.3**	**55.3**	55.3	49.7	**51.7**	**53.2**	**52.8**	**51.2**	50.1	**52.2**	53.0	**54.6**	**56.3**	50.3	**52.5**	**53.2**	**54.2**	**54.2**

Table 3: TPR@1%FPR results on MIMIR benchmark. The best results are bolded, and the second best results are underlined.

Method	Wikipedia					Github					Pile CC					PubMed Central				
	160M	1.4B	2.8B	6.9B	12B	160M	1.4B	2.8B	6.9B	12B	160M	1.4B	2.8B	6.9B	12B	160M	1.4B	2.8B	6.9B	12B
Loss	0.7	0.8	0.6	0.7	1.0	15.7	19.6	22.2	22.6	23.1	0.7	0.5	0.8	0.8	0.8	0.8	0.8	0.7	0.8	0.4
Ref	**1.2**	0.7	**0.8**	1.0	1.4	13.8	10.8	10.4	14.0	14.8	**0.9**	0.7	0.9	1.2	**1.4**	0.4	0.9	0.8	0.9	0.9
Zlib	0.9	0.7	0.7	0.9	1.0	**17.3**	**22.8**	**24.0**	**26.0**	**25.8**	0.5	0.6	0.9	1.1	1.1	0.5	0.5	0.3	0.6	0.5
Min-K%	1.1	0.8	0.6	0.8	1.0	15.2	20.1	21.6	22.8	23.1	0.6	0.6	0.7	0.7	0.9	0.7	0.4	0.6	0.6	0.7
Min-K%++	0.8	1.1	0.6	1.2	1.1	15.0	18.1	18.8	21.0	23.2	0.5	0.6	1.0	1.2	1.3	0.7	0.6	0.9	1.1	1.3
ReCaLL	1.2	0.7	0.6	0.8	1.1	11.4	18.0	20.7	18.5	22.3	0.6	0.4	0.5	0.6	0.7	**0.8**	1.0	0.3	1.1	0.4
ReproMIA	0.8	**1.3**	**0.8**	**1.8**	**1.9**	15.0	19.4	19.1	23.2	23.8	0.5	**0.8**	**1.7**	**1.4**	1.4	0.7	**1.7**	**1.4**	**1.8**	**1.9**
Method	Arxiv					DM Mathematics					HackerNews					Average				
	160M	1.4B	2.8B	6.9B	12B	160M	1.4B	2.8B	6.9B	12B	160M	1.4B	2.8B	6.9B	12B	160M	1.4B	2.8B	6.9B	12B
Loss	0.5	0.4	0.6	0.7	1.1	0.7	0.6	1.1	1.2	1.2	0.9	0.6	0.6	0.8	0.8	0.7	0.6	0.8	0.9	1.0
Ref	**1.1**	1.7	1.7	1.6	1.9	0.8	0.9	0.8	0.8	0.8	1.5	1.2	1.2	1.2	1.2	1.1	1.3	1.3	1.2	1.3
Zlib	0.6	0.3	0.4	0.4	0.7	**1.2**	0.7	1.0	1.0	1.0	1.0	0.9	1.0	1.3	1.2	**0.9**	0.7	0.8	0.9	1.0
Min-K%	0.5	0.4	0.5	0.5	1.0	0.8	0.4	0.2	0.4	0.4	1.3	0.8	0.7	0.9	0.9	0.9	0.6	0.5	0.6	0.8
Min-K%++	0.9	1.3	1.5	1.3	1.7	0.7	0.8	1.1	0.7	1.0	0.9	0.4	1.0	1.3	0.8	0.9	0.8	1.2	1.1	1.2
ReCaLL	0.3	0.8	0.8	1.0	2.6	0.3	0.2	0.3	0.3	0.2	**1.8**	1.9	1.5	2.0	0.8	0.8	1.0	0.9	1.1	1.2
ReproMIA	0.9	**2.0**	**2.4**	**1.6**	**2.7**	0.7	**1.6**	**1.4**	**1.7**	**1.2**	0.9	**2.0**	**1.7**	**2.0**	**1.6**	0.9	**1.9**	**1.9**	**1.8**	**1.8**

we introduce a hard example mining strategy into $\mathcal{L}_{\text{LLM}}$. Specifically, we rank the scores within a batch of members $\mathcal{D}_m$ and non-members $\mathcal{D}_{nm}$, and define hard member set $\mathcal{H}_m$ as the k-percentile of members with the lowest scores, and the hard non-member set $\mathcal{H}_{nm}$ as the k-percentile of non-members with the highest scores. The final loss of ReproMIA for LLM is formulated as:

$$\mathcal{L}_{\text{LLM}} = \mathbb{E}_{x\in\mathcal{H}_m, z\in\mathcal{H}_{nm}} \left[\text{softplus}\left(\log S(z) - \log S(x) + \gamma\right)\right]. \quad (15)$$

Through this loss function, the soft prompt $\mathbf{P}$ learns a specific activation pattern that resonates with the embeddings of member data. It increases the certainty of long-tail token predictions, and disrupts the contextual coherence of non-member data, thereby exacerbating the entropy of its long-tail predictions.

With the learned $\mathbf{P}$, to determine the membership of a sample, we just need to append $\mathbf{P}$ and derive its score and compare with the predefined threshold.

5.2 Experimental Setup

5.2.1 Datasets. To rigorously validate the performance of ReproMIA, we selected two prominent benchmarks: WikiMIA [73] and MIMIR [18]. WikiMIA comprises textual corpora harvested from Wikipedia, partitioned into four distinct subsets based on fixed sequence lengths

of 32, 64, 128, and 256 tokens. The ground-truth membership status of each sample is determined by the temporal alignment with the model's knowledge cutoff. MIMIR is derived from The Pile [26] dataset and utilizes n-gram filtering to curate member and non-member samples from the same underlying distribution, so it is more difficult compared to WikiMIA.

5.2.2 Models. For the evaluation on the WikiMIA benchmark, we conducted experiments across a diverse array of Transformer-based [82] LLMs, including Pythia-6.9B [4], LLaMA-13B [79], GPT-NeoX-20B [5], LLaMA-30B [79], and OPT-66B [94]. We also include the new state-space model architecture Mamba-1.4B [29]. Regarding the MIMIR benchmark, and consistent with [18, 93], our analysis focused on the Pythia model family, spanning a broad spectrum of parameter scales: 160M, 1.4B, 2.8B, 6.9B, and 12B. For baseline methodologies necessitated by a reference model, we follow [73, 93] by utilizing a smaller version of the target architecture as the reference model.

5.2.3 Baselines. To validate the performance of ReproMIA, we evaluate it against 7 state-of-the-art baseline methods. Loss [90] employs the raw cross-entropy loss as the primary discriminative feature, predicated on the principle that perplexity in LLMs serves as a robust proxy for the occurrence of training data. Ref [8] incorporates a reference model to calibrate the likelihood of the sample. Zlib [8] utilizes Zlib compression as reference signals for statistical normalization. Neighbor [59] generates perturbed variants of the input to construct a local neighborhood, utilizing the mean loss across these neighbors to calibrate the target sample's loss. Min-K% [73] computes the average log-likelihood of the $K\%$ tokens with the lowest probabilities to discern membership. This was further refined by Min-K%++ [93], which standardizes these values using the mean and standard deviation. ReCaLL [87] exploits relative variations in conditional log-likelihood, assessing membership by the score degradation observed when the target text is prepended with a non-member prefix.

5.3 Evaluations

5.3.1 MIA Performance. We conducted extensive evaluations on LLMs to substantiate the superiority of ReproMIA. Table 1 presents a comparative analysis of ReproMIA against various state-of-the-art baselines using the WikiMIA dataset. The results consistently show that ReproMIA significantly outperforms all baselines, particularly in terms of AUC and TPR@1%FPR. Specifically, at sequence lengths of 32, 64, and 128 tokens, ReproMIA exceeds the runner-up method, ReCaLL, by 6.12%, 1.62%, and 8.02% in AUC, and by 4.39%, 6.89%, and 20.77% in TPR@1%FPR, respectively. Furthermore, the efficacy of ReproMIA transcends diverse architectures and parameter scales. Notably, performance gains tend to scale positively with model size, underscoring the practical viability of ReproMIA for massive commercial models in real-world scenarios.

On the more formidable MIMIR benchmark, ReproMIA maintains its robust performance edge. It is imperative to note that the MIMIR dataset presents a substantially more rigorous challenge, as it deliberately deviates from the standard MIA setting by minimizing the distributional shift between member and non-member samples. This proximity renders most existing MIA approaches nearly indistinguishable from random guessing, highlighting the profound similarity between the two cohorts. Notwithstanding these challenges, Tables 2 and 3 illustrate the comparative AUC and TPR@1%FPR metrics, where ReproMIA achieves state-of-the-art results under most circumstances. With the exception of the Github subset, ReproMIA secures the highest performance across all other data distributions. Across varying model scales of 1.4B, 2.8B, 6.9B, and 12B parameters, our method yields an average AUC improvement over the runner-up Zlib baseline of 0.79%, 1.16%, 1.53%, and 1.33%, respectively, while enhancing TPR@1%FPR by 0.84%, 0.52%, 1.32%, and 0.87%. Given the inherent difficulty and near-random baseline performance characteristic of the MIMIR benchmark, these incremental numerical gains represent a statistically significant and substantial advancement in detection capability.

For more experimental results, including ablation studies of prompt length, and parameter analysis of shadow sample number and Min-K% ratio, please refer to Appendix D.1.

Table 4: MIA robustness under logits perturbation defense of different levels.

Noise	Mamba		LLaMA-13B		LLaMA-30B		OPT	
Scale	AUC	T1%F	AUC	T1%F	AUC	T1%F	AUC	T1%F
Clean	89.60	36.07	94.60	49.18	98.84	59.02	94.08	21.31
0.1	90.35	31.15	93.15	37.70	94.95	47.54	93.93	19.67
0.5	90.81	37.70	94.71	54.10	97.61	60.66	94.36	24.59
1.0	86.16	14.75	91.75	36.07	96.91	40.98	98.27	39.34
1.5	87.88	21.31	91.99	27.87	95.89	55.74	96.68	29.51
2.0	86.78	9.84	89.63	24.59	94.30	45.90	88.91	24.59
2.5	78.72	4.92	79.01	19.67	90.94	29.51	89.67	19.67

5.3.2 Robustness against Defenses. A proficient MIA must remain robust against potential defensive countermeasures. To evaluate ReproMIA's resilience, we conducted robustness stress tests across 4 target models using the WikiMIA dataset with length 128. Specifically, we subjected the model outputs to stochastic perturbations with varying standard deviations to assess whether ReproMIA could sustain its superior MIA efficacy under such conditions.

Table 4 delineates the AUC and TPR@1%FPR metrics across the target models following the injection of these multi-level perturbations. It is observable that while an increase in the perturbation standard deviation precipitates a non-negligible decay in both AUC and TPR@1%FPR, ReproMIA preserves a commendable level of attack performance even at a substantial noise threshold of std=2.0. These results empirically substantiate the fortified robustness of our approach.

6 ReproMIA for Diffusion Models

6.1 Methodology

DDPMs [36] are generative frameworks that utilize a two-stage stochastic process. In the forward phase, an image $\boldsymbol{x}_0$ is systematically transformed into Gaussian noise through a fixed Markov chain, where noise is injected at each timestep t according to:

$$q(\boldsymbol{x}_t|\boldsymbol{x}_{t-1}) = \mathcal{N}\left(\sqrt{1-\beta_t}\boldsymbol{x}_{t-1}, \beta_t\mathbf{I}\right). \tag{16}$$

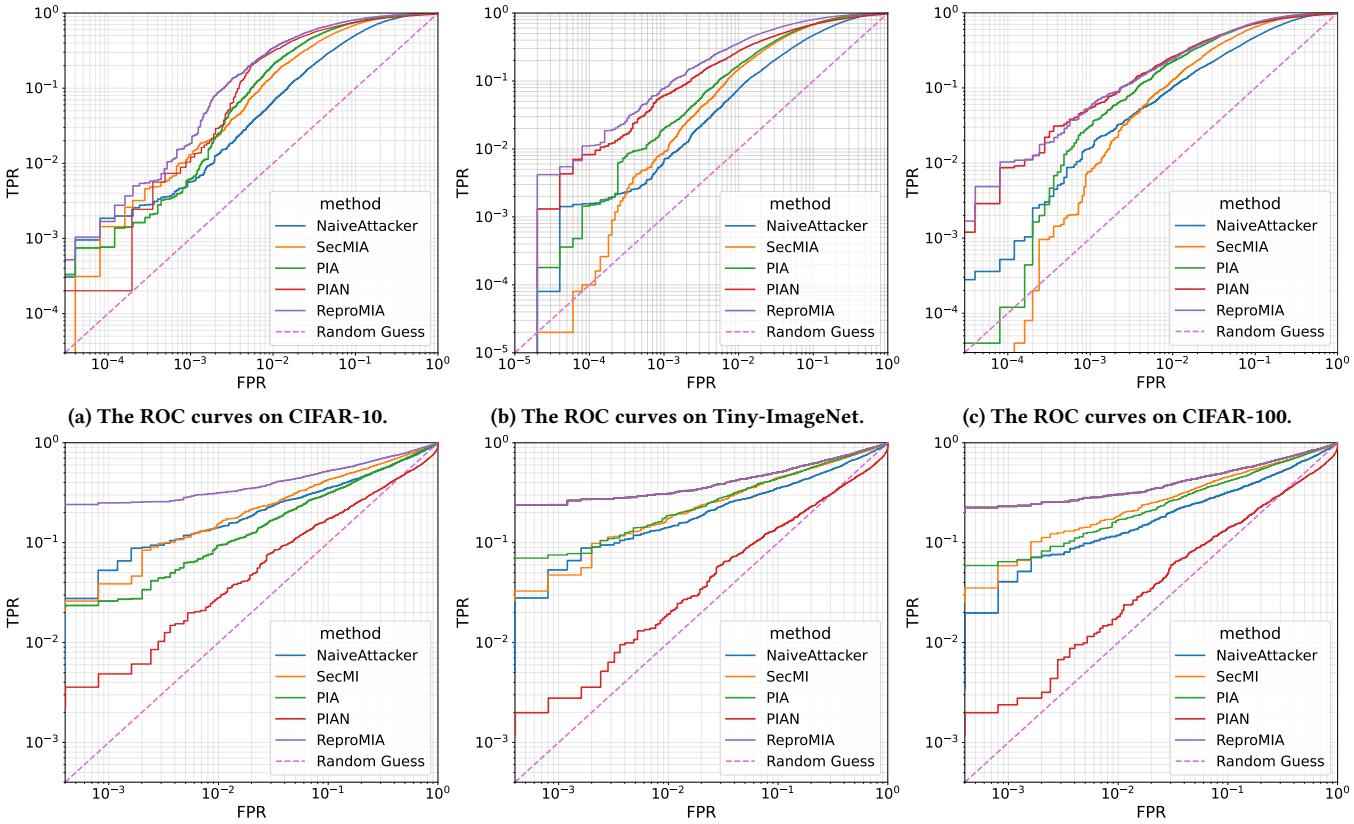

(a) The ROC curves on CIFAR-10.

(b) The ROC curves on Tiny-ImageNet.

(c) The ROC curves on CIFAR-100.

(d) The ROC curves on LAION-5B.

(e) The ROC curves on LAION-5B w/o text.

(f) The ROC curves on LAION-5B Blip text.

Figure 5: The log-scaled ROC curves of different methods on different datasets.

The reverse process trains a model to reconstruct the original data by predicting and removing this noise. This is achieved by learning the transition $p_\theta(\boldsymbol{x}_{t-1}|\boldsymbol{x}_t)$, optimized via a simplified loss function $\mathcal{L}_{\text{simple}}$ that minimizes the error between the added noise and the model's prediction:

$$\mathcal{L}_{\text{simple}} = \mathbb{E}_{\mathbf{x}_0,\epsilon\sim\mathcal{N}(\mathbf{0},\mathbf{I})}\left[\|\epsilon - \epsilon_\theta(\boldsymbol{x}_t, t)\|^2\right] \tag{17}$$

To address the high computational cost of sampling, methods like DDIM [15, 76, 86] enable faster inference by traversing the diffusion trajectory more efficiently without retraining.

For diffusion models, ReproMIA leverages the trajectory determinism of the generative process to propose a MIA framework predicated on proximal initialization [43]. The fundamental insight resides in the observation that diffusion models exhibit a significantly higher manifold adsorption force toward training data. If the reverse generation process is initiated from a deterministic intermediate state, member data tends to regress precisely along a defined trajectory, whereas non-member data is prone to significant trajectory deviation.

In ReproMIA, we utilize reprogramming to learn a specialized initial perturbation pattern δ, which is added onto the input image x_0 to construct a perturbed starting point. As demonstrated by Kong et al. [43], within the DDIM [76] framework, the entire deterministic trajectory can be uniquely identified if the original sample x_0 and any point x_k along the trajectory are known. Consequently, rather than initiating the process from the final timestep T, we calculate the noise estimate $\epsilon_\theta(x_0)$ at $t = 0$ and utilize this as the foundation for constructing proximal noise.

Formally, we define the reprogrammed input as $\tilde{x} = \text{clamp}(x + \delta, 0, 1)$. Drawing upon the principles of DDIM Inversion, we derive the state x_t at timestep t via a single-step forward formulation:

$$x_t(\tilde{x}) = \sqrt{\bar{\alpha}_t}\tilde{x} + \sqrt{1-\bar{\alpha}_t}\epsilon_\theta(\tilde{x}, 0). \tag{18}$$

By substituting random sampling with the predicted noise $\epsilon_\theta(\tilde{x}, 0)$ at $t = 0$, we ensure that the trajectory's origin is entirely deterministic and situated in close proximity to the data manifold.

To quantify membership, we measure the reconstruction error incurred when attempting to recover x_0 from x_t. We define the reconstruction discrepancy as the norm of the difference between the model's predicted noise at timestep t and the initial noise:

$$\mathcal{E}(\tilde{x}, \delta) = \|\epsilon_\theta(x_t(\tilde{x}), t) - \epsilon_\theta(\tilde{x}, 0)\|_p. \tag{19}$$

The value of $\epsilon_\theta(\tilde{x}, 0)$ may not conform to a standard normal distribution, so we use the following equation to normalize them:

$$\hat{\epsilon}_\theta(\tilde{x}, 0) = \frac{\epsilon_\theta(\tilde{x}, 0)}{\mathbb{E}_{x\sim\mathcal{N}(0,1)}(|x|)\frac{\|\epsilon_\theta(\tilde{x},0)\|_1}{N}} = N\sqrt{\frac{2}{\pi}}\frac{\epsilon_\theta(\tilde{x}, 0)}{\|\epsilon_\theta(\tilde{x}, 0)\|_1}, \tag{20}$$

where N represents the number of elements in the sample. We replace $\epsilon_\theta(\tilde{x}, 0)$ in Equation (19) with $\hat{\epsilon}_\theta(\tilde{x}, 0)$.

Our objective is to optimize δ such that the perturbation acts as a diagnostic probe: for member data, the model's familiarity with the underlying distribution ensures that the denoising process remains robust to δ, resulting in a minimal $\mathcal{E}$. Conversely, for non-member data, the effect of δ is amplified, causing the model's predicted noise direction at timestep t to deviate substantially from the initial direction at $t = 0$. To this end, we formulate the following trajectory deviation loss to train δ:

$$\mathcal{L}_{\text{Diff}} = \text{softplus}(\log(\mathcal{E}(x_m, \delta)) - \log(\mathcal{E}(x_{nm}, \delta)) + \eta) + \lambda \|\delta\|_2. \quad (21)$$

By minimizing this objective over the shadow dataset, ReproMIA identifies vulnerability points on the diffusion manifold. These points are inherently unstable for unseen non-member data, thereby significantly magnifying the membership inference signal for superior attack performance.

With the learned pattern δ^*, to determine the membership of a sample x, we add δ^* to the sample and derive its score $\mathcal{E}(\tilde{x}, \delta^*)$ and compare with the predefined threshold.

6.2 Experimental Setup

6.2.1 Datasets and Models. For our evaluation of diffusion models, we selected CIFAR-10 [44], TinyImageNet [13], CIFAR-100 [44], LAION-5B [68], and COCO [52] as the benchmark datasets, following the experimental setups established in [16]. TinyImageNet serves as a compact subset of the ImageNet corpus, comprising 200 distinct categories with 500 training images and 50 validation images per class, all rendered at a 64×64 resolution. LAION-5B represents a massive-scale collection of approximately 5.8 billion image-text pairs harvested from the web. COCO constitutes a high-fidelity dataset featuring roughly 330,000 real-world images spanning 80 object categories.

We adopted DDPM [36] and Stable Diffusion [66] as the target models. Specifically, DDPM was paired with the CIFAR-10/100 and TinyImageNet datasets, while Stable Diffusion was paired with LAION-5B and COCO. To ensure empirical consistency and reproducibility, all configurations regarding dataset partitioning, model training paradigms, and the selection of diffusion timesteps were strictly aligned with the settings prescribed by [43].

6.2.2 Baselines. We evaluate the performance of ReproMIA in comparison to three SOTA baselines. Naive Attacker [58] utilizes the noise estimation error as a proxy for the sample's loss value, then applying a threshold-based decision criterion to determine membership status. SecMI [17] exploits step-wise error discrepancies, identifing members by analyzing the variance in posterior estimation errors between the training set and the non-member population during the denoising process. PIA/PIAN [43] introduces a proximal initialization paradigm to streamline the query procedure, achieving high-precision adversarial inference with only two queries.

6.3 Evaluations

6.3.1 MIA Performance. We conducted a comprehensive series of experiments on diffusion models to substantiate the superior attack efficacy of ReproMIA. Table 5 delineates the comparative performance of ReproMIA against established baselines for MIA targeting DDPMs across diverse datasets. The results indicate that ReproMIA consistently outperforms all baseline methodologies by a substantial margin. On average, it exceeds the runner-up PIAN by 4.07% in AUC and 5.40% in TPR@1%FPR. Notably, our framework requires only two queries to the target model, demonstrating that ReproMIA achieves significantly enhanced MIA performance while remaining highly query-efficient.

Table 5: AUC and TPR@1%FPR results of different methods on DDPM. The best results are bolded, and the second best results are underlined.

Method	CIFAR-10		T-ImageNet		CIFAR-100		Query
	AUC	T1%F	AUC	T1%F	AUC	T1%F	
NA	78.52	6.60	81.97	7.56	77.85	10.47	1
SecMI	87.77	15.59	86.12	14.88	83.48	13.05	10+2
PIA	87.11	20.19	89.00	16.91	85.30	19.84	1+1
PIAN	88.34	31.09	89.55	28.57	87.77	22.08	1+1
ReproMIA	**92.83**	**34.14**	**94.05**	**37.71**	**91.00**	**26.10**	1+1

Table 6: AUC and TPR@1%FPR results of different methods on Stable Diffusion. L-5B w/o t. and L-5B Blip t. represent LAION-5B w/o text and LAION-5B with Blip text, respectively. The best results are bolded, and the second best results are underlined.

Method	LAION-5B		L-5B w/o t.		L-5B Blip t.		Query
	AUC	T1%F	AUC	T1%F	AUC	T1%F	
NA	69.62	15.36	66.16	14.12	69.26	12.84	1
SecMI	71.68	16.84	72.22	19.61	73.30	19.27	10+2
PIA	67.62	9.44	72.52	17.76	71.12	17.42	1+1
PIAN	55.74	2.80	56.84	1.98	54.30	1.88	1+1
ReproMIA	**76.16**	**31.52**	**76.07**	**30.96**	**76.08**	**30.44**	1+1

Furthermore, we evaluated the vulnerability of Stable Diffusion as a target architecture, with the corresponding results summarized in Table 6. ReproMIA continues to exhibit superior performance metrics, surpassing the runner-up SecMI by an average of 3.70% in AUC and a remarkable 12.40% in TPR@1%FPR, all while maintaining its characteristic query efficiency. These findings underscore the generalizability and dataset agnosticism of our ReproMIA.

To provide further visual evidence of this superiority, we present the ROC curves for various MIA baselines across the six datasets, with DDPM and Stable Diffusion as target models in Figure 5.

6.3.2 Robustness against Defenses. Table 7 shows the ReproMIA's robustness against various defenses, specifically DP-SGD [1] and input smoothing. The results indicate that ReproMIA sustains high MIA efficacy even under strict privacy constricts of DP-SGD. Interestingly, low-level input smoothing slightly improves performance, suggesting that moderate noise acts as a regularizer that refines ReproMIA's ability to distinguish membership distributions.

Table 7: MIA performance of ReproMIA under defenses.

Defense	CIFAR-10		T-ImageNet		CIFAR-100	
	AUC	T1%F	AUC	T1%F	AUC	T1%F
No defense	92.83	34.14	94.05	37.71	91.00	26.10
DP-SGD(0.2)	91.80	27.18	89.59	31.88	90.69	25.92
DP-SGD(0.5)	91.51	25.93	87.76	27.04	90.41	25.64
DP-SGD(0.8)	91.50	24.18	84.74	23.90	90.11	25.01
DP-SGD(1.1)	91.40	23.64	79.93	17.47	89.89	24.25
Smooth (0.3)	93.92	34.53	94.88	38.18	92.72	32.13
Smooth (0.5)	92.89	34.30	94.12	38.02	91.23	29.97
Smooth (0.7)	91.67	28.30	93.59	36.95	90.78	27.46
Smooth (0.8)	90.10	24.03	92.94	32.52	90.04	25.20
Smooth (0.9)	86.34	20.59	89.86	26.86	88.96	22.48

7 Discussion

7.1 An Information-Theoretic Perspective

We can further elucidate the advantages of model reprogramming through the lens of mutual information. The fundamental objective of a MIA is to maximize $\mathcal{I}(\text{membership}; \text{observation})$, where $\mathcal{I}$ denotes the mutual information and the observation encompasses all signals accessible to the attacker from the target model $\mathcal{M}_\theta$.In the absence of model reprogramming, the raw observation for a sample x is simply $\mathcal{M}_\theta(x)$, where its membership information is inherently constrained by the model's natural generalization gap, defined as $\mathcal{I}_0 = \mathcal{I}(\mathbb{1}[x \in \mathcal{D}_m]; \mathcal{M}_\theta(x))$. Upon ReproMIA, the observation shifts to $\mathcal{M}_\theta(x \oplus \delta^*)$, with the corresponding mutual information denoted as $\mathcal{I}_{\delta^*} = \mathcal{I}(\mathbb{1}[x \in \mathcal{D}_m]; \mathcal{M}_\theta(x \oplus \delta^*))$.

Proposition 2. *For a pattern δ^* optimized via Equation (3), under some conditions of the score model Φ, we have:*

$$\mathcal{I}_{\delta^*} \geq \mathcal{I}_0, \tag{22}$$

with strict inequality whenever the model exhibits any degree of memorization, characterized by an overfitting ratio $\rho > 1$.

The intuition behind this proposition is straightforward: $\mathcal{M}_\theta(x \oplus \delta^*)$ represents an engineered variant of the raw observation, where the transformation $x \mapsto x \oplus \delta^*$ is explicitly optimized to maximize class separability. While the Data Processing Inequality posits that arbitrary transformations cannot increase mutual information, the adversarial optimization of the transformation bypasses the DPI's assumption of label-independent processing. Consequently, it succeeds in extracting latent membership signals that remain dormant under vanilla observation. The full proof of Proposition 2 is provided in the Appendix A.4.

This theoretical framework also clarifies why ReproMIA maintains superior performance even under stringent low FPR constraints. A heightened $\mathcal{I}_{\delta^*}$ translates directly into a more distinctively separated score distribution, effectively pushing the densities of the two classes apart and minimizing their overlap at the decision threshold, which is validated in Figure 4 as well.

7.2 Limitations

While ReproMIA shows consistent gains across architectures and modalities, several limitations remain. First, optimizing the reprogramming pattern δ requires a shadow dataset with known membership labels, which may not always be available. Even though shadow data need not match the target model's training distribution, large mismatches can reduce pattern transferability. Second, our method assumes access to output logits or loss values; with only hard labels or top-k outputs, the gradient signal weakens, potentially lowering attack performance. Third, while ReproMIA withstands logits perturbation and input smoothing, its robustness against stronger adaptive defenses is still unexplored, especially where defenders anticipate ReproMIA attacks. Extending ReproMIA to more restrictive settings are key directions for future work.

8 Related Work

MIA on Classification Models. Early MIAs used shadow models to approximate a target model's behavior [74], while later work showed that simple signals such as loss thresholds [90] or confidence scores without shadow models [67] can already be effective. Subsequent studies explored more realistic threat models but often faced the practical constraint of maintaining extremely low false-positive rates [10, 48, 50]. LiRA [6] substantially improved precision via likelihood-ratio testing and careful calibration, inspiring follow-up work on calibration and scalability [3, 34, 47, 56, 57, 70, 83, 89].

MIA on Generative Models. As generative modeling advanced, MIAs were adapted to GANs and VAEs by exploiting reconstruction- and likelihood-related signals. LOGAN [32] provided early white-/black-box MIAs for GANs [27], and later work compared leakage across model families and refined reconstruction-based strategies [9, 35, 55]. With diffusion models [14, 36, 66], recent MIAs leverage diffusion-specific losses and estimation errors, including white-box approaches [17] and query-based or initialization-based attacks [43, 58]. Emerging directions further exploit cross-modal correlations between prompts and generated images for membership inference [49, 84, 92].

MIA on LLMs. MIAs for LLMs typically fall into *reference-based* and *reference-free* categories. Reference-based methods build calibrated tests using auxiliary data or models, e.g., self-prompt calibration to synthesize references [25] or constructing augmented datasets for stronger calibration [39]. Reference-free methods avoid external resources and rely only on the target model's outputs, using signals such as negative log-likelihood [90], compressibility [8], token-level likelihood statistics (Min-K% and variants) [73, 93], or prefix-based likelihood fluctuations [87].

9 Conclusion

We introduce ReproMIA, a unified framework that uses model reprogramming as an active signal amplifier for MIAs. By learning a lightweight input-space transformation on frozen models, it proactively magnifies behavioral discrepancies between members and non-members, which fundamentally departure from passive paradigms. Supported by rigorous theory and validated across LLMs, diffusion, and classification models, ReproMIA consistently outperforms SOTA baselines on 10+ benchmarks, especially in low-FPR regimes, establishing a new paradigm for active privacy auditing.

References

[1] Martin Abadi, Andy Chu, Ian Goodfellow, H. Brendan McMahan, Ilya Mironov, Kunal Talwar, and Li Zhang. 2016. Deep Learning with Differential Privacy. In *Proceedings of the 2016 ACM SIGSAC Conference on Computer and Communications Security* (Vienna, Austria) *(CCS '16)*. Association for Computing Machinery, New York, NY, USA, 308–318. doi:10.1145/2976749.2978318

[2] Hyojin Bahng, Ali Jahanian, Swami Sankaranarayanan, and Phillip Isola. 2022. Exploring Visual Prompts for Adapting Large-Scale Models. arXiv:2203.17274 [cs.CV] https://arxiv.org/abs/2203.17274

[3] Martin Bertran, Shuai Tang, Michael Kearns, Jamie Morgenstern, Aaron Roth, and Zhiwei Steven Wu. 2023. Scalable membership inference attacks via quantile regression. In *Proceedings of the 37th International Conference on Neural Information Processing Systems* (New Orleans, LA, USA) *(NIPS '23)*. Curran Associates Inc., Red Hook, NY, USA, Article 16, 17 pages.

[4] Stella Biderman, Hailey Schoelkopf, Quentin Gregory Anthony, Herbie Bradley, Kyle O'Brien, Eric Hallahan, Mohammad Aflah Khan, Shivanshu Purohit, Usvsn Sai Prashanth, Edward Raff, Aviya Skowron, Lintang Sutawika, and Oskar Van Der Wal. 2023. Pythia: A Suite for Analyzing Large Language Models Across Training and Scaling. In *Proceedings of the 40th International Conference on Machine Learning (Proceedings of Machine Learning Research, Vol. 202)*, Andreas Krause, Emma Brunskill, Kyunghyun Cho, Barbara Engelhardt, Sivan Sabato, and Jonathan Scarlett (Eds.). PMLR, 2397–2430. https://proceedings.mlr.press/v202/biderman23a.html

[5] Sidney Black, Stella Biderman, Eric Hallahan, Quentin Anthony, Leo Gao, Laurence Golding, Horace He, Connor Leahy, Kyle McDonell, Jason Phang, Michael Pieler, Usvsn Sai Prashanth, Shivanshu Purohit, Laria Reynolds, Jonathan Tow, Ben Wang, and Samuel Weinbach. 2022. GPT-NeoX-20B: An Open-Source Autoregressive Language Model. In *Proceedings of BigScience Episode #5 – Workshop on Challenges & Perspectives in Creating Large Language Models*. Association for Computational Linguistics, virtual+Dublin, 95–136. doi:10.18653/v1/2022.bigscience-1.9

[6] Nicholas Carlini, Steve Chien, Milad Nasr, Shuang Song, Andreas Terzis, and Florian Tramèr. 2022. Membership Inference Attacks From First Principles. In *2022 IEEE Symposium on Security and Privacy (SP)*. 1897–1914. doi:10.1109/SP46214.2022.9833649

[7] Nicholas Carlini, Chang Liu, Úlfar Erlingsson, Jernej Kos, and Dawn Song. 2019. The secret sharer: evaluating and testing unintended memorization in neural networks. In *Proceedings of the 28th USENIX Conference on Security Symposium* (Santa Clara, CA, USA) *(SEC'19)*. USENIX Association, USA, 267–284.

[8] Nicholas Carlini, Florian Tramèr, Eric Wallace, Matthew Jagielski, Ariel Herbert-Voss, Katherine Lee, Adam Roberts, Tom Brown, Dawn Song, Úlfar Erlingsson, Alina Oprea, and Colin Raffel. 2021. Extracting Training Data from Large Language Models. In *30th USENIX Security Symposium (USENIX Security 21)*. USENIX Association, 2633–2650. https://www.usenix.org/conference/usenixsecurity21/presentation/carlini-extracting

[9] Dingfan Chen, Ning Yu, Yang Zhang, and Mario Fritz. 2020. GAN-Leaks: A Taxonomy of Membership Inference Attacks against Generative Models. In *Proceedings of the 2020 ACM SIGSAC Conference on Computer and Communications Security* (Virtual Event, USA) *(CCS '20)*. Association for Computing Machinery, New York, NY, USA, 343–362. doi:10.1145/3372297.3417238

[10] Christopher A. Choquette-Choo, Florian Tramer, Nicholas Carlini, and Nicolas Papernot. 2021. Label-Only Membership Inference Attacks. In *Proceedings of the 38th International Conference on Machine Learning (Proceedings of Machine Learning Research, Vol. 139)*, Marina Meila and Tong Zhang (Eds.). PMLR, 1964–1974. https://proceedings.mlr.press/v139/choquette-choo21a.html

[11] Adam Coates, Andrew Ng, and Honglak Lee. 2011. An Analysis of Single-Layer Networks in Unsupervised Feature Learning. In *Proceedings of the Fourteenth International Conference on Artificial Intelligence and Statistics (Proceedings of Machine Learning Research, Vol. 15)*, Geoffrey Gordon, David Dunson, and Miroslav Dudík (Eds.). PMLR, Fort Lauderdale, FL, USA, 215–223. https://proceedings.mlr.press/v15/coates11a.html

[12] Luke N. Darlow, Elliot J. Crowley, Antreas Antoniou, and Amos J. Storkey. 2018. CINIC-10 is not ImageNet or CIFAR-10. arXiv:1810.03505 [cs.CV] https://arxiv.org/abs/1810.03505

[13] Jia Deng, Wei Dong, Richard Socher, Li-Jia Li, Kai Li, and Li Fei-Fei. 2009. ImageNet: A large-scale hierarchical image database. In *2009 IEEE Conference on Computer Vision and Pattern Recognition*. 248–255. doi:10.1109/CVPR.2009.5206848

[14] Prafulla Dhariwal and Alexander Quinn Nichol. 2021. Diffusion Models Beat GANs on Image Synthesis. In *Advances in Neural Information Processing Systems*, A. Beygelzimer, Y. Dauphin, P. Liang, and J. Wortman Vaughan (Eds.). https://openreview.net/forum?id=AAWuCvzaVt

[15] Tim Dockhorn, Arash Vahdat, and Karsten Kreis. 2022. Score-Based Generative Modeling with Critically-Damped Langevin Diffusion. In *International Conference on Learning Representations*. https://openreview.net/forum?id=CzceR82CYc

[16] Jeff Donahue, Philipp Krähenbühl, and Trevor Darrell. 2017. Adversarial Feature Learning. In *International Conference on Learning Representations*. https://openreview.net/forum?id=BJtNZAFgg

[17] Jinhao Duan, Fei Kong, Shiqi Wang, Xiaoshuang Shi, and Kaidi Xu. 2023. Are Diffusion Models Vulnerable to Membership Inference Attacks?. In *Proceedings of the 40th International Conference on Machine Learning (Proceedings of Machine Learning Research, Vol. 202)*, Andreas Krause, Emma Brunskill, Kyunghyun Cho, Barbara Engelhardt, Sivan Sabato, and Jonathan Scarlett (Eds.). PMLR, 8717–8730. https://proceedings.mlr.press/v202/duan23b.html

[18] Michael Duan, Anshuman Suri, Niloofar Mireshghallah, Sewon Min, Weijia Shi, Luke Zettlemoyer, Yulia Tsvetkov, Yejin Choi, David Evans, and Hannaneh Hajishirzi. 2024. Do Membership Inference Attacks Work on Large Language Models?. In *First Conference on Language Modeling*. https://openreview.net/forum?id=av0D19pSkU

[19] Vasisht Duddu, Antoine Boutet, and Virat Shejwalkar. 2020. Quantifying Privacy Leakage in Graph Embedding. *MobiQuitous 2020 - 17th EAI International Conference on Mobile and Ubiquitous Systems: Computing, Networking and Services* (2020). https://api.semanticscholar.org/CorpusID:222125006

[20] Christophe Dupuy, Radhika Arava, Rahul Gupta, and Anna Rumshisky. 2022. An Efficient DP-SGD Mechanism for Large Scale NLU Models. In *ICASSP 2022 - 2022 IEEE International Conference on Acoustics, Speech and Signal Processing (ICASSP)*. 4118–4122. doi:10.1109/ICASSP43922.2022.9746975

[21] Gamaleldin F. Elsayed, Ian Goodfellow, and Jascha Sohl-Dickstein. 2019. Adversarial Reprogramming of Neural Networks. In *International Conference on Learning Representations*. https://openreview.net/forum?id=Syx_Ss05tm

[22] Andre Esteva, Brett Kuprel, Roberto A. Novoa, Justin Ko, Susan M. Swetter, Helen M. Blau, and Sebastian Thrun. 2017. Dermatologist-level classification of skin cancer with deep neural networks. *Nature* 542 (2017), 115–118. doi:10.1038/nature21056

[23] Xingli Fang and Jung-Eun Kim. 2024. Center-based relaxed learning against membership inference attacks. In *Proceedings of the Fortieth Conference on Uncertainty in Artificial Intelligence* (Barcelona, Spain) *(UAI '24)*. JMLR.org, Article 60, 13 pages.

[24] Thomas Fischer and Christopher Krauss. 2018. Deep learning with long short-term memory networks for financial market predictions. *European Journal of Operational Research* 270, 2 (2018), 654–669. doi:10.1016/j.ejor.2017.11.054

[25] Wenjie Fu, Huandong Wang, Chen Gao, Guanghua Liu, Yong Li, and Tao Jiang. 2024. Membership Inference Attacks against Fine-tuned Large Language Models via Self-prompt Calibration. In *Advances in Neural Information Processing Systems*, A. Globerson, L. Mackey, D. Belgrave, A. Fan, U. Paquet, J. Tomczak, and C. Zhang (Eds.), Vol. 37. Curran Associates, Inc., 134981–135010. doi:10.52202/079017-4290

[26] Leo Gao, Stella Biderman, Sid Black, Laurence Golding, Travis Hoppe, Charles Foster, Jason Phang, Horace He, Anish Thite, Noa Nabeshima, Shawn Presser, and Connor Leahy. 2020. The Pile: An 800GB Dataset of Diverse Text for Language Modeling. arXiv:2101.00027 [cs.CL] https://arxiv.org/abs/2101.00027

[27] Ian J. Goodfellow, Jean Pouget-Abadie, Mehdi Mirza, Bing Xu, David Warde-Farley, Sherjil Ozair, Aaron Courville, and Yoshua Bengio. 2014. Generative adversarial nets. In *Proceedings of the 28th International Conference on Neural Information Processing Systems - Volume 2* (Montreal, Canada) *(NIPS'14)*. MIT Press, Cambridge, MA, USA, 2672–2680.

[28] Aaron Grattafiori et al. 2024. The Llama 3 Herd of Models. arXiv:2407.21783 [cs.AI] https://arxiv.org/abs/2407.21783

[29] Albert Gu and Tri Dao. 2024. Mamba: Linear-Time Sequence Modeling with Selective State Spaces. In *First Conference on Language Modeling*. https://openreview.net/forum?id=tEYskw1VY2

[30] Chuan Guo, Geoff Pleiss, Yu Sun, and Kilian Q. Weinberger. 2017. On Calibration of Modern Neural Networks. In *Proceedings of the 34th International Conference on Machine Learning (Proceedings of Machine Learning Research, Vol. 70)*, Doina Precup and Yee Whye Teh (Eds.). PMLR, 1321–1330. https://proceedings.mlr.press/v70/guo17a.html

[31] William L. Hamilton, Rex Ying, and Jure Leskovec. 2017. Inductive representation learning on large graphs. In *Proceedings of the 31st International Conference on Neural Information Processing Systems* (Long Beach, California, USA) *(NIPS'17)*. Curran Associates Inc., Red Hook, NY, USA, 1025–1035.

[32] Jamie Hayes, Luca Melis, George Danezis, and Emiliano De Cristofaro. 2018. LOGAN: Membership Inference Attacks Against Generative Models. arXiv:1705.07663 [cs.CR] https://arxiv.org/abs/1705.07663

[33] Kaiming He, Xiangyu Zhang, Shaoqing Ren, and Jian Sun. 2016. Deep Residual Learning for Image Recognition. In *2016 IEEE Conference on Computer Vision and Pattern Recognition (CVPR)*. 770–778. doi:10.1109/CVPR.2016.90

[34] Yu He, Boheng Li, Yao Wang, Mengda Yang, Juan Wang, Hongxin Hu, and Xingyu Zhao. 2024. Is Difficulty Calibration All We Need? Towards More Practical Membership Inference Attacks. In *Proceedings of the 2024 on ACM SIGSAC Conference on Computer and Communications Security* (Salt Lake City, UT, USA) *(CCS '24)*. Association for Computing Machinery, New York, NY, USA, 1226–1240. doi:10.1145/3658644.3690316

[35] Benjamin Hilprecht, Martin Härterich, and Daniel Bernau. 2019. Monte Carlo and Reconstruction Membership Inference Attacks against Generative Models. In *Proceedings on Privacy Enhancing Technologies*, Vol. 2019. doi:10.2478/popets-2019-0067

[36] Jonathan Ho, Ajay Jain, and Pieter Abbeel. 2020. Denoising Diffusion Probabilistic Models. In *Advances in Neural Information Processing Systems*, H. Larochelle, M. Ranzato, R. Hadsell, M.F. Balcan, and H. Lin (Eds.), Vol. 33. Curran Associates, Inc., 6840–6851. https://proceedings.neurips.cc/paper_files/paper/2020/file/4c5bcfec8584af0d967f1ab10179ca4b-Paper.pdf

[37] Yuke Hu, Zheng Li, Zhihao Liu, Yang Zhang, Zhan Qin, Kui Ren, and Chun Chen. 2025. Membership inference attacks against vision-language models. In *Proceedings of the 34th USENIX Conference on Security Symposium* (Seattle, WA, USA) *(SEC '25)*. USENIX Association, USA, Article 83, 20 pages.

[38] Gao Huang, Zhuang Liu, Laurens Van Der Maaten, and Kilian Q. Weinberger. 2017. Densely Connected Convolutional Networks. In *2017 IEEE Conference on Computer Vision and Pattern Recognition (CVPR)*. 2261–2269. doi:10.1109/CVPR.2017.243

[39] Zhiheng Huang, Yannan Liu, Daojing He, and Yu Li. 2025. DF-MIA: a distribution-free membership inference attack on fine-tuned large language models. In *Proceedings of the Thirty-Ninth AAAI Conference on Artificial Intelligence and Thirty-Seventh Conference on Innovative Applications of Artificial Intelligence and Fifteenth Symposium on Educational Advances in Artificial Intelligence (AAAI'25/IAAI'25/EAAI'25)*. AAAI Press, Article 39, 9 pages. doi:10.1609/aaai.v39i1.32012

[40] Yigitcan Kaya, Sanghyun Hong, and Tudor Dumitras. 2020. On the Effectiveness of Regularization Against Membership Inference Attacks. arXiv:2006.05336 [cs.LG] https://arxiv.org/abs/2006.05336

[41] Mishaal Kazmi, Hadrien Lautraite, Alireza Akbari, Qiaoyue Tang, Mauricio Soroco, Tao Wang, Sébastien Gambs, and Mathias Lécuyer. 2024. PANORAMIA: privacy auditing of machine learning models without retraining. In *Proceedings of the 38th International Conference on Neural Information Processing Systems* (Vancouver, BC, Canada) *(NIPS '24)*. Curran Associates Inc., Red Hook, NY, USA, Article 1825, 39 pages.

[42] Nitish Shirish Keskar, Dheevatsa Mudigere, Jorge Nocedal, Mikhail Smelyanskiy, and Ping Tak Peter Tang. 2017. On Large-Batch Training for Deep Learning: Generalization Gap and Sharp Minima. In *International Conference on Learning Representations*. https://openreview.net/forum?id=H1oyRlYgg

[43] Fei Kong, Jinhao Duan, RuiPeng Ma, Heng Tao Shen, Xiaoshuang Shi, Xiaofeng Zhu, and Kaidi Xu. 2024. An Efficient Membership Inference Attack for the Diffusion Model by Proximal Initialization. In *The Twelfth International Conference on Learning Representations*. https://openreview.net/forum?id=rpH9FcCEV6

[44] Alex Krizhevsky. 2009. Learning Multiple Layers of Features from Tiny Images. https://api.semanticscholar.org/CorpusID:18268744

[45] Meghdad Kurmanji, Peter Triantafillou, Jamie Hayes, and Eleni Triantafillou. 2023. Towards Unbounded Machine Unlearning. In *Thirty-seventh Conference on Neural Information Processing Systems*. https://openreview.net/forum?id=OveBaTtUAT

[46] Yann LeCun, Yoshua Bengio, and Geoffrey Hinton. 2015. Deep Learning. *Nature* 521 (2015), 436–444. doi:10.1038/nature14539

[47] Hao Li, Zheng Li, Siyuan Wu, Chengrui Hu, Yutong Ye, Min Zhang, Dengguo Feng, and Yang Zhang. 2024. SeqMIA: Sequential-Metric Based Membership Inference Attack. In *Proceedings of the 2024 on ACM SIGSAC Conference on Computer and Communications Security* (Salt Lake City, UT, USA) *(CCS '24)*. Association for Computing Machinery, New York, NY, USA, 3496–3510. doi:10.1145/3658644.3690335

[48] Jiacheng Li, Ninghui Li, and Bruno Ribeiro. 2021. Membership Inference Attacks and Defenses in Classification Models. arXiv:2002.12062 [cs.CR] doi:10.1145/3422337.3447836

[49] Qiao Li, Xiaomeng Fu, Xi Wang, Jin Liu, Xingyu Gao, Jiao Dai, and Jizhong Han. 2024. Unveiling Structural Memorization: Structural Membership Inference Attack for Text-to-Image Diffusion Models. In *Proceedings of the 32nd ACM International Conference on Multimedia* (Melbourne VIC, Australia) *(MM '24)*. Association for Computing Machinery, New York, NY, USA, 10554–10562. doi:10.1145/3664647.3681170

[50] Zheng Li and Yang Zhang. 2021. Membership Leakage in Label-Only Exposures. In *Proceedings of the 2021 ACM SIGSAC Conference on Computer and Communications Security* (Virtual Event, Republic of Korea) *(CCS '21)*. Association for Computing Machinery, New York, NY, USA, 880–895. doi:10.1145/3460120.3484575

[51] Jiacheng Liang, Ren Pang, Changjiang Li, and Ting Wang. 2024. Model Extraction Attacks Revisited. In *Proceedings of the 19th ACM Asia Conference on Computer and Communications Security* (Singapore, Singapore) *(ASIA CCS '24)*. Association for Computing Machinery, New York, NY, USA, 1231–1245. doi:10.1145/3634737.3657002

[52] Tsung-Yi Lin, Michael Maire, Serge Belongie, James Hays, Pietro Perona, Deva Ramanan, Piotr Dollár, and C. Lawrence Zitnick. 2014. Microsoft COCO: Common Objects in Context. In *Computer Vision – ECCV 2014*. Springer International Publishing, Cham, 740–755.

[53] Gaoyang Liu, Chen Wang, Kai Peng, Haojun Huang, Yutong Li, and Wenqing Cheng. 2019. SocInf: Membership Inference Attacks on Social Media Health Data With Machine Learning. *IEEE Transactions on Computational Social Systems* 6, 5 (2019), 907–921. doi:10.1109/TCSS.2019.2916086

[54] Han Liu, Yuhao Wu, Zhiyuan Yu, and Ning Zhang. 2024. Please Tell Me More: Privacy Impact of Explainability through the Lens of Membership Inference Attack. In *2024 IEEE Symposium on Security and Privacy (SP)*. 4791–4809. doi:10.1109/SP54263.2024.00120

[55] Kin Sum Liu, Chaowei Xiao, Bo Li, and Jie Gao. 2019. Performing Co-membership Attacks Against Deep Generative Models. In *2019 IEEE International Conference on Data Mining (ICDM)*. 459–467. doi:10.1109/ICDM.2019.00056

[56] Yugeng Liu, Zheng Li, Michael Backes, Yun Shen, and Yang Zhang. 2023. Backdoor Attacks Against Dataset Distillation. arXiv:2301.01197 [cs.CR] https://arxiv.org/abs/2301.01197

[57] Yiyong Liu, Zhengyu Zhao, Michael Backes, and Yang Zhang. 2022. Membership Inference Attacks by Exploiting Loss Trajectory. In *Proceedings of the 2022 ACM SIGSAC Conference on Computer and Communications Security* (Los Angeles, CA, USA) *(CCS '22)*. Association for Computing Machinery, New York, NY, USA, 2085–2098. doi:10.1145/3548606.3560684

[58] Tomoya Matsumoto, Takayuki Miura, and Naoto Yanai. 2023. Membership Inference Attacks against Diffusion Models. arXiv:2302.03262 [cs.CR] https://arxiv.org/abs/2302.03262

[59] Justus Mattern, Fatemehsadat Mireshghallah, Zhijing Jin, Bernhard Schölkopf, Mrinmaya Sachan, and Taylor Berg-Kirkpatrick. 2023. Membership Inference Attacks against Language Models via Neighbourhood Comparison. In *Findings of the Association for Computational Linguistics: ACL 2023*, Anna Rogers, Jordan Boyd-Graber, and Naoaki Okazaki (Eds.). Association for Computational Linguistics, Toronto, Canada, 11330–11343. doi:10.18653/v1/2023.findings-acl.719

[60] Sasi Kumar Murakonda and Reza Shokri. 2020. ML Privacy Meter: Aiding Regulatory Compliance by Quantifying the Privacy Risks of Machine Learning. arXiv:2007.09339 [cs.CR] https://arxiv.org/abs/2007.09339

[61] Milad Nasr, Reza Shokri, and Amir Houmansadr. 2019. Comprehensive Privacy Analysis of Deep Learning: Passive and Active White-box Inference Attacks against Centralized and Federated Learning. In *2019 IEEE Symposium on Security and Privacy (SP)*. 739–753. doi:10.1109/SP.2019.00065

[62] Milad Nasr, Shuang Songi, Abhradeep Thakurta, Nicolas Papernot, and Nicholas Carlin. 2021. Adversary Instantiation: Lower Bounds for Differentially Private Machine Learning. In *2021 IEEE Symposium on Security and Privacy (SP)*. 866–882. doi:10.1109/SP40001.2021.00069

[63] Behnam Neyshabur, Srinadh Bhojanapalli, David McAllester, and Nathan Srebro. 2017. Exploring generalization in deep learning. In *Proceedings of the 31st International Conference on Neural Information Processing Systems* (Long Beach, California, USA) *(NIPS'17)*. Curran Associates Inc., Red Hook, NY, USA, 5949–5958.

[64] Nicolas Papernot, Patrick McDaniel, Arunesh Sinha, and Michael P. Wellman. 2018. SoK: Security and Privacy in Machine Learning. In *2018 IEEE European Symposium on Security and Privacy (EuroS&P)*. 399–414. doi:10.1109/EuroSP.2018.00035

[65] Shahbaz Rezaei, Zubair Shafiq, and Xin Liu. 2023. Accuracy-Privacy Trade-off in Deep Ensemble: A Membership Inference Perspective. In *2023 IEEE Symposium on Security and Privacy (SP)*. 364–381. doi:10.1109/SP46215.2023.10179463

[66] Robin Rombach, Andreas Blattmann, Dominik Lorenz, Patrick Esser, and Björn Ommer. 2022. High-Resolution Image Synthesis With Latent Diffusion Models. In *Proceedings of the IEEE/CVF Conference on Computer Vision and Pattern Recognition (CVPR)*. 10684–10695.

[67] Ahmed Salem, Yang Zhang, Mathias Humbert, Mario Fritz, and Michael Backes. 2019. ML-Leaks: Model and Data Independent Membership Inference Attacks and Defenses on Machine Learning Models. In *Network and Distributed Systems Security*. https://dx.doi.org/10.14722/ndss.2019.23119

[68] Christoph Schuhmann, Romain Beaumont, Richard Vencu, Cade W Gordon, Ross Wightman, Mehdi Cherti, Theo Coombes, Aarush Katta, Clayton Mullis, Mitchell Wortsman, Patrick Schramowski, Srivatsa R Kundurthy, Katherine Crowson, Ludwig Schmidt, Robert Kaczmarczyk, and Jenia Jitsev. 2022. LAION-5B: An open large-scale dataset for training next generation image-text models. In *Thirty-sixth Conference on Neural Information Processing Systems Datasets and Benchmarks Track*. https://openreview.net/forum?id=M3Y74vmsMcY

[69] Prithviraj Sen, Galileo Namata, Mustafa Bilgic, Lise Getoor, Brian Galligher, and Tina Eliassi-Rad. 2008. Collective Classification in Network Data. *AI Magazine* 29, 3 (Sep. 2008), 93. doi:10.1609/aimag.v29i3.2157

[70] Shlomit Shachor, Natalia Razinkov, and Abigail Goldsteen. 2024. Improved Membership Inference Attacks Against Language Classification Models. arXiv:2310.07219 [cs.LG] https://arxiv.org/abs/2310.07219

[71] Moshe Shaked and J. George Shanthikumar. 2007. *Stochastic Orders*. Springer New York, New York.

[72] Haonan Shi, Tu Ouyang, and An Wang. 2024. Learning-Based Difficulty Calibration for Enhanced Membership Inference Attacks. In *2024 IEEE 9th European Symposium on Security and Privacy (EuroS&P)*. 62–77. doi:10.1109/EuroSP60621.2024.00012

[73] Weijia Shi, Anirudh Ajith, Mengzhou Xia, Yangsibo Huang, Daogao Liu, Terra Blevins, Danqi Chen, and Luke Zettlemoyer. 2024. Detecting Pretraining Data from Large Language Models. In *The Twelfth International Conference on Learning Representations*. https://openreview.net/forum?id=zWqr3MQuNs

[74] Reza Shokri, Marco Stronati, Congzheng Song, and Vitaly Shmatikov. 2017. Membership Inference Attacks Against Machine Learning Models. In *2017 IEEE Symposium on Security and Privacy (SP)*. 3–18. doi:10.1109/SP.2017.41

[75] K Simonyan and A Zisserman. 2015. Very deep convolutional networks for large-scale image recognition, In 3rd International Conference on Learning Representations (ICLR 2015). *3rd International Conference on Learning Representations (ICLR 2015)*, 1–14.

[76] Jiaming Song, Chenlin Meng, and Stefano Ermon. 2021. Denoising Diffusion Implicit Models. In *International Conference on Learning Representations*. https://openreview.net/forum?id=St1giarCHLP

[77] Lukas Struppek, Dominik Hintersdorf, and Kristian Kersting. 2024. Be Careful What You Smooth For: Label Smoothing Can Be a Privacy Shield but Also a Catalyst for Model Inversion Attacks. In *The Twelfth International Conference on Learning Representations*. https://openreview.net/forum?id=1SbkubNdbW

[78] Yonglong Tian, Dilip Krishnan, and Phillip Isola. 2020. Contrastive multiview coding. In *Computer Vision–ECCV 2020: 16th European Conference, Glasgow, UK, August 23–28, 2020, Proceedings, Part XI 16*. Springer, 776–794.

[79] Hugo Touvron, Thibaut Lavril, Gautier Izacard, Xavier Martinet, Marie-Anne Lachaux, Timothée Lacroix, Baptiste Rozière, Naman Goyal, Eric Hambro, Faisal Azhar, Aurelien Rodriguez, Armand Joulin, Edouard Grave, and Guillaume Lample. 2023. LLaMA: Open and Efficient Foundation Language Models. arXiv:2302.13971 [cs.CL] https://arxiv.org/abs/2302.13971

[80] Florian Tramèr, Fan Zhang, Ari Juels, Michael K. Reiter, and Thomas Ristenpart. 2016. Stealing machine learning models via prediction APIs. In *Proceedings of the 25th USENIX Conference on Security Symposium* (Austin, TX, USA) *(SEC'16)*. USENIX Association, USA, 601–618.

[81] Yun-Yun Tsai, Pin-Yu Chen, and Tsung-Yi Ho. 2020. Transfer Learning without Knowing: Reprogramming Black-box Machine Learning Models with Scarce Data and Limited Resources. In *Proceedings of the 37th International Conference on Machine Learning (Proceedings of Machine Learning Research, Vol. 119)*, Hal Daumé III and Aarti Singh (Eds.). PMLR, 9614–9624. https://proceedings.mlr.press/v119/tsai20a.html

[82] Ashish Vaswani, Noam Shazeer, Niki Parmar, Jakob Uszkoreit, Llion Jones, Aidan N. Gomez, Łukasz Kaiser, and Illia Polosukhin. 2017. Attention is all you need. In *Proceedings of the 31st International Conference on Neural Information Processing Systems* (Long Beach, California, USA) *(NIPS'17)*. Curran Associates Inc., Red Hook, NY, USA, 6000–6010.

[83] Lauren Watson, Chuan Guo, Graham Cormode, and Alexandre Sablayrolles. 2022. On the Importance of Difficulty Calibration in Membership Inference Attacks. In *The Tenth International Conference on Learning Representations, ICLR 2022, Virtual Event, April 25-29, 2022*. OpenReview.net. https://openreview.net/forum?id=3eIrli0TwQ

[84] Yuxin Wen, Yuchen Liu, Chen Chen, and Lingjuan Lyu. 2024. Detecting, Explaining, and Mitigating Memorization in Diffusion Models. In *The Twelfth International Conference on Learning Representations*. https://openreview.net/forum?id=84n3UwkH7b

[85] YUTONG WU, Han Qiu, Shangwei Guo, Jiwei Li, and Tianwei Zhang. 2024. You Only Query Once: An Efficient Label-Only Membership Inference Attack. In *The Twelfth International Conference on Learning Representations*. https://openreview.net/forum?id=7WsivwyHrS

[86] Zhisheng Xiao, Karsten Kreis, and Arash Vahdat. 2022. Tackling the Generative Learning Trilemma with Denoising Diffusion GANs. In *International Conference on Learning Representations*. https://openreview.net/forum?id=JprM0p-q0Co

[87] Roy Xie, Junlin Wang, Ruomin Huang, Minxing Zhang, Rong Ge, Jian Pei, Neil Zhenqiang Gong, and Bhuwan Dhingra. 2024. ReCaLL: Membership Inference via Relative Conditional Log-Likelihoods. In *Proceedings of the 2024 Conference on Empirical Methods in Natural Language Processing*, Yaser Al-Onaizan, Mohit Bansal, and Yun-Nung Chen (Eds.). Association for Computational Linguistics, Miami, Florida, USA, 8671–8689. doi:10.18653/v1/2024.emnlp-main.493

[88] Zhilin Yang, William Cohen, and Ruslan Salakhudinov. 2016. Revisiting Semi-Supervised Learning with Graph Embeddings. In *Proceedings of The 33rd International Conference on Machine Learning (Proceedings of Machine Learning Research, Vol. 48)*, Maria Florina Balcan and Kilian Q. Weinberger (Eds.). PMLR, New York, New York, USA, 40–48. https://proceedings.mlr.press/v48/yanga16.html

[89] Jiayuan Ye, Aadyaa Maddi, Sasi Kumar Murakonda, Vincent Bindschaedler, and Reza Shokri. 2022. Enhanced Membership Inference Attacks against Machine Learning Models. In *Proceedings of the 2022 ACM SIGSAC Conference on Computer and Communications Security* (Los Angeles, CA, USA) *(CCS '22)*. Association for Computing Machinery, New York, NY, USA, 3093–3106. doi:10.1145/3548606.3560675

[90] Samuel Yeom, Irene Giacomelli, Matt Fredrikson, and Somesh Jha. 2018. Privacy Risk in Machine Learning: Analyzing the Connection to Overfitting. In *2018 IEEE 31st Computer Security Foundations Symposium (CSF)*. 268–282. doi:10.1109/CSF.2018.00027

[91] Sergey Zagoruyko and Nikos Komodakis. 2016. Wide Residual Networks. In *Proceedings of the British Machine Vision Conference (BMVC)*, Edwin R. Hancock Richard C. Wilson and William A. P. Smith (Eds.). BMVA Press, Article 87, 12 pages. doi:10.5244/C.30.87

[92] Shengfang Zhai, Huanran Chen, Yinpeng Dong, Jiajun Li, Qingni Shen, Yansong Gao, Hang Su, and Yang Liu. 2024. Membership Inference on Text-to-Image Diffusion Models via Conditional Likelihood Discrepancy. In *The Thirty-eighth Annual Conference on Neural Information Processing Systems*. https://openreview.net/forum?id=DztaBt4wP5

[93] Jingyang Zhang, Jingwei Sun, Eric Yeats, Yang Ouyang, Martin Kuo, Jianyi Zhang, Hao Frank Yang, and Hai Li. 2025. Min-K%++: Improved Baseline for Pre-Training Data Detection from Large Language Models. In *The Thirteenth International Conference on Learning Representations*. https://openreview.net/forum?id=ZGkfoufDaU

[94] Susan Zhang, Stephen Roller, Naman Goyal, Mikel Artetxe, Moya Chen, Shuohui Chen, Christopher Dewan, Mona Diab, Xian Li, Xi Victoria Lin, Todor Mihaylov, Myle Ott, Sam Shleifer, Kurt Shuster, Daniel Simig, Punit Singh Koura, Anjali Sridhar, Tianlu Wang, and Luke Zettlemoyer. 2022. OPT: Open Pre-trained Transformer Language Models. arXiv:2205.01068 [cs.CL] https://arxiv.org/abs/2205.01068

A Theoretical Proofs

A.1 Notations

Prior to proceeding with the formal proof, it is essential to standardize the notation and establish several fundamental lemmas that will be invoked repeatedly throughout this derivation.

Let $f_\theta : \mathbb{R}^d \to \mathbb{R}^K$ denote a neural network parameterized by θ, where K represents the total number of distinct classes. For a given input x and its corresponding label y, we define the pre-activation logit vector as $z(x) = f_\theta(x) \in \mathbb{R}^K$. The associated Softmax probability vector is defined as follows:

$$p(x) = \mathrm{softmax}(z(x)) = \left(\frac{e^{z_k(x)}}{\sum_{j=1}^K e^{z_j(x)}} \right)_{k=1}^K \in \Delta^{K-1}, \tag{23}$$

and the Cross Entropy loss as:

$$\mathcal{L}(x) = \ell(f_\theta(x), y) = -\log p_y(x) = -\log \mathrm{softmax}(f_\theta(x))_y. \tag{24}$$

We define the two core matrices, input-space Jacobian matrix $\mathbf{J}(x)$ and the Covariance matrix after softmax $\mathbf{C}(p)$ as follows:

$$\mathbf{J}(x) = \frac{\partial f_\theta(x)}{\partial x} \in \mathbb{R}^{K \times d}, \tag{25}$$

$$\mathbf{C}(p) = \mathrm{diag}(p) - pp^\top \in \mathbb{R}^{K \times K}. \tag{26}$$

Lemma 1 (Hessian matrix decomposition). *The input-space Hessian matrix* $\mathbf{H}(x) = \nabla_x^2 \mathcal{L}(x)$ *has a precise decomposition:*

$$\mathbf{H}(x) = \mathbf{J}(x)^\top \mathbf{C}(p(x)) \mathbf{J}(x) + \mathbf{R}(x) \tag{27}$$

where the residual term is:

$$\mathbf{R}(x) = \sum_{k=1}^K (p_k(x) - \mathbb{1}[k = y]) \cdot \nabla_x^2 f_\theta(x)_k \tag{28}$$

Proof. Applying the chain rule, we compute the first-order partial derivative of the loss function $\mathcal{L}(x) = -\log p_y(x)$ with respect to the input component x_i as follows:

$$\frac{\partial \mathcal{L}}{\partial x_i} = \sum_{k=1}^K \frac{\partial \mathcal{L}}{\partial z_k} \cdot \frac{\partial z_k}{\partial x_i}. \tag{29}$$

As $\mathcal{L} = -\log p_y = -z_y + \log(\sum_j \exp z_j)$, take the derivative of it and we have $\frac{\partial \mathcal{L}}{\partial z_k} = p_k - \mathbb{1}[k = y]$. Then we apply derivative with

respect to x_j invoking the product rule:

$$\begin{aligned}\frac{\partial^2 \mathcal{L}}{\partial x_i \partial x_j} &= \frac{\partial}{\partial x_j}\left(\sum_{k=1}^{K} \frac{\partial \mathcal{L}}{\partial z_k} \cdot \frac{\partial z_k}{\partial x_i}\right) \\ &= \underbrace{\sum_{k=1}^{K} \frac{\partial}{\partial x_j}\left(\frac{\partial \mathcal{L}}{\partial z_k}\right)\frac{\partial z_k}{\partial x_i}}_{\text{Term 1}} + \underbrace{\sum_{k=1}^{K} \frac{\partial \mathcal{L}}{\partial z_k}\frac{\partial^2 z_k}{\partial x_i \partial x_j}}_{\text{Term 2}}.\end{aligned} \tag{30}$$

We apply the chain rule on $\frac{\partial \mathcal{L}}{\partial z_k}$ again:

$$\frac{\partial}{\partial x_j}\left(\frac{\partial \mathcal{L}}{\partial z_k}\right) = \sum_{l=1}^{K} \frac{\partial^2 \mathcal{L}}{\partial z_k \partial z_l} \cdot \frac{\partial z_l}{\partial x_j}. \tag{31}$$

Since we know $\frac{\partial \mathcal{L}}{\partial z_k} = p_k - y_k$, so:

$$\frac{\partial^2 \mathcal{L}}{\partial z_k \partial z_l} = \frac{\partial p_k}{\partial z_l} = \begin{cases} p_k(1-p_k) & \text{if } k = l \\ -p_k p_l & \text{if } k \neq l \end{cases}, \tag{32}$$

which is exactly the definition of the Covariance matrix after softmax $\mathbf{C}(p)$. Therefore we have:

$$[\text{Term 1}]_{ij} = \sum_{k,l} \frac{\partial z_k}{\partial x_i} \cdot \mathbf{C}(p)_{kl} \cdot \frac{\partial z_l}{\partial x_j} = [\mathbf{J}^\top \mathbf{C}(p)\mathbf{J}]_{ij}. \tag{33}$$

For Term 2, we directly substitute $\frac{\partial \mathcal{L}}{\partial z_k} = p_k - \mathbb{1}[k = y]$ to obtain:

$$\begin{aligned}\mathbf{R}(x) &= \sum_{k=1}^{K} (p_k(x) - \mathbb{1}[k=y]) \cdot \frac{\partial^2 z_k}{\partial x_i \partial x_j} \\ &= \sum_{k=1}^{K} (p_k(x) - \mathbb{1}[k=y]) \cdot \nabla_x^2 f_\theta(x)_k.\end{aligned} \tag{34}$$

□

A.2 Proof for Proposition 1

We formulate a more precise description of Proposition 1.

Proposition (1. Spectral Gap of Hessian Eigenvalues). *Let $\mathcal{M}_\theta$ be a model with an overfitting ratio $\rho = \mathcal{L}_{test}/\mathcal{L}_{train} > 1$. Following the notations in Section 4, and under the following assumptions:*

- ***A1*** *The model training loss satisfies $\mathbb{E}_{x_m \sim \mathcal{D}_m}[\mathcal{L}(x_m)] = \varepsilon_{train}$ and $\mathbb{E}_{x_{nm} \sim \mathcal{D}_{nm}}[\mathcal{L}(x_{nm})] = \rho\varepsilon_{train}$, where $\rho > 1$.*
- ***A2*** *For all x, the Jacobian matrix satisfies $\sigma_{\min}(\mathbf{J}(x)) \geq \sigma > 0$ and $\sigma_{\max}(\mathbf{J}(x)) \leq S < \infty$.*
- ***A3*** *For all k and x, the residual term satisfies $\|\nabla_x^2 f_\theta(x)_k\|_2 \leq B < \infty$.*
- ***A4*** *Define the dispersion function for non-member outputs as:*

$$\alpha(\rho) := 1 - \mathbb{E}_{x_{nm} \sim \mathcal{D}_{nm}}\left[\|p(x_{nm})\|_2^2\right] \in (0,1), \quad \forall \rho \geq 1, \tag{35}$$

which quantifies the expected degree of dispersion in the model's output distribution when evaluated on non-member data. $\alpha(\rho)$ is monotonically increasing with respect to ρ, and there exist constants $\beta > 0$ such that $\frac{d\alpha}{d\rho} \geq \beta > 0$.

Then, the following spectral gap bound holds:

$$\begin{aligned}&\mathbb{E}_{x_{nm}}\left[\lambda_{\max}(\mathbf{H}(x_{nm}))\right] - \mathbb{E}_{x_m}\left[\lambda_{\max}(\mathbf{H}(x_m))\right] \\ &\geq \frac{\sigma^2 \alpha(\rho)}{K-1} - \left(2B\rho + 2S^2 + 2B\right)\varepsilon_{train}.\end{aligned} \tag{36}$$

Proof. We will derive the upper/lower bound for member/non-member Hessian spectral radius in two separate parts.

Part A: Upper bound for member Hessian spectral radius

Lemma 2 (Trace Bound of the Covariance Matrix). *If $p_y \geq 1 - \varepsilon$ (i.e., the model exhibits high predictive confidence for member samples), then:*

$$\operatorname{tr}(\mathbf{C}(p)) = 1 - \|p\|_2^2 \leq 2\varepsilon. \tag{37}$$

Proof. Since we have:

$$\|p\|_2^2 = p_y^2 + \sum_{k \neq y} p_k^2 \geq p_y^2 \geq (1-\varepsilon)^2 = 1 - 2\varepsilon + \varepsilon^2. \tag{38}$$

Then:

$$\operatorname{tr}(\mathbf{C}(p)) = 1 - \|p\|_2^2 \leq 1 - (1-\varepsilon)^2 = 2\varepsilon - \varepsilon^2 \leq 2\varepsilon. \tag{39}$$

□

Lemma 3 (Relationship between Loss and Confidence). *Invoking the inequality $-\log t \geq 1 - t$ for $t \in (0,1)$, we have:*

$$\mathcal{L}(x_m) = -\log p_y(x_m) \geq 1 - p_y(x_m) = \varepsilon_m, \tag{40}$$

which means $\varepsilon_m \leq \mathcal{L}(x_m)$, implying that the degree of predictive uncertainty is upper-bounded by the empirical training loss.

Lemma 4 (Relationship between the Spectral Radius and the Trace). *For any positive semi-definite matrix $\mathbf{A}$, the inequality $\lambda_{\max}(\mathbf{A}) \leq \operatorname{tr}(\mathbf{A})$ holds (since $\lambda_{\max} \leq \sum_i \lambda_i = \operatorname{tr}$).*

For a member sample x_m, let $\varepsilon_m = 1 - p_y(x_m)$. From Lemma 2, we have $\varepsilon_m \leq \mathcal{L}(x_m) = \ell_m$. Utilizing Lemma 1, we have:

$$\lambda_{\max}(\mathbf{H}(x_m)) \leq \lambda_{\max}(\mathbf{J}^\top \mathbf{C}(p_m)\mathbf{J}) + \lambda_{\max}(\mathbf{R}(x_m)). \tag{41}$$

Utilizing the eigenvalue calculus of variation $\lambda_{\max}(\mathbf{J}^\top \mathbf{C}\mathbf{J}) = \max_{\|v\|=1, v \in \mathbb{R}^d} v^\top \mathbf{J}^\top \mathbf{C}\mathbf{J} v = \max_{\|v\|=1} (\mathbf{J}v)^\top \mathbf{C}(\mathbf{J}v)$, and we have:

$$(\mathbf{J}v)^\top \mathbf{C}(\mathbf{J}v) \leq \lambda_{\max}(\mathbf{C}) \cdot \|\mathbf{J}v\|^2 \leq \lambda_{\max}(\mathbf{C}) \cdot \|\mathbf{J}\|_2^2 \cdot \|v\|^2 = \lambda_{\max}(\mathbf{C}) \cdot \|\mathbf{J}\|_2^2. \tag{42}$$

Therefore, with Lemmas 2 and 4, we have:

$$\lambda_{\max}(\mathbf{J}^\top \mathbf{C}\mathbf{J}) \underbrace{\leq \|\mathbf{J}\|_2^2 \cdot \lambda_{\max}(\mathbf{C})}_{\text{Assumption A2}} \leq S^2 \cdot \lambda_{\max}(\mathbf{C}) \underbrace{\leq S^2 \cdot \operatorname{tr}(\mathbf{C}(p_m))}_{\text{Lemma 4}} \underbrace{\leq S^2 \cdot 2\varepsilon_m}_{\text{Lemma 2}}. \tag{43}$$

For the residual term, we have:

$$\begin{aligned}\|\mathbf{R}(x_m)\|_2 &\leq \sum_k |p_k(x_m) - 1[k=y]| \cdot \|\nabla_x^2 f_\theta(x_m)_k\|_2 \\ &\leq B \sum_k |r_k| \\ &= B\left(|p_y - 1| + \sum_{k \neq y} p_k\right) \\ &= B\left((1-p_y) + (1-p_y)\right) \\ &= 2B\varepsilon_m \leq 2B\ell_m.\end{aligned} \tag{44}$$

Therefore, we have $\lambda_{\max}(\mathbf{H}(x_m)) \leq (2S^2 + 2B)\ell_m$, with the expectation form of:

$$\mathbb{E}_{x_m}[\lambda_{\max}(\mathbf{H}(x_m))] \leq 2(S^2 + B)\varepsilon_{train}. \tag{45}$$

Part B: Lower bound for non-member Hessian spectral radius

Lemma 5 (Trace-derived Lower Bound for Eigenvalues). *Let* $\mathbf{A}$ *be a* $n \times n$ *positive semi-definite matrix such that* $\text{rank}(\mathbf{A}) \leq r$. *Then:*

$$\lambda_{\max}(\mathbf{A}) \geq \frac{\text{tr}(\mathbf{A})}{r}. \tag{46}$$

Proof. Denote the non-zero eigenvalues of $\mathbf{A}$ as $\lambda_1 \geq \cdots \geq \lambda_r > 0$. By the arithmetic mean inequality, we have: $\lambda_1 \geq \frac{\lambda_1+\cdots+\lambda_r}{r} = \frac{\text{tr}(\mathbf{A})}{r}$. □

Lemma 6 (Trace Lower Bound for $\mathbf{J}^\top\mathbf{C}\mathbf{J}$). *Under the assumption of* ***A2****, we have:*

$$\text{tr}(\mathbf{J}^\top\mathbf{C}(p)\mathbf{J}) \geq \sigma^2 \cdot \text{tr}(\mathbf{C}(p)). \tag{47}$$

Proof. Note that $\text{tr}(\mathbf{J}^\top\mathbf{C}\mathbf{J}) = \text{tr}(\mathbf{C}\mathbf{J}\mathbf{J}^\top)$ by the cyclic property of the trace. As Assumption **A2** specifies $\sigma_{\min}(\mathbf{J}) \geq \sigma$, which implies $\mathbf{J}\mathbf{J}^\top \succeq \sigma^2\mathbf{I}$, we can derive that $\mathbf{C}(p) \succeq 0$ and $\mathbf{J}\mathbf{J}^\top \succeq \sigma^2\mathbf{I}_K$.

Applying the trace inequality for PSD matrices, for $\mathbf{A} \succeq 0$ and $\mathbf{B} \succeq c\mathbf{I}$, it holds that $\text{tr}(\mathbf{A}\mathbf{B}) = \sum_i \lambda_i(\mathbf{A})\langle v_i, \mathbf{B}v_i\rangle \geq c\sum_i \lambda_i(\mathbf{A}) = c \cdot \text{tr}(\mathbf{A})$.

By setting $\mathbf{A} = \mathbf{C}(p)$, $\mathbf{B} = \mathbf{J}\mathbf{J}^\top$, and $c = \sigma^2$ in the above inequality, we obtain $\text{tr}(\mathbf{C}\mathbf{J}\mathbf{J}^\top) \geq \sigma^2\text{tr}(\mathbf{C}(p))$.

□

For a non-member x_{nm}, it follows from Assumption **A4** that: $\mathbb{E}_{x_{nm}}[\text{tr}(\mathbf{C}(p(x_{nm})))] = 1 - \mathbb{E}_{x_{nm}}[\|p(x_{nm})\|_2^2] \geq \alpha_\circ$.

By invoking the Hessian decomposition Lemma 1 and the triangle inequality, we have:

$$\lambda_{\max}(\mathbf{H}(x_{nm})) \geq \lambda_{\max}(\mathbf{J}^\top\mathbf{C}(p_{nm})\mathbf{J}) - \|\mathbf{R}(x_{nm})\|_2. \tag{48}$$

Regarding the first term, by leveraging Lemma 5 ($\text{rank}(\mathbf{J}^\top\mathbf{C}\mathbf{J}) \leq \text{rank}(\mathbf{C}(p)) = K - 1$) and Lemma 6, we obtain:

$$\lambda_{\max}(\mathbf{J}^\top\mathbf{C}(p_{nm})\mathbf{J}) \geq \frac{\text{tr}(\mathbf{J}^\top\mathbf{C}(p_{nm})\mathbf{J})}{K-1} \geq \frac{\sigma^2 \cdot \text{tr}(\mathbf{C}(p_{nm}))}{K-1}. \tag{49}$$

Regarding the second term, the analysis mirrors that for members, and we have:

$$\|\mathbf{R}(x_{nm})\|_2 \leq B\sum_k |r_k| = B \cdot 2(1 - p_y) \leq 2B\mathcal{L}(x_{nm}) \tag{50}$$

Taking the expectation and invoking **A1** and **A4**, we obtain:

$$\mathbb{E}_{x_{nm}}[\lambda_{\max}(\mathbf{H}(x_{nm}))] \geq \frac{\sigma^2\alpha(\rho)}{K-1} - 2B \cdot \rho\varepsilon_{train}. \tag{51}$$

All together, we can derive the spectral gap:

$$\begin{aligned}\underbrace{\mathbb{E}_{x_{nm}}[\lambda_{\max}(\mathbf{H}(x_{nm}))]}_{\geq \frac{\sigma^2\alpha}{K-1} - 2B\rho\varepsilon_{train}} - \underbrace{\mathbb{E}_{x_m}[\lambda_{\max}(\mathbf{H}(x_m))]}_{\leq 2(S^2+B)\varepsilon_{train}} \\ \geq \frac{\sigma^2\alpha(\rho)}{K-1} - \left(2B\rho + 2S^2 + 2B\right)\varepsilon_{train}.\end{aligned} \tag{52}$$

Denote the right hand side as $\Delta(\rho)$, then its derivative with respect to ρ satisfies:

$$\frac{d\Delta}{d\rho} = \frac{\sigma^2\alpha'(\rho)}{K-1} - 2B\varepsilon_{train} \geq \frac{\sigma^2\beta}{K-1} - 2B\varepsilon_{train}. \tag{53}$$

When the training is sufficiently converged, specifically when $\varepsilon_{train} < \min\left\{\frac{\sigma^2\alpha(1)}{(4B+2S^2)(K-1)}, \frac{\sigma^2\beta}{2B(K-1)}\right\}$, the right term becomes strictly positive, and the first term in the min{} is to make sure $\Delta(1) > 0$. Consequently, the lower bound of the spectral gap exhibits a strictly monotonic increase with respect to the overfitting ratio ρ.

□

Remark 1 (Practical Validity of Assumption **A2**). *The uniform lower bound* $\sigma_{\min}(\mathbf{J}(x)) \geq \sigma > 0$ *depends on the activation function. Models such as LLaMA [79], Mamba [29], DDPM [36], and Stable Diffusion [66] use SiLU, while Pythia [4] and GPT-NeoX [5] use GELU; both are* C^∞*, making* $\mathbf{J}(x)$ *continuous. On compact supports,* $\sigma_{\min}(\mathbf{J}(x))$ *attains its infimum, which is strictly positive for generic (non-degenerate) weights, since smooth networks with* $|\delta| \gg K$ *have full row rank almost everywhere in parameter space.*

OPT [94] and classification models like WideResNet [91], VGG [75], DenseNet [38], and ResNet [33] use ReLU, yielding a piecewise-constant Jacobian. Within each linear region, $\mathbf{J}(x) = \mathbf{W}_L\mathbf{D}_L \cdots \mathbf{W}_1\mathbf{D}_1$*, where* $\mathbf{D}_i$ *are diagonal 0/1 matrices. For generic* $\mathbf{W}_i$*, these products are full row rank (since* $|\delta| \gg K$*), so* $\sigma_{\min} > 0$ *locally. Region boundaries form hyperplanes of Lebesgue measure zero and thus do not affect expectation-based bounds in Proposition 1.*

In practice, the uniform bound $\sigma > 0$ *can be relaxed to* $\sigma_{\min}(\mathbf{J}(x)) > 0$ *almost everywhere under* $\mathcal{D}$*. The spectral gap inequality (6) still holds in expectation via dominated convergence, provided* $\sigma_{\min}(\mathbf{J}(x))$ *is bounded below by a positive constant on a set of probability* $1 - \varepsilon$ *for arbitrarily small* ε*.*

Remark 2 (Practical Validity of Assumption **A4**). *The monotonicity of* $\alpha(\rho) = 1 - \mathbb{E}x_{nm}[|p(x_{nm})|2^2]$ *in the overfitting ratio* ρ *follows from the link between overfitting and calibration degradation. As* ρ *increases, the model memorizes training data, yielding sharper predictions on members* ($p_y(x_m) \to 1$) *and poorer calibration on non-members. This shifts probability mass away from the correct class, decreasing* $\|p(x_{nm})\|_2^2$ *and increasing* $\alpha(\rho)$*.*

For a K*-class classifier, when* $\rho = 1$ *(perfect generalization), members and non-members are treated identically, so* α *equals the Bayes-optimal baseline. As* ρ *increases,* $\mathcal{L}_{train} \to 0$ *enforces* $p_y(x_m) \to 1$*, while non-member predictions degrade toward* $\|p(xnm)\|_2^2 \to 1/K$ *(uniform), implying* $\alpha \to 1 - 1/K$ *as* $\rho \to \infty$*. This transition is monotonic, since additional memorization cannot improve non-member calibration once overfitting begins.*

This behavior is well supported empirically. Guo et al. [30] show that neural networks become less calibrated as they overfit, and Kaya et al. [40] show that the confidence gap between members and non-members grows with overfitting. Figure 3 further confirms that the loss gap (positively correlated with $\alpha(\rho)$*) is consistently positive and amplified by* ReproMIA*.*

A.3 Proof for Gradient Flow

We formalize and prove the claim that the non-member gradient stream $\mathbf{G}_2$ dominates the member stream $\mathbf{G}_1$ in the optimization of the reprogramming pattern δ, thereby steering δ^* toward a configuration that maximally destabilizes non-member outputs.

Proposition (Non-Member Stream Dominance). *Let* $\mathcal{M}_\theta$ *be a model trained on* $\mathcal{D}_m$ *with overfitting ratio* $\rho = \mathcal{L}_{test}/\mathcal{L}_{train} > 1$*. Following the notations in Section 4.4, and under the following assumptions:*

- ***A1*** *The perturbation dimension satisfies* $|\delta| \geq K$*, and the Jacobian* $\mathbf{J}(x) \in \mathbb{R}^{K\times|\delta|}$ *satisfies* $\sigma_{\min}(\mathbf{J}(x)) \geq \sigma > 0$ *(i.e.,* $\mathbf{J}$ *has full row rank with all* K *singular values bounded below) and* $\sigma_{\max}(\mathbf{J}(x)) \leq S < \infty$ *for all* x*.*

A2 *The score-sensitivity vectors* $w_m = \nabla_{o_m}\phi_1(o_m) \in \mathbb{R}^K$ *and* $w_{nm} = \nabla_{o_{nm}}\phi_2(o_{nm}) \in \mathbb{R}^K$ *satisfy:*

$$\mathbb{E}_{x_m}\left[\|w_m\|^2\right] \le C_1\,\varepsilon_{train}, \tag{54}$$

$$\mathbb{E}_{x_{nm}}\left[\|w_{nm}\|^2\right] \ge C_2\,\alpha(\rho), \tag{55}$$

where $C_1, C_2 > 0$ *are constants determined by the scoring function and model architecture, and* $\alpha(\rho)$ *is the dispersion function defined in Assumption **A4** of Proposition 1.*

A3 *The model exhibits memorization such that* $\mathbb{E}_{x_m}[\varepsilon_m] = \varepsilon_{train}$ *and* $\mathbb{E}_{x_{nm}}[\varepsilon_{nm}] = \rho\,\varepsilon_{train}$*, where* $\varepsilon = 1 - p_y(x)$*.*

Then, the expected squared norms of the two gradient streams satisfy:

$$\mathbb{E}_{x_{nm}}\left[\|\mathbf{G}_2\|^2\right] > \mathbb{E}_{x_m}\left[\|\mathbf{G}_1\|^2\right], \tag{56}$$

provided $\rho > \rho^*$ *for a threshold* ρ^* *depending on the model and scoring function constants. Since* $\sqrt{\cdot}$ *is monotonically increasing on* $[0, +\infty)$*, applying it to both sides of inequality norms (56) directly yields* $\sqrt{\mathbb{E}[\|\mathbf{G}_2\|^2]} > \sqrt{\mathbb{E}[\|\mathbf{G}_1\|^2]}$*, confirming that the non-member stream governs the aggregate gradient magnitude.*

Proof. We proceed in three steps: establishing per-sample norm bounds, deriving expected bounds for each stream, and combining them to prove the dominance.

Step 1: Per-sample squared norm bounds.

Recall from Equation (10) that the per-sample gradient contributions are:

$$\mathbf{G}_1(x_m) = \mathbf{J}(\tilde{x}_m)^\top w_m, \quad \mathbf{G}_2(x_{nm}) = \mathbf{J}(\tilde{x}_{nm})^\top w_{nm}, \tag{57}$$

where $w_m = \nabla_{o_m}\phi_1 \in \mathbb{R}^K$, $w_{nm} = \nabla_{o_{nm}}\phi_2 \in \mathbb{R}^K$, and $\mathbf{J}(\tilde{x}) \in \mathbb{R}^{K\times|\delta|}$ is the model's input-space Jacobian at the reprogrammed input $\tilde{x} = x \oplus \delta$. We bound the squared norms of these quantities using the singular value structure of $\mathbf{J}$.

Upper bound of member stream. For any vector $w \in \mathbb{R}^K$ and matrix $\mathbf{J} \in \mathbb{R}^{K\times|\delta|}$, the submultiplicativity of the operator norm yields:

$$\|\mathbf{G}_1(x_m)\|^2 = \|\mathbf{J}(\tilde{x}_m)^\top w_m\|^2 \le \sigma^2_{\max}(\mathbf{J}(\tilde{x}_m))\,\|w_m\|^2 \le S^2\,\|w_m\|^2, \tag{58}$$

where the last inequality invokes Assumption **A1**.

Lower bound of non-member stream. Since $|\delta| \ge K$ by Assumption **A1**, the Jacobian $\mathbf{J}(\tilde{x}_{nm}) \in \mathbb{R}^{K\times|\delta|}$ is a fat matrix. Combined with the lower bound $\sigma_{\min}(\mathbf{J}(\tilde{x}_{nm})) \ge \sigma > 0$, this ensures that all K singular values of $\mathbf{J}(\tilde{x}_{nm})$ are at least σ. Equivalently, $\mathbf{J}(\tilde{x}_{nm})$ has full row rank, and the linear map $w \mapsto \mathbf{J}(\tilde{x}_{nm})^\top w : \mathbb{R}^K \to \mathbb{R}^{|\delta|}$ is injective. Therefore, by the variational characterization of singular values, for all $w \in \mathbb{R}^K$:

$$\|\mathbf{J}^\top w\|^2 = w^\top \mathbf{J}\mathbf{J}^\top w \ge \lambda_{\min}(\mathbf{J}\mathbf{J}^\top)\|w\|^2 = \sigma^2_{\min}(\mathbf{J})\|w\|^2, \tag{59}$$

where the equality $\lambda_{\min}(\mathbf{J}\mathbf{J}^\top) = \sigma^2_{\min}(\mathbf{J})$ holds precisely because $\mathbf{J}\mathbf{J}^\top \in \mathbb{R}^{K\times K}$ is positive definite under the full-row-rank condition. Applying this to the non-member stream:

$$\begin{aligned}\|\mathbf{G}_2(x_{nm})\|^2 &= \|\mathbf{J}(\tilde{x}_{nm})^\top w_{nm}\|^2 \\ &\ge \sigma^2_{\min}(\mathbf{J}(\tilde{x}_{nm}))\,\|w_{nm}\|^2 \\ &\ge \sigma^2\,\|w_{nm}\|^2.\end{aligned} \tag{60}$$

Remark 3. *The two bounds in (58) and (60) are tight in complementary regimes. The upper bound in (58) is attained when* w_m *aligns with the leading right singular vector of* $\mathbf{J}$*, while the lower bound in (60) is attained when* w_{nm} *aligns with the right singular vector corresponding to* $\sigma_{\min}(\mathbf{J})$*. In practice, the actual norms lie between these extremes, but the bounds suffice for establishing dominance.*

The fat Jacobian condition $|\delta| \ge K$ *is indispensable for the lower bound: when* $|\delta| < K$*, the matrix* $\mathbf{J}^\top$ *has a non-trivial kernel of dimension* $K - |\delta|$*, so there exist non-zero* w_{nm} *for which* $\mathbf{J}^\top w_{nm} = 0$*, invalidating (60). In all practical instantiations of* `ReproMIA`*,* $|\delta| \gg K$ *holds by a wide margin.*

Step 2: Expected squared norm bounds for each stream.

Taking expectations of (58) and (60) and applying Assumption **A2**:

Member stream upper bound.

$$\mathbb{E}_{x_m}\left[\|\mathbf{G}_1\|^2\right] \le S^2\,\mathbb{E}_{x_m}\left[\|w_m\|^2\right] \le S^2\,C_1\,\varepsilon_{train}. \tag{61}$$

This bound reflects a fundamental property of memorization: for well-trained models, member samples reside near local minima where the model's output is highly confident ($p_y \approx 1$), causing the score-sensitivity vector w_m to vanish. The operator norm bound S ensures that even the maximal amplification by the Jacobian cannot overcome this vanishing sensitivity.

Non-member stream lower bound.

$$\mathbb{E}_{x_{nm}}\left[\|\mathbf{G}_2\|^2\right] \ge \sigma^2\,\mathbb{E}_{x_{nm}}\left[\|w_{nm}\|^2\right] \ge \sigma^2\,C_2\,\alpha(\rho). \tag{62}$$

For non-member samples, the model's predictive uncertainty quantified by the dispersion function $\alpha(\rho) > 0$, ensures that the score-sensitivity vector w_{nm} maintains a non-trivial norm. The minimum singular value σ guarantees that this sensitivity is faithfully transmitted through the Jacobian into the perturbation space.

Step 3: Establishing the dominance of $\mathbf{G}_2$.

Combining (61) and (62), the dominance condition $\mathbb{E}[\|\mathbf{G}_2\|^2] > \mathbb{E}[\|\mathbf{G}_1\|^2]$ is satisfied whenever:

$$\sigma^2\,C_2\,\alpha(\rho) > S^2\,C_1\,\varepsilon_{train}. \tag{63}$$

We now show that this condition holds for sufficiently large overfitting ratio ρ. By Assumption **A4** of Proposition 1, the dispersion function $\alpha(\rho)$ is monotonically increasing with $\frac{d\alpha}{d\rho} \ge \beta > 0$, which implies:

$$\alpha(\rho) \ge \alpha(1) + \beta\,(\rho - 1). \tag{64}$$

Since $\rho = \mathcal{L}_{test}/\mathcal{L}_{train} = \rho\,\varepsilon_{train}/\varepsilon_{train}$, Inequality (63) can be rewritten as:

$$\frac{\alpha(\rho)}{\varepsilon_{train}} > \frac{S^2\,C_1}{\sigma^2\,C_2}. \tag{65}$$

For models trained to small training loss ($\varepsilon_{train} \to 0$) with non-trivial generalization gap ($\rho > 1$), the left-hand side grows without bound because $\alpha(\rho) \ge \beta(\rho - 1) > 0$ remains positive while ε_{train} vanishes. More precisely, since $\mathcal{L}_{test} = \rho\,\varepsilon_{train}$ and $\alpha(\rho) \ge \beta(\rho - 1)$, we have:

$$\frac{\alpha(\rho)}{\varepsilon_{train}} \ge \frac{\beta(\rho-1)}{\varepsilon_{train}} = \frac{\beta(\mathcal{L}_{test} - \mathcal{L}_{train})}{\mathcal{L}^2_{train}}, \tag{66}$$

which diverges as $\mathcal{L}_{train} \to 0$ with $\mathcal{L}_{test}$ bounded away from zero.

Consequently, there exists a threshold:

$$\rho^* = 1 + \frac{1}{\beta}\left(\frac{S^2\,C_1\,\varepsilon_{train}}{\sigma^2\,C_2} - \alpha(1)\right)^+, \tag{67}$$

where $(x)^+ = \max(x, 0)$, such that for all $\rho > \rho^*$, the non-member gradient stream strictly dominates the member stream in expected squared norm.

For models exhibiting non-trivial overfitting ($\rho > \rho^*$), the aggregate gradient $\nabla_\delta \mathcal{F}(\delta) = \mathbf{G}_1 - \mathbf{G}_2$ is predominantly governed by the non-member contribution, steering δ toward the direction that most rapidly destabilizes non-member output distributions while preserving the relative stability of member outputs. □

Remark 4. *The dominance condition in (63) is readily satisfied in practice. For high-capacity models trained to near-zero training loss, the overfitting ratio ρ is typically large (empirically $\rho \gg 1$), which ensures that $\alpha(\rho)$ is substantial while ε_{train} is negligible.*

The bounds in Step 1 can be further refined through the lens of the Jacobian Frobenius norm, which provides additional geometric insight into the member–non-member divergence. Specifically, for the member stream, the Cauchy–Schwarz inequality for matrix–vector products yields the alternative per-sample bound:

$$\|\mathbf{J}(\tilde{x}_m)^\top w_m\|^2 \le \|\mathbf{J}(\tilde{x}_m)\|_F^2 \, \|w_m\|^2, \tag{68}$$

*where $\|\mathbf{J}\|_F^2 = \mathrm{tr}(\mathbf{J}\mathbf{J}^\top)$ is bounded above by $\min(K, |\delta|)\, S^2$ from Assumption **A1** (since $\mathbf{J}$ has at most $\min(K, |\delta|)$ singular values, each bounded by S). While this Frobenius-based bound is in general no tighter than the operator-norm bound (58) for individual samples, the average Frobenius norm $\mathbb{E}[\|\mathbf{J}(\tilde{x}_m)\|_F^2]$ can be substantially smaller than the worst-case $\min(K, |\delta|)\, S^2$ when the Jacobian is approximately low-rank at memorized points.*

For the non-member stream, the Hessian decomposition from Lemma 1 provides a structural lower bound on the Jacobian Frobenius norm. From Lemma 6:

$$\mathrm{tr}\big(\mathbf{C}(p_{nm})\mathbf{J}\mathbf{J}^\top\big) \ge \sigma^2 \ \mathrm{tr}(\mathbf{C}(p_{nm})), \tag{69}$$

and since $\mathrm{tr}(\mathbf{C}(p_{nm})\mathbf{J}\mathbf{J}^\top) \le \lambda_{\max}(\mathbf{C}(p_{nm}))\, \|\mathbf{J}\|_F^2 \le \|\mathbf{J}\|_F^2$ (because $\lambda_{\max}(\mathbf{C}(p)) \le 1$ for any probability vector), we obtain:

$$\|\mathbf{J}(\tilde{x}_{nm})\|_F^2 \ge \sigma^2 \big(1 - \|p(x_{nm})\|_2^2\big)\,. \tag{70}$$

Taking the expectation yields $\mathbb{E}[\|\mathbf{J}(\tilde{x}_{nm})\|_F^2] \ge \sigma^2\, \alpha(\rho)$, confirming that the non-member Jacobian possesses richer spectral content. While this Frobenius norm bound is not directly required by the dominance proof above, which relies on the operator norm and sensitivity bounds, it provides complementary evidence that the model's feature representation is more active for non-member inputs, further supporting the amplification mechanism of ReproMIA.

A.4 Proof for Proposition 2

We formulate a more precise description of Proposition 2.

Proposition (2. Mutual Information Improvement). *Denote $M \in \{0, 1\}$ as the membership label. Following the notations in Section 4, and under the following assumptions:*

- ***A1*** *Equal priors $P(M = 1) = P(M = 0) = 1/2$.*
- ***A2*** *For all perturbations δ and classes $i \in \{0, 1\}$, the conditional distribution of the score variable $s_\delta(x) = \phi(\mathcal{M}_\theta(x \oplus \delta))$ satisfies:*

$$s_\delta \mid M = i \sim \mathcal{N}(\mu_i^\delta, \sigma^2), \tag{71}$$

where the mean $\mu_i^\delta \in \mathbb{R}$ depends on both the class and the perturbation, while the variance $\sigma^2 > 0$ is uniform across i and δ.

- ***A3*** *For the objective function $\mathcal{F}(\delta) = \mathbb{E}_{x\sim\mathcal{D}_m^s, z\sim\mathcal{D}_{nm}^s}[\Phi(\mathcal{M}_\theta(x \oplus \delta), \mathcal{M}_\theta(z \oplus \delta))]$, we have $\mathcal{F}(\delta^*) > \mathcal{F}(0)$, which is guaranteed by Proposition 1 (see Lemma 10 for a rigorous justification).*
- ***A4*** *The vanilla mean separation satisfies $\Delta^0 := \mu_1^0 - \mu_0^0 \ge 0$, i.e., member samples achieve no lower expected score than non-members under the unperturbed model. This is the standard prerequisite for MIA to be meaningful, as a negative separation would indicate that the scoring function inversely correlates with membership status.*

Then, we have:

$$\mathcal{I}_{\delta^*} := \mathcal{I}(M; s_{\delta^*}) > \mathcal{I}(M; s_0) =: \mathcal{I}_0. \tag{72}$$

Proof. We establish the result through a sequence of four lemmas, followed by the main argument. Lemma 7 establishes a monotonic correspondence between the optimization objective and the mean separation; Lemma 8 equates mutual information with JSD under equal priors; Lemma 9 proves the strict monotonicity of JSD with respect to the mean separation; and Lemma 10 provides sufficient conditions for $\mathcal{F}(\delta^*) > \mathcal{F}(0)$.

Lemma 7 (Objective and Mean Difference Correspondence). *Under Assumptions **A2** and **A3**, define $\Delta^\delta := \mu_1^\delta - \mu_0^\delta$. The training objective $\mathcal{F}(\delta)$ satisfies:*

$$\mathcal{F}(\delta) = H(\Delta^\delta), \tag{73}$$

where $H : \mathbb{R} \to \mathbb{R}$ is a strictly increasing function, which means maximizing $\mathcal{F}(\delta)$ is equivalent to maximizing Δ^δ.

Proof. Under Assumption **A2**, the member and non-member score distributions share an identical variance σ^2, so the score difference $D^\delta := s_\delta(x_m) - s_\delta(x_{nm})$, where $x_m \sim \mathcal{D}_m^s, x_{nm} \sim \mathcal{D}_{nm}^s$ are drawn independently, satisfies:

$$D^\delta \sim \mathcal{N}\left(\mu_1^\delta - \mu_0^\delta, 2\sigma^2\right) = \mathcal{N}\left(\Delta^\delta, 2\sigma^2\right). \tag{74}$$

Substituting into the objective from Assumption **A3**, we have:

$$\mathcal{F}(\delta) = \mathbb{E}_{x,z}[\phi(s_\delta(x) - s_\delta(z))] = \mathbb{E}_{D^\delta\sim\mathcal{N}(\Delta^\delta, 2\sigma^2)}[\phi(D^\delta)] =: H(\Delta^\delta). \tag{75}$$

It remains to show that $H(\Delta) = \mathbb{E}_{D\sim\mathcal{N}(\Delta, 2\sigma^2)}[\phi(D)]$ is strictly increasing with respect to Δ.

Suppose $\Delta_1 > \Delta_2$, let $D_1 \sim \mathcal{N}(\Delta_1, 2\sigma^2)$ and $D_2 \sim \mathcal{N}(\Delta_2, 2\sigma^2)$. Since the two distributions share an identical variance, D_1 exhibits First-Order Stochastic Dominance over D_2, that is for any $t \in \mathbb{R}$:

$$P(D_1 > t) = \Phi\left(\frac{t - \Delta_1}{\sqrt{2}\sigma}\right)^c \ge \Phi\left(\frac{t - \Delta_2}{\sqrt{2}\sigma}\right)^c = P(D_2 > t). \tag{76}$$

where $\Phi^c = 1 - \Phi$ denotes the survival function of the standard normal distribution. The strict inequality is guaranteed by $\Delta_1 > \Delta_2$ for t over a set of positive Lebesgue measure.

By the fundamental properties of First-Order Stochastic Dominance [71], if $D_1 \succ_{FSD} D_2$ and ϕ is strictly increasing, then:

$$H(\Delta_1) = \mathbb{E}[\phi(D_1)] > \mathbb{E}[\phi(D_2)] = H(\Delta_2), \tag{77}$$

The strict inequality holds because the FSD is strict as the distributions of D_1 and D_2 are non-identical, and ϕ is strictly increasing, so the difference in expectations is strictly positive as the set on which $\phi(D_1)$ exceeds $\phi(D_2)$ has positive probability.

Thus H is a strictly increasing continuous function on $\mathbb{R}$. Consequently, there exists a strictly increasing inverse function H^{-1}. It follows that:

$$\Delta^\delta = H^{-1}(\mathcal{F}(\delta)) \tag{78}$$

That is, there exists a strictly monotonic correspondence between the mean difference Δ^δ and the optimization objective $\mathcal{F}(\delta)$.

□

Lemma 8 (Equivalence of Mutual Information and JSD). *Under Assumption **A1**, denote P_1^δ and P_0^δ as the marginal distributions of the score for member and non-member samples under the score function s_δ, respectively. Then for any perturbation δ:*

$$\mathcal{I}(M; s_\delta) = \mathrm{JSD}(P_1^\delta \parallel P_0^\delta), \tag{79}$$

where $\mathrm{JSD}(P\|Q) := \frac{1}{2}D_{\mathrm{KL}}\left(P\|\frac{P+Q}{2}\right) + \frac{1}{2}D_{\mathrm{KL}}\left(Q\|\frac{P+Q}{2}\right)$.

Proof. From the standard decomposition of mutual information, we have:

$$\begin{aligned}\mathcal{I}(M; s_\delta) &= D_{\mathrm{KL}}(P_{M,s_\delta} \parallel P_M \otimes P_{s_\delta}) \\ &= \mathbb{E}_{M,s}\left[\log \frac{P_{s_\delta|M}(s \mid M)}{P_{s_\delta}(s)}\right] \\ &= \sum_{i\in\{0,1\}} P(M=i)\cdot D_{\mathrm{KL}}(P_i^\delta \parallel P_{s_\delta})\end{aligned} \tag{80}$$

The marginal distribution is determined by the uniform prior:

$$P_{s_\delta} = P(M=1)P_1^\delta + P(M=0)P_0^\delta = \frac{1}{2}(P_1^\delta + P_0^\delta) \tag{81}$$

Substituting the uniform prior coefficients:

$$\mathcal{I}(M; s_\delta) = \frac{1}{2}D_{\mathrm{KL}}\left(P_1^\delta \middle\| \frac{P_1^\delta + P_0^\delta}{2}\right) + \frac{1}{2}D_{\mathrm{KL}}\left(P_0^\delta \middle\| \frac{P_1^\delta + P_0^\delta}{2}\right), \tag{82}$$

which is precisely the definition of $\mathrm{JSD}(P_1^\delta \parallel P_0^\delta)$.

□

Lemma 9 (Strict Monotonicity of JSD). *Under Assumption **A2**, the function:*

$$\tilde{h}(\Delta) := \mathrm{JSD}\left(\mathcal{N}\left(\frac{\Delta}{2}, \sigma^2\right) \| \mathcal{N}\left(-\frac{\Delta}{2}, \sigma^2\right)\right) \tag{83}$$

is strictly monotonically increasing for $\Delta \geq 0$, satisfying $\tilde{h}(0) = 0$ and $\lim_{\Delta\to\infty}\tilde{h}(\Delta) = \log 2$.

Proof. When $\Delta = 0$ the two distributions are identical, so $\tilde{h}(0) = 0$. When $\Delta > 0$, the two distributions have distinct means, and since $\sigma^2 > 0$ ensures both densities have full support, the JSD is strictly positive.

For any $\Delta_1 > \Delta_2 \geq 0$, set $r = \Delta_2/\Delta_1 \in [0, 1)$, we construct the following Degraded Channel:

$$X_{\Delta_2} = r \cdot X_{\Delta_1} + Z, \quad Z \sim \mathcal{N}(0, (1-r^2)\sigma^2) \perp X_{\Delta_1}. \tag{84}$$

To verify the validity of this construction: given $M = i$, then $X_{\Delta_1} \sim \mathcal{N}(i_\pm\Delta_1/2, \sigma^2)$ where $i_+ = 1, i_- = -1$ correspond to $M = 1, 0$ respectively, thus:

$$\begin{aligned}\mathbb{E}[X_{\Delta_2} \mid M] &= r\cdot\frac{\pm\Delta_1}{2} = \frac{\pm\Delta_2}{2} \\ \mathrm{Var}(X_{\Delta_2} \mid M) &= r^2\sigma^2 + (1-r^2)\sigma^2 = \sigma^2\end{aligned} \tag{85}$$

Consequently, $X_{\Delta_2} \mid M = i \sim \mathcal{N}(\pm\Delta_2/2, \sigma^2)$, which is perfectly consistent with the model parameterized by the mean difference Δ_2 in Assumption **A2**.

Observe that $M \to X_{\Delta_1} \to X_{\Delta_2}$ constitutes a Markov chain. By the standard Data Processing Inequality:

$$\mathcal{I}(M; X_{\Delta_2}) \leq \mathcal{I}(M; X_{\Delta_1}) \tag{86}$$

Equality in the DPI holds if and only if X_{Δ_2} is a sufficient statistic for M with respect to X_{Δ_1}, which is equivalent to the Markov chain $M - X_{\Delta_2} - X_{\Delta_1}$, i.e., $X_{\Delta_1} \perp M \mid X_{\Delta_2}$.

However, within the expression $X_{\Delta_2} = rX_{\Delta_1} + Z$ and $r < 1$, the noise term Z is non-degenerate as $\mathrm{Var}(Z) = (1-r^2)\sigma^2 > 0$. Consequently, X_{Δ_2} constitutes a lossy observation of X_{Δ_1}. Given the realization $X_{\Delta_2} = x_2$, the conditional distribution of X_{Δ_1} follows a non-degenerate Gaussian distribution:

$$X_{\Delta_1} \mid X_{\Delta_2} = x_2, M = i \sim \mathcal{N}\left((1-r^2)\mu_i + rx_2, (1-r^2)\sigma^2\right). \tag{87}$$

Since $r < 1$, the coefficient $(1-r^2) > 0$, so the conditional mean retains the M-dependent component $(1-r^2)\mu_i$. Consequently, $X_{\Delta_1} \not\perp M \mid X_{\Delta_2}$, the equality in DPI does not hold, so we have:

$$\mathcal{I}(M; X_{\Delta_2}) < \mathcal{I}(M; X_{\Delta_1}) \tag{88}$$

For the case where $\Delta_2 = 0$, $\mathcal{I}(M; X_0) = \mathcal{I}(M; \mathcal{N}(0, \sigma^2)) = 0$, while $\mathcal{I}(M; X_{\Delta_1}) > 0$ for $\Delta_1 > 0$, so strict monotonicity follows.

□

Lemma 10 (Optimization Objective). *Under the conditions of the Hessian spectral gap in Proposition 1 and the assumptions of the gradient flow analysis in Appendix A.3, with the following additional regularity condition:*

***A5** The aggregated non-member gradient stream evaluated at $\delta = 0$ is non-degenerate:*

$$\left\|\mathbb{E}_{x_{nm}\sim\mathcal{D}_{nm}^s}\left[\nabla_{o_{nm}}\phi_2(o_{nm})\cdot\mathbf{J}_x(x_{nm})\right]\right\| \geq c_{nm} > 0, \tag{89}$$

where c_{nm} is a positive constant. Then, for any model with sufficiently small training loss $\varepsilon_{\text{train}}$, the optimal perturbation $\delta^* = \arg\max_\delta \mathcal{F}(\delta)$ satisfies $\mathcal{F}(\delta^*) > \mathcal{F}(0)$.

Proof. It suffices to show that $\delta = 0$ is not a stationary point of $\mathcal{F}$, i.e., $\nabla_\delta\mathcal{F}(\delta)\big|_{\delta=0} \neq \mathbf{0}$.

From Equation (7), evaluating at $\delta = 0$ gives:

$$\begin{aligned}g := \nabla_\delta\mathcal{F}(\delta)|_{\delta=0} = &\underbrace{\mathbb{E}_{x_m}\left[\nabla_{o_m}\phi_1(o_m)\cdot\mathbf{J}_x(x_m)\right]}_{\mathbf{G}_1} \\ &- \underbrace{\mathbb{E}_{x_{nm}}\left[\nabla_{o_{nm}}\phi_2(o_{nm})\cdot\mathbf{J}_x(x_{nm})\right]}_{\mathbf{G}_2},\end{aligned} \tag{90}$$

where $\mathbf{G}_1, \mathbf{G}_2 \in \mathbb{R}^{|\delta|}$ are the aggregated (i.e., expected) member and non-member gradient streams, respectively.

Upper bound on $\|\mathbf{G}_1\|$. Denoting $w_m := \nabla_{o_m}\phi_1(o_m) \in \mathbb{R}^K$ as the score-sensitivity vector for a member sample, the triangle inequality and the submultiplicativity of the operator norm yield:

$$\begin{aligned}\|\mathbf{G}_1\| &= \left\|\mathbb{E}_{x_m}\left[\mathbf{J}(x_m)^\top w_m\right]\right\| \\ &\leq \mathbb{E}_{x_m}\left[\|\mathbf{J}(x_m)^\top w_m\|\right] \\ &\leq \mathbb{E}_{x_m}\left[\sigma_{\max}(\mathbf{J}(x_m))\|w_m\|\right].\end{aligned} \tag{91}$$

By Assumption **A1** of the gradient flow analysis in Appendix A.3, $\sigma_{\max}(\mathbf{J}(x)) \le S$ for all x. By Assumption **A2** therein, $\mathbb{E}_{x_m}[\|w_m\|^2] \le C_1\varepsilon_{\text{train}}$. Applying the Cauchy–Schwarz inequality:

$$\|\mathbf{G}_1\| \le S \cdot \mathbb{E}_{x_m}[\|w_m\|] \le S\sqrt{\mathbb{E}_{x_m}[\|w_m\|^2]} \le S\sqrt{C_1\,\varepsilon_{\text{train}}}. \quad (92)$$

This bound reflects the fundamental consequence of memorization: for well-trained models, member samples reside near local minima where the model's output is highly confident ($p_y(x_m) \approx 1$), causing the score-sensitivity vector w_m to vanish.

Lower bound on $\|\mathbf{G}_2\|$. By the Directional Coherence condition in Equation (89):

$$\|\mathbf{G}_2\| = \left\|\mathbb{E}_{x_{nm}}\left[\mathbf{J}(x_{nm})^\top w_{nm}\right]\right\| \ge c_{nm} > 0. \quad (93)$$

Combining. By the reverse triangle inequality:

$$\|g\| = \|\mathbf{G}_1 - \mathbf{G}_2\| \ge \|\mathbf{G}_2\| - \|\mathbf{G}_1\| \ge c_{nm} - S\sqrt{C_1\,\varepsilon_{\text{train}}}. \quad (94)$$

For sufficiently well-trained models satisfying:

$$\varepsilon_{\text{train}} < \frac{c_{nm}^2}{S^2 C_1}, \quad (95)$$

we obtain $\|g\| > 0$, establishing that $\delta = 0$ is not a stationary point of $\mathcal{F}$.

Consequently, choosing the unit vector $v := g/\|g\|$ and invoking the first-order Taylor expansion of $\mathcal{F}$ at $\delta = 0$, there exists a sufficiently small $\epsilon > 0$ such that:

$$\mathcal{F}(\epsilon v) = \mathcal{F}(0) + \epsilon \cdot \nabla_\delta \mathcal{F}|_{\delta=0}^\top v + o(\epsilon) = \mathcal{F}(0) + \epsilon\|g\| + o(\epsilon) > \mathcal{F}(0). \quad (96)$$

Therefore, $\mathcal{F}(\delta^*) \ge \mathcal{F}(\epsilon v) > \mathcal{F}(0)$.

□

Remark 5 (Justification of the Directional Coherence Condition). *The Directional Coherence condition (89) requires that the per-sample non-member gradient contributions $\mathbf{J}(x_{nm})^\top w_{nm}$ do not perfectly cancel upon aggregation over the non-member population. This condition is generically satisfied for neural networks in practice, for three reasons:*

(1) ***Systematic score-sensitivity:*** *The non-member score-sensitivity vector $w_{nm} = \nabla_{o_{nm}}\phi_2(o_{nm})$ possesses a systematic nonzero component. For cross-entropy-derived scoring, $w_{nm} = p(x_{nm}) - \mathbf{e}_{y_{nm}}$ has a consistently negative entry in the true-label coordinate, since $p_{y_{nm}}(x_{nm}) < 1$ for non-members. This directional consistency prevents the score-sensitivity vectors from averaging to zero.*

(2) ***High-dimensional perturbation space:*** *In all instantiations of* ReproMIA, *$|\delta| \gg K$. The mapping $w_{nm} \mapsto \mathbf{J}(x_{nm})^\top w_{nm}$ projects K-dimensional vectors into a $|\delta|$-dimensional space. Exact cancellation of $\mathbb{E}[\mathbf{J}^\top w_{nm}] = \mathbf{0}$ in this high-dimensional space would require a pathological alignment between the Jacobian and the score-sensitivity across the entire non-member distribution.*

(3) ***Generic position:*** *For any continuous data distribution with non-degenerate support, the event $\|\mathbb{E}[\mathbf{J}^\top w_{nm}]\| = 0$ is a measure-zero phenomenon in the space of model parameters θ, since the Jacobian $\mathbf{J}(x_{nm})$ varies smoothly with both x_{nm} and θ.*

We note that the per-sample norm lower bound $\mathbb{E}[\|\mathbf{J}(x_{nm})^\top w_{nm}\|^2] \ge \sigma^2 C_2 \alpha(\rho)$ from the gradient flow analysis in Appendix A.3 guarantees that individual gradient contributions are non-negligible; the Directional Coherence condition additionally ensures that these contributions do not destructively interfere upon averaging.

Main proof of Proposition 2. We now assemble the four lemmas to establish the main result.

Step 1: From $\mathcal{F}(\delta^*) > \mathcal{F}(0)$ to $\Delta^{\delta^*} > \Delta^0$. From Lemma 7, H is strictly increasing with a strictly increasing inverse H^{-1}. Together with Assumption **A3** (justified by Lemma 10):

$$\begin{aligned} &\mathcal{F}(\delta^*) > \mathcal{F}(0) \\ &\Delta^{\delta^*} = H^{-1}(\mathcal{F}(\delta^*)) > H^{-1}(\mathcal{F}(0)) = \Delta^0. \end{aligned} \quad (97)$$

Step 2: Expressing mutual information via $\tilde{h}$. From Lemma 8, $\mathcal{I}_\delta = \text{JSD}(P_1^\delta \,\|\, P_0^\delta)$. Under Assumption **A2**, $P_i^\delta = \mathcal{N}(\mu_i^\delta, \sigma^2)$. By the translation invariance of the KL divergence (and hence JSD) for distributions differing only in their means,[1] we obtain:

$$\mathcal{I}_\delta = \text{JSD}(P_1^\delta \,\|\, P_0^\delta) = \tilde{h}(\Delta^\delta), \quad (98)$$

where $\tilde{h}$ is the function defined in Lemma 9. Here we note that $\tilde{h}$ is an even function (i.e., $\tilde{h}(\Delta) = \tilde{h}(-\Delta)$) since swapping the two Gaussian arguments does not alter the JSD, and hence $\tilde{h}(\Delta) = \tilde{h}(|\Delta|)$. Consequently, $\text{JSD}(P_1^\delta \,\|\, P_0^\delta) = \tilde{h}(|\Delta^\delta|)$.

Step 3: Concluding the mutual information improvement. From Step 1, $\Delta^{\delta^*} > \Delta^0$. By Assumption **A4**, $\Delta^0 \ge 0$, which implies $\Delta^{\delta^*} > \Delta^0 \ge 0$. Therefore $|\Delta^{\delta^*}| > |\Delta^0|$, and both arguments lie in the non-negative domain where $\tilde{h}$ is strictly increasing by Lemma 9. It follows that:

$$\mathcal{I}_{\delta^*} = \tilde{h}(\Delta^{\delta^*}) > \tilde{h}(\Delta^0) = \mathcal{I}_0. \quad (99)$$

□

Remark 6 (Practical Validity of Assumption **A2**). *The Gaussian assumption for conditional score distributions (Equation (71)) is made for analytical tractability; the qualitative result $\mathcal{I}_{\delta^*} > \mathcal{I}_0$ holds much more generally.*

The proof of Proposition 2 relies on two properties: (i) $F(\delta)$ is strictly increasing in the mean separation Δ^δ (Lemma 7), and (ii) $\mathcal{I}(M; s_\delta)$ is strictly increasing in $|\Delta^\delta|$ (Lemma 9). Property (i) holds for any location family $D^\delta \sim G(\cdot - \Delta^\delta)$, since the stochastic dominance argument requires only a location shift. Property (ii) also generalizes: for $\Delta_1 > \Delta_2 \ge 0$, one can construct a degraded channel $X_{\Delta_2} = rX_{\Delta_1} + Z$ with $r = \Delta_2/\Delta_1$ and independent non-degenerate noise Z, and the Data Processing Inequality gives $\mathcal{I}(M; X_{\Delta_2}) < \mathcal{I}(M; X_{\Delta_1})$. The Gaussian assumption is only used for closed-form results in Equations (74)-(76) and Lemma 9; strict monotonicity holds for any continuous, full-support location family.

[1] Specifically, for equal-variance Gaussians, $\text{JSD}(\mathcal{N}(\mu_1, \sigma^2)\|\mathcal{N}(\mu_0, \sigma^2)) = \text{JSD}(\mathcal{N}(\Delta/2, \sigma^2)\|\mathcal{N}(-\Delta/2, \sigma^2))$ where $\Delta = \mu_1 - \mu_0$. This follows from the fact that shifting both distributions by $-(\mu_1 + \mu_0)/2$ preserves all KL divergence terms in the JSD definition.

Table 8: TPR@Low FPR regions of different MIA methods across datasets. The best results are bolded, and the second best results are underlined.

Method	CIFAR-10						CIFAR-100						CINIC-10			STL-10			ImageNet		
	WRN28-10			VGG-16			Dense-121			Res-18			VGG-16			WRN28-10			WRN28-10		
(FPR)	0.01%	0.10%	1%	0.01%	0.10%	1%	0.01%	0.10%	1%	0.01%	0.10%	1%	0.01%	0.10%	1%	0.01%	0.10%	1%	0.01%	0.10%	1%
Salem	0.01	0.15	1.47	0.01	0.13	1.33	0.00	0.07	2.76	0.00	0.14	7.90	0.02	0.15	1.52	0.00	0.16	5.04	0.01	0.08	0.84
Yeom	0.02	0.16	1.56	0.01	0.15	1.49	0.00	0.06	2.57	0.00	0.12	6.61	0.02	0.19	1.88	0.00	0.16	4.96	0.01	0.08	0.82
Watson	0.46	0.98	3.73	0.14	0.94	4.42	0.26	2.02	8.31	0.41	2.94	10.06	0.16	0.94	4.83	0.08	0.72	4.88	0.04	0.66	5.79
LDC-MIA	0.46	1.86	8.49	0.26	1.24	6.75	4.25	14.60	45.54	12.90	30.78	68.49	0.23	1.84	9.32	1.68	**2.64**	26.64	0.54	3.24	12.64
ReproMIA	**0.62**	**2.20**	**9.20**	**0.47**	**1.77**	**7.56**	**6.52**	**16.30**	**48.20**	**14.22**	**33.71**	**70.37**	**0.31**	**2.44**	**10.63**	**1.93**	2.33	**31.66**	**0.60**	**3.41**	**13.95**

Table 9: Accuracy and ROC of different MIA methods across datasets. The best results are bolded, and the second best results are underlined.

Method	CIFAR-10				CIFAR-100				CINIC-10		STL-10		ImageNet	
	WRN28-10		VGG-16		DenseNet-121		ResNet18		VGG-16		WRN28-10		WRN28-10	
	Acc.	AUC	Acc.	AUC	Acc.	AUC	Acc.	AUC	Acc.	AUC	Acc.	AUC	Acc.	AUC
Salem et al.	69.66	78.60	65.19	70.42	92.04	94.98	93.24	96.91	73.46	75.25	84.08	92.46	73.98	74.05
Yeom et al.	70.14	78.81	69.81	72.39	92.67	95.24	94.37	97.86	77.03	78.79	84.68	92.75	75.08	74.73
Watson et al.	66.23	68.15	65.05	68.02	72.05	77.28	73.78	79.37	68.40	70.71	71.32	73.86	65.87	70.96
LDC-MIA	73.21	80.48	69.82	77.20	92.63	97.26	95.61	98.86	76.07	84.33	87.40	93.94	75.21	80.92
ReproMIA	**73.23**	**81.31**	**70.17**	**77.88**	**93.09**	**97.84**	**95.65**	**99.04**	**77.16**	**85.06**	**88.03**	**94.63**	**75.65**	**81.01**

B More Details

B.1 Dataset Details

- **WikiMIA** is a benchmark dataset for evaluating membership inference attacks on LLMs. It uses Wikipedia article texts from specific temporal splits labeled as member vs non-member, enabling researchers to assess whether an LLM memorizes its training corpus and is susceptible to MIA.
- **MIMIR** is a benchmark suite designed to evaluate membership inference attack methods on LLMs' pretraining corpora, with multiple sources such as Wikipedia, Arxiv, Github, etc., and features both member and non-member samples plus auxiliary neighbour lists for more detailed analysis.
- **CIFAR-10** is a classic image classification dataset containing 60,000 32×32 color images across 10 classes, split into 50,000 training and 10,000 test images, widely used as a baseline for vision and generative modeling research.
- **TinyImageNet** is a mid-scale vision dataset derived from ImageNet, covering 200 classes with around 500 training images, 50 validation images, and 50 test images per class at 64×64 resolution, often used for intermediate-complexity classification and generative experiments.
- **CIFAR-100** is an extended image classification dataset similar to CIFAR-10 but spanning 100 classes with 600 32×32 color images per class, providing both coarse (20 superclass) and fine (100 class) labels for more granular evaluation.
- **LAION-5B** is a large open multimodal dataset encompassing around 5.85 billion image-text pairs filtered using CLIP for semantic alignment and categorized into English, multilingual, and ambiguous language subsets, widely used for pretraining large multimodal and diffusion models.
- **COCO** is a widely used computer vision dataset for object detection, segmentation, and captioning, featuring around 328,000 images with over 2.5 million labeled instances across 80 object categories, complete with bounding box, segmentation, and caption annotations.
- **CINIC-10** is an extended image classification dataset that augments CIFAR-10 by incorporating an additional 210,000 downsampled ImageNet images for the same 10 classes, totaling 270,000 images equally split into train, validation, and test subsets, serving as a bridge dataset between CIFAR-10 and larger image collections.
- **STL-10** is an image recognition dataset inspired by CIFAR-10 with 10 classes of 96×96 RGB images, featuring a limited labeled training set, a separate test set, and a large unlabeled pool for unsupervised or self-supervised feature learning research.
- **ImageNet-100** refers to a 100-category subset of the extensive ImageNet dataset, retaining diverse natural images and serving as a medium-scale classification benchmark for testing transfer learning and generative model behavior derived from the larger ImageNet corpus.
- **Cora** is a citation network dataset with 2,708 scientific publication nodes, 5,429 citation edges, and 1,433-dimensional bag-of-words features annotated into 7 subject categories, widely used for node classification and graph representation learning.
- **Citeseer** is a citation graph dataset with approximately 3,312 nodes representing publications, 4,732 citation edges, and 3,703 feature dimensions per node, labelled across 6

categories and commonly used in graph neural network research.

- **PubMed** is a biomedical citation network dataset with 19,717 nodes, 44,338 citation edges, and 500-dimensional word vector features, classified into 3 categories, and widely used for evaluating graph neural network methods on larger graphs.

B.2 Experimental Setup Details

We evaluate our methods on a dual-socket server featuring Intel(R) Xeon(R) Gold 5318Y processors, providing a total of 96 logical cores at a base frequency of 2.10 GHz (up to 3.40 GHz). For hardware acceleration, we utilize an NVIDIA H800 GPU with 80 GB of HBM3 memory, running on CUDA 12.8.

For all baseline methods, we download their official code and rerun the experiments with their default hyper-parameters.

For all the models not trained locally, we use the official checkpoints on huggingface. Specifically, Mamba-1.4B[2], Mamba-130M[3], Pythia-12B[4], Pythia-6.9B[5], Pythia-2.8B[6], Pythia-1.4B[7], Pythia-160M[8], Pythia-70M[9], LLaMA-30B[10], LLaMA-13B[11], LLaMA-7B[12], GPT-NeoX-20B[13], GPT-Neo-2.7B[14], OPT-66B[15], OPT-13B[16] and Stable Diffusion v1.5[17] are downloaded.

We implement the DDPM using a U-Net backbone with 128 base channels, 2 residual blocks per resolution and self-attention. The diffusion process follows a linear schedule of $T = 1000$, $\beta_1 = 10^{-4}$ to $\beta_T = 0.02$. We train the model for 800k steps using the Adam optimizer with $lr = 2 \times 10^{-4}$, a 5k-step warmup and a batch size of 128. For robust generation, an EMA with a decay of 0.9999 is applied.

We implement the image classification baselines using different model architectures across multiple datasets, including CIFAR-10/100, CINIC-10, STL-10, ImageNet-100. The model is trained using an SGD optimizer with a momentum of 0.9 and a cosine learning rate decay starting at 0.01, and the epoch varies across model architectures.

C ReproMIA for Classification Models

C.1 Methodology

In the context of classification tasks, ReproMIA aims to reshape the classifier's decision boundaries through subtle input-space reprogramming, strategically propelling member data into high-confidence regions while relegating non-member data to high-entropy zones. To rigorously validate the universality of the ReproMIA paradigm, we extend our methodological design from traditional image classification models to GNNs.

Visual Reprogramming: We propose a simple reprogramming strategy for visual data. The first involves learning a full-dimensional global perturbation δ_{global}.

Topological Reprogramming: For graph-structured data, directly modifying the adjacency matrix is often non-differentiable and risk-prone regarding structural integrity. Consequently, we opt for reprogramming within the feature space. We learn a generalized node feature perturbation, $\delta_{feat} \in \mathbb{R}^F$, which is broadcasted and added onto the global node feature matrix X:

$$\tilde{X} = X + \mathbf{1}\delta_{feat}^T, \tag{100}$$

This nuanced feature shift effectively pushes nodes toward or away from class prototypes, facilitating the discovery of subspaces that most acutely expose the model's overfitting characteristics. To optimize these perturbation patterns δ, we formulate a joint objective comprising three integral components.

Preservation Loss: This component ensures that member data remains correctly classified post-reprogramming, preventing δ from degenerating into a noise pattern that completely obliterates the semantic content of the original input:

$$\mathcal{L}_{preserve} = \mathbb{E}_{(x,y)\sim\mathcal{D}_m}[\mathcal{L}_{CE}(f(\tilde{x}), y)]. \tag{101}$$

Separation Loss: We employ a separation loss predicated on a free-energy-based scoring function to forcibly maximize the discrepancy between the mean scores of member and non-member populations:

$$\mathcal{L}_{sep} = \text{softplus}\left(\gamma - (\bar{\mathcal{S}}_m - \bar{\mathcal{S}}_{nm})\right). \tag{102}$$

For image classification models, the score $\mathcal{S}$ consists of membership score s and calibration membership score s_{cal}, which eliminates sample-specific difficulty by subtracting the reference model's prediction from the target model's prediction:

$$s(f, \tilde{x}, y) = \log(f(\tilde{x})_y). \tag{103}$$

$$s_{cal} = [s(f, \tilde{x}, y) - s(g, \tilde{x}, y)] \cdot \text{NI}(\tilde{x}). \tag{104}$$

where f and g are the target model and the reference model respectively, and $\text{NI}(\tilde{x})$ is the Neighborhood Information of $\tilde{x}$ [72].

Regularization Loss: To ensure the reprogramming pattern δ remains a subtle perturbation and prevents overfitting to the shadow set, we introduce L_2 regularization on the perturbation parameters:

$$\mathcal{L}_{reg} = |\delta|_2^2. \tag{105}$$

The overall optimization objective is defined as:

$$\mathcal{L}_{\text{cls}} = \mathcal{L}_{preserve} + \alpha\mathcal{L}_{sep} + \beta\mathcal{L}_{reg}. \tag{106}$$

We utilize a lightweight MLP as the final attack classifier, which is designed to learn a non-linear decision boundary across the multi-dimensional feature space. Specifically, for each sample, we construct a combined feature vector $[s, s_{cal}, y]$, which integrates the membership score, the calibration membership score, and the one-hot target label. The MLP then outputs a membership probability, and we use it as a signal for membership status determination.

Through this architecture, ReproMIA effectively constructs a member-exclusive channel within the input space, ensuring that only previously encountered samples maintain a low-energy state

[2] https://huggingface.co/state-spaces/mamba-1.4b-hf
[3] https://huggingface.co/state-spaces/mamba-130m-hf
[4] https://huggingface.co/EleutherAI/pythia-12b
[5] https://huggingface.co/EleutherAI/pythia-6.9b
[6] https://huggingface.co/EleutherAI/pythia-2.8b
[7] https://huggingface.co/EleutherAI/pythia-1.4b
[8] https://huggingface.co/EleutherAI/pythia-160m
[9] https://huggingface.co/EleutherAI/pythia-70m
[10] https://huggingface.co/huggyllama/llama-30b
[11] https://huggingface.co/huggyllama/llama-13b
[12] https://huggingface.co/huggyllama/llama-7b
[13] https://huggingface.co/EleutherAI/gpt-neox-20b
[14] https://huggingface.co/EleutherAI/gpt-neo-2.7B
[15] https://huggingface.co/facebook/opt-66b
[16] https://huggingface.co/facebook/opt-13b
[17] https://huggingface.co/stable-diffusion-v1-5/stable-diffusion-v1-5

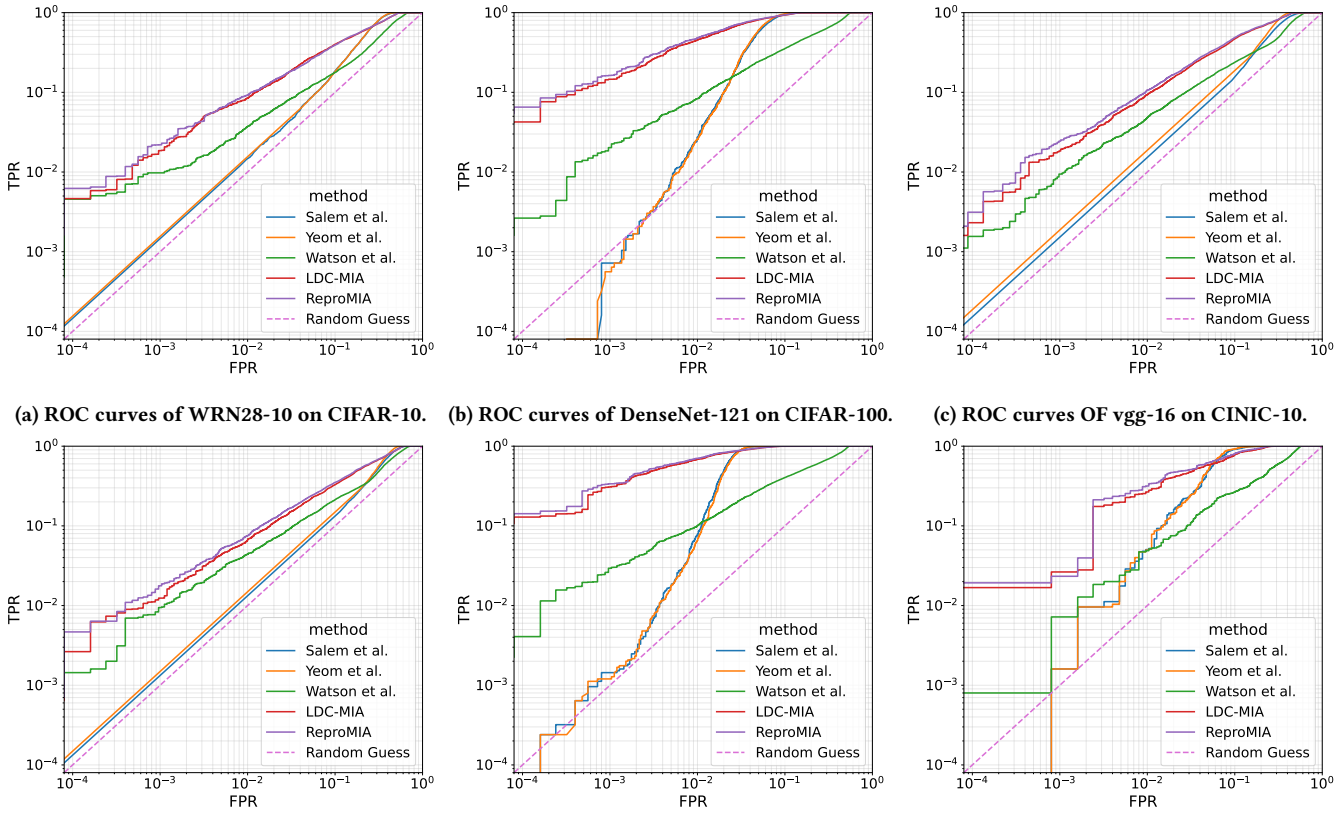

(a) ROC curves of WRN28-10 on CIFAR-10. (b) ROC curves of DenseNet-121 on CIFAR-100. (c) ROC curves OF vgg-16 on CINIC-10.

(d) ROC curves of VGG-16 on CIFAR-10. (e) ROC curves of ResNet-18 on CIFAR-100. (f) ROC curves of WRN28-10 on STL-10.

Figure 6: The log-scaled ROC curves of different methods on different datasets.

upon the injection of δ, thereby enabling precise membership identification.

C.2 Experimental Setup

C.2.1 Datasets. To evaluate the proposed methodology, we conduct experiments across three datasets of varying complexity: CIFAR-10 [44], CIFAR-100 [44], and CINIC-10 [12]. CIFAR-10 comprises 60,000 $32 \times 32 \times 3$ color images, uniformly distributed across 10 distinct classes. Similarly, CIFAR-100 consists of 60,000 images of identical dimensions, though partitioned into 100 fine-grained categories. CINIC-10 serves as an augmented hybrid derived from CIFAR-10 and downsampled ImageNet [13], encompassing a more extensive collection of 270,000 images distributed over 10 classes.

In our experimental evaluations, each dataset is meticulously partitioned into six disjoint subsets: $\mathcal{D}_{tar}^{train}$, $\mathcal{D}_{tar}^{held}$, $\mathcal{D}_{shadow}^{train}$, $\mathcal{D}_{shadow}^{held}$, $\mathcal{D}_{ref}^{train}$, and $\mathcal{D}^{test}$. Specifically, $\mathcal{D}_{tar}^{train}$ is utilized for the optimization of the target model, while $\mathcal{D}_{tar}^{held}$ functions as the set of non-members relative to that model. $\mathcal{D}_{shadow}^{train}$ is employed to train the shadow model, with $\mathcal{D}_{shadow}^{held}$ serving as its respective non-member population. $\mathcal{D}_{ref}^{train}$ is used for the training of the reference model, and $\mathcal{D}^{test}$ serves as a universal test set to assess the performance of all models.

C.2.2 Models. Following Shi et al. [72], we selected diverse architectural benchmarks to serve as the target models across our evaluated datasets. For the CIFAR-10 dataset, we utilized WideResNet-28-10 [91] and VGG-16 [75]. For CIFAR-100, the evaluation was conducted using DenseNet-121 [38] and ResNet-18 [33]. For the CINIC-10 dataset, VGG-16 [75] was adopted as the target model. For STL-10 [11] and ImageNet-100 [78] datasets, we both use WideResNet-28-10 [91] as well. The default architectures of the shadow models and reference models were maintained as identical to those of the respective target models, we also extended to different model architectures across the shadow and reference models.

C.2.3 Baselines. In our evaluations, we benchmark `ReproMIA` against five SOTA baseline methodologies to rigorously assess its efficacy. Salem et al. [67] utilize the posterior probabilities of target samples obtained from the target model to train shadow models, subsequently optimizing a binary classifier as the adversarial engine based on confidence vectors. Yeom et al. [90] dispense with auxiliary models entirely, adjudicating membership status solely by analyzing the target samples' loss values or prediction error rates relative to the target model. Watson et al. [83] introduce calibration factors by training reference models to facilitate a comparative analysis of output distributions. LiRA [6] advances this paradigm

Table 10: TPR@5%FPR and TPR@0.1%FPR results on WikiMIA benchmark. The best results are bolded, and the second best results are underlined.

Len.	Method	Mamba-1.4B		Pythia-6.9B		LLaMA-13B		NeoX-20B		LLaMA-30B		OPT-66B		Average	
		T5%F	T0.1%F	T5%F	T0.1%F	T5%F	T0.1%F	T5%F	T0.1%F	T5%F	T0.1%F	T5%F	T0.1%F	T5%F	T0.1%F
32	Loss	11.28	1.19	13.95	1.48	12.17	2.37	20.18	2.97	16.32	2.97	16.32	2.97	15.04	1.98
	Ref	7.42	0.59	5.93	0.30	4.15	0.00	19.29	0.00	10.39	0.00	10.39	0.00	9.60	0.45
	Zlib	13.06	1.48	15.73	2.08	10.39	1.19	19.58	2.97	13.65	2.97	13.65	2.97	14.34	2.13
	Min-K%	14.24	2.67	18.40	6.82	17.80	3.56	25.82	3.26	20.18	3.26	20.18	2.67	19.44	4.30
	Min-K%++	11.87	1.19	14.54	2.37	35.01	1.48	18.10	5.04	28.19	5.04	27.30	4.15	22.50	2.97
	ReCaLL	38.87	2.67	42.14	7.72	38.28	10.09	39.76	5.34	44.81	5.34	25.82	4.45	38.28	7.42
	ReproMIA	**39.17**	**3.26**	**50.45**	**10.68**	**59.64**	**13.06**	**45.90**	**6.13**	**55.19**	**6.13**	**46.88**	**5.64**	**49.54**	**8.38**
64	Loss	10.58	0.96	14.90	0.96	10.58	1.92	12.02	1.92	12.50	1.92	12.50	1.92	12.18	1.60
	Ref	4.33	0.48	10.58	0.00	3.37	0.00	20.67	3.85	10.10	0.00	10.10	0.00	9.86	0.72
	Zlib	14.90	2.40	15.38	1.44	13.46	3.37	17.79	2.88	14.42	3.85	14.42	3.85	15.06	2.97
	Min-K%	17.31	3.37	21.63	3.37	19.23	3.85	22.12	3.85	21.63	1.92	21.63	5.77	20.59	3.69
	Min-K%++	13.94	6.73	25.48	4.33	34.13	4.81	21.15	**5.77**	32.21	0.96	28.85	1.44	25.96	4.01
	ReCaLL	53.37	9.13	54.81	1.44	61.06	25.48	**42.62**	3.37	62.02	6.73	21.63	2.40	49.25	8.09
	ReproMIA	**57.69**	**11.06**	**70.67**	**25.00**	**73.77**	**32.79**	35.10	4.91	**67.31**	**9.62**	**46.63**	**8.17**	**58.53**	**15.26**
128	Loss	14.81	0.00	13.11	0.00	22.54	9.86	19.67	2.97	27.87	8.20	22.95	3.28	20.16	4.05
	Ref	13.58	3.70	6.56	0.00	8.45	0.00	13.11	0.00	11.48	0.00	6.56	4.92	9.96	1.44
	Zlib	20.99	9.88	16.39	4.92	19.72	11.27	14.75	2.97	22.95	6.56	21.31	14.75	19.35	8.39
	Min-K%	14.81	2.47	16.39	6.56	25.35	14.08	29.51	3.26	34.43	6.56	27.87	3.28	24.73	6.04
	Min-K%++	13.58	1.23	18.03	6.56	42.25	8.45	26.23	5.04	42.62	8.20	22.95	1.64	27.61	5.19
	ReCaLL	49.18	16.39	36.07	26.23	45.90	19.67	45.90	11.27	37.70	1.64	26.23	6.56	40.16	13.63
	ReproMIA	**50.82**	**18.03**	**75.41**	**45.90**	**65.57**	**37.70**	**50.82**	**14.75**	**96.72**	**55.74**	**47.54**	**18.03**	**64.48**	**31.69**

Table 11: Accuracy of target models on different datasets.

Dataset	Target Model	Train Acc.	Test Acc.
CIFAR-10	WideResNet28-10	100.00	77.82
CIFAR-10	VGG-16	100.00	69.08
CIFAR-100	DenseNet-121	99.98	41.89
CIFAR-100	ResNet18	100.00	36.77
CINIC-10	VGG-16	99.98	57.80
STL-10	WideResNet28-10	100.00	59.38
ImageNet-100	WideResNet28-10	99.99	64.89

by training multiple shadow models both including and excluding a specific target sample, and employing a likelihood ratio test to achieve high-precision membership inference. LDC-MIA [72] implements a specialized difficulty classifier designed to extract intrinsic sample features, determining membership by quantifying the discrepancy between the target model's empirical scores and their calibrated values.

C.3 Evaluations

C.3.1 Image Classification. We conducted a comprehensive series of experiments on image classification models to substantiate the technical sophistication and state-of-the-art performance of ReproMIA. The target models were initially optimized using SGD with a learning rate of 0.1, a momentum coefficient of 0.9, and a cosine learning rate schedule; the resulting training and test accuracies are detailed in Table 11.

Tables 8, 9, and the accuracy metrics delineate the comparative performance between existing baselines and ReproMIA across various datasets and architectural paradigms. The empirical evidence indicates that ReproMIA consistently maintains SOTA performance regardless of the specific dataset or target architecture. Specifically, ReproMIA surpasses the runner-up method, LDC-MIA, with an average increase in TPR@0.01%FPR, TPR@0.1%FPR, and TPR@1%FPR of 0.62%, 0.85%, and 1.96%, respectively. Furthermore, it achieves a margin of improvement in Accuracy and AUC of 0.43% and 0.54%. These results further validate the universal adaptability of ReproMIA, demonstrating its capacity to deliver superior performance across diverse adversarial scenarios.

To provide further visual evidence of the efficacy of ReproMIA, we present the ROC curves in Figure 6. These curves illustrate the performance of various MIA baselines alongside ReproMIA for different target models and datasets, highlighting the consistent superiority of our approach.

Robustness against Defenses. In Table 12, we rigorously evaluate the robustness of ReproMIA against a spectrum of prevalent defense mechanisms. Specifically, we investigate the countermeasures of Differential Privacy and Input Smoothing as primary defenses to MIAs. The empirical results demonstrate that ReproMIA maintains exceptional adversarial efficacy under Input Smoothing; even at a noise standard deviation of 0.5, the attack performance remains remarkably stable. Notably, when the noise level escalates to 0.9, ReproMIA continues to sustain an AUC exceeding 60%, and all baselines typically suffer complete degradation of discriminative power. In the presence of Differential Privacy, arguably the most

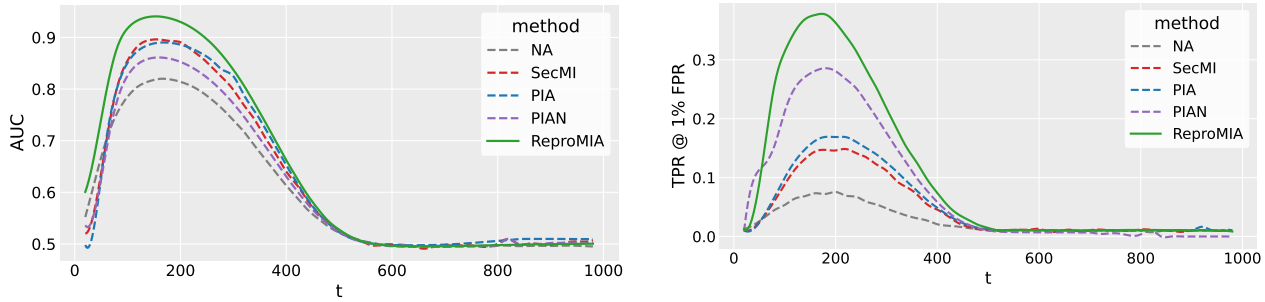

Figure 7: The AUC and TPR@1%FPR results of different methods on Tiny-ImageNet as t varies.

Table 12: Target model accuracy and MIA AUC and TPR@Low FPR of ReproMIA under different defense mechanisms.

Defense	Model Acc	AUC	T@0.1%F	T@1%F
No defense	77.82	81.31	2.20	9.20
DP-SGD(0,∞)	64.82	60.68	0.32	2.08
DP-SGD(0.2,1000)	50.73	54.92	0.28	1.83
DP-SGD(0.3,100)	46.87	54.78	0.22	1.72
DP-SGD(0.6,10)	43.96	53.74	0.20	1.63
DP-SGD(1,1)	43.05	53.54	0.16	1.54
Smooth (0.3)	76.42	81.22	2.17	9.17
Smooth (0.5)	74.86	81.08	2.06	9.12
Smooth (0.7)	61.99	71.56	1.85	6.53
Smooth (0.8)	54.46	65.95	1.14	5.08
Smooth (0.9)	47.30	61.85	0.40	3.95

formidable defensive paradigm, while a non-negligible attenuation in attack potency is observed, ReproMIA consistently preserves a superior performance margin over all baseline methods across every evaluated privacy budget.

C.3.2 Graph Classification. For the task of graph classification, we utilize the Cora, PubMed, and Citeseer datasets [69, 88], the descriptive statistics of which are detailed in Appendix B.1. Given the relative paucity of literature concerning MIA specifically tailored for graph classification, we focus our evaluation on the GraphSAGE architecture [31] as the target model. We employ the methodology proposed by Duddu et al. [19] as our primary baseline. The performance is quantified using Accuracy, AUC, and Inference Advantage, a metric designed to evaluate the volume of leaked information relative to random guessing, formulated as $Adv. = 2 \times (Acc. - 0.5)$.

Table 13 delineates the comparative results of Accuracy, Inference Advantage, and AUC between the baseline and ReproMIA. Our framework consistently achieves superior performance, exceeding the baseline by average margins of 2.15%, 4.31%, and 3.74%, respectively.

Furthermore, Figure 8 illustrates the interplay between the intrinsic classification accuracy of GraphSAGE and its susceptibility to MIA as measured by AUC across varying network depths. It is observable that excessive layer depth induces a precipitous decline in model accuracy due to the over-smoothing phenomenon; this degradation consequently precipitates a moderate reduction in MIA efficacy, although ReproMIA nevertheless sustains a high level of discriminative power.

Table 13: Model accuracy and MIA attack performance comparison. Adv. represents the inference advantage. The best results are bolded.

Dataset	Methods	Model Acc.	Acc.	Adv.	AUC
Cora	Duddu et al.	81.20	70.54	41.08	73.13
	ReproMIA	81.20	**72.46**	**44.92**	**77.92**
Pubmed	Duddu et al.	78.50	74.60	49.20	78.87
	ReproMIA	78.50	**77.78**	**55.56**	**82.18**
Citeseer	Duddu et al.	71.30	63.75	27.48	67.06
	ReproMIA	71.30	**65.10**	**30.21**	**70.19**

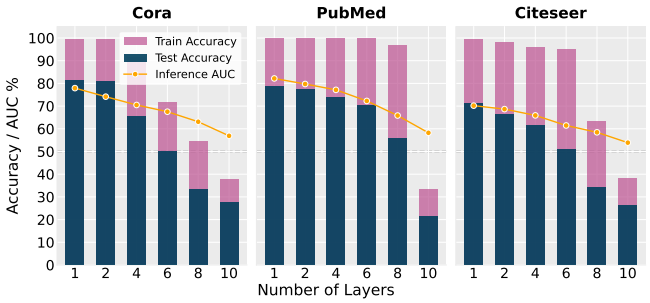

Figure 8: The train, test accuracy and membership inference attack AUC drop of different layers due to feature over-smoothing.

D More Experimental Results

D.1 More Results on LLMs

In this section, we present a comparative analysis of TPR@5%FPR and TPR@0.1%FPR for various baselines and ReproMIA on the WikiMIA dataset, evaluated across target models of varying parameter scales, as detailed in Table 10. The empirical results demonstrate that ReproMIA consistently maintains state-of-the-art performance across all configurations. Specifically, ReproMIA exceeds the runner-up method, ReCaLL, by an average margin of 14.95% in TPR@5%FPR and 8.73% in TPR@0.1%FPR. These findings provide

Table 14: MIA performance of ReproMIA when varying the prompt length.

Prompt	Mamba		Pythia		LLaMA-13B		LLaMA-30B	
Length	AUC	T1%F	AUC	T1%F	AUC	T1%F	AUC	T1%F
10	81.43	9.84	78.19	16.90	87.37	16.39	95.89	36.07
20	83.53	4.92	81.46	18.03	92.13	24.59	96.40	44.26
30	87.91	6.56	76.77	15.49	93.95	31.15	90.38	19.67
40	90.06	13.11	86.90	29.51	89.98	40.98	95.94	39.35
50	87.77	6.56	91.33	27.87	92.42	34.43	94.36	44.26
60	86.35	11.48	91.08	36.07	93.93	49.18	95.35	32.79
70	89.60	36.07	90.07	39.34	90.51	31.15	96.43	47.54
80	89.79	22.95	96.96	49.18	94.60	49.18	96.69	59.02
90	85.06	16.39	96.83	18.03	91.51	32.79	96.72	44.26
100	88.61	9.84	84.20	26.23	94.20	44.26	98.84	59.02
110	87.80	4.92	81.59	13.11	90.43	29.51	95.35	42.62
120	90.38	14.75	82.80	3.28	93.20	39.34	98.39	62.30

Table 15: MIA performance of ReproMIA when varying the Min-K% ratio.

Min-K%	Mamba		Pythia		LLaMA-13B		LLaMA-30B	
Ratio	AUC	T1%F	AUC	T1%F	AUC	T1%F	AUC	T1%F
0.05	79.76	6.56	74.43	13.11	90.46	37.70	93.23	27.87
0.10	86.29	19.67	88.82	24.59	93.79	11.48	92.45	29.51
0.15	89.22	37.70	84.79	23.94	91.86	26.23	97.34	59.02
0.20	89.60	36.07	96.96	49.18	94.60	49.18	98.84	59.02
0.25	89.98	26.23	81.19	31.15	91.43	29.51	89.84	37.70
0.30	87.15	16.39	94.60	49.18	92.26	22.95	97.74	49.18
0.35	89.36	11.48	95.41	37.88	91.83	27.87	96.08	44.26
0.40	91.28	6.56	74.16	8.64	92.64	44.26	91.02	24.59

compelling evidence that ReproMIA achieves superior membership inference efficacy across diverse and stringent low-FPR regimes.

A critical hyperparameter influencing the efficacy of ReproMIA is the soft prompt length, and we will analyze its impact in this section. To empirically investigate this relationship, we evaluated the MIA performance of ReproMIA across four target models of varying parameter scales using the WikiMIA dataset with the length of 128, systematically adjusting the prompt length. As detailed in Table 14, the metrics for AUC and TPR@1%FPR peak when the prompt length is around 80 tokens. While either increases or decreases in the prompt length result in a slight degradation of performance, the attack consistently maintains a high level of efficacy throughout the tested range.

Another pivotal hyperparameter governing the efficacy of ReproMIA is the Min-K% ratio, for which we conducted a parametric sensitivity analysis using the WikiMIA dataset with a sequence length of 128. The empirical results, summarized in Table 15, reveal that both too small or large Min-K% ratios precipitate varying degrees of attenuation in membership inference performance. Consequently, we identified $K = 0.2$ as the optimal threshold, as it yields the most robust discriminative signal by balancing the filtration of high-probability tokens with the retention of informative tail-distribution residuals.

Table 16: MIA performance of ReproMIA with different numbers of accessible shadow data.

Shadow	Mamba		Pythia		LLaMA-13B		LLaMA-30B	
Num	AUC	T1%F	AUC	T1%F	AUC	T1%F	AUC	T1%F
10	78.28	6.93	77.75	17.28	90.04	11.18	87.74	31.68
20	77.12	19.78	84.70	19.78	92.20	15.38	93.59	39.56
30	79.61	20.99	92.04	27.16	91.94	23.46	92.44	40.74
40	84.39	30.99	96.38	42.25	94.11	35.29	94.27	40.98
50	89.60	36.07	96.96	49.18	95.20	37.70	98.84	59.02
60	91.08	29.41	89.16	31.37	93.93	47.06	98.58	84.31
70	93.04	46.34	90.48	51.22	96.73	41.46	94.29	78.05
80	89.70	29.03	97.50	64.52	97.40	74.19	98.75	90.32

We further conducted a parametric analysis regarding the volume of accessible shadow data, the results of which are summarized in Table 16. It is observable that when the available shadow data is extremely scarce, the MIA performance of ReproMIA is marginally attenuated. However, with a modest threshold of approximately 50 samples, ReproMIA achieves commendable membership inference efficacy. Generally, an expansion in the shadow dataset size facilitates a monotonic improvement in attack performance.

In practice, the assumption that an adversary can acquire a substantial volume of non-member data is highly realistic. As noted by Hu et al. [37], data generated subsequent to the completion of a model's training phase can effectively serve as non-member samples. Consequently, the adversarial requirement is reduced to obtaining a nominal set of member samples, a task that remains fundamentally feasible in real-world auditing scenarios [37].

D.2 More Results on Diffusion Models

In this section, we provide a parametric sensitivity analysis regarding the diffusion timestep t. Specifically, we employed DDPM as the target model on TinyImageNet to systematically record the AUC and TPR@1%FPR for both the baseline methods and ReproMIA as t varies. As illustrated in Figure 7, all evaluated methods exhibit a similar pattern, wherein optimal MIA performance is localized around the $t = 150$ interval. Notably, ReproMIA consistently demonstrates superior discriminative capability across the entire spectrum of t.

Our ablation study on the maximum permissible perturbation magnitude δ_m, summarized in Table 17, reveals that optimal MIA performance is typically achieved when δ_m is set between 4/255 and 64/255. This bell-shaped trend stems from a fundamental trade-off: overly small δ_m provides insufficient optimization space for ReproMIA to encode discriminative features for signal amplification, while excessively large δ_m leads to stochastic saturation, where the reprogramming pattern acts as high-intensity noise that obscures semantic information and sharply degrades membership inference efficacy.

E On the Scope of Unification

The unification in ReproMIA resides in the *signal amplification mechanism*: all instantiations share the bilevel optimization formulation of Equation (3), the frozen-model constraint, and the learnable

Table 17: MIA performance on DDPM with different reprogramming threshold δ_m.

δ_m	CIFAR-10		Tiny-ImageNet		CIFAR-100	
	AUC	T@1%F	AUC	T@1%F	AUC	T@1%F
2/255	92.52	28.67	93.65	30.67	91.00	22.88
4/255	92.60	29.21	94.05	37.71	91.07	23.76
8/255	92.57	32.36	94.05	30.89	90.84	22.72
16/255	92.83	34.14	93.30	29.49	90.90	24.96
32/255	92.54	31.58	93.11	29.06	91.00	26.09
64/255	92.54	26.56	89.38	11.32	91.00	26.10
96/255	80.01	7.58	76.30	3.79	73.96	3.68

input-space transformation δ, which together constitute the active probing paradigm that distinguishes ReproMIA from all prior passive MIA methods. The theoretical guarantees established in Propositions 1 and 2 apply universally to any instantiation satisfying Equation (3), as the proofs depend only on the monotonicity and differentiability of Φ and the memorization property $\rho > 1$, not on the specific form of the scoring function.

The downstream scoring pipeline, which is how the reprogrammed model output $\mathcal{M}_\theta(x \oplus \delta^*)$ is converted into a scalar membership score, is intentionally domain-specific. This is a structural necessity rather than a design limitation: an LLM produces a sequence of token-level log-probabilities, a diffusion model produces noise predictions $\epsilon_\theta(x_t, t)$ along a temporal trajectory, and a classification model produces a K-dimensional softmax vector. No single scoring function can meaningfully operate across these heterogeneous output spaces. Requiring implementation-level identity across such fundamentally different output modalities would render cross-domain unification trivially impossible for any framework.

Regarding the classification instantiation's use of shadow and reference models, our opening motivation targets the prohibitive cost of shadow models in the era of LLMs with billions of parameters. For classification models with small parameters, training shadow models is computationally inexpensive and is the universal practice among all competing methods [6, 72, 83, 90]. ReproMIA's contribution in this domain is the reprogramming-based signal amplification, which demonstrably improves over all baselines that also employ shadow models under identical conditions.

F Ethical Considerations

This study does not introduce new ethical risks. All datasets leveraged in our experiments were originally collected and released by prior work and are publicly available. We follow the usage conditions and ethical safeguards described by their original authors. All evaluated models are also publicly available. Our work focuses on benchmarking and analysis of existing artifacts rather than collecting new data. The study does not involve human participants, user studies, or the acquisition of new user data, and therefore does not raise concerns related to informed consent, privacy, or the handling of personally identifiable information beyond what is already covered by the source datasets.